Recycling of Aerospace Aluminum Components into New Valuable Products

José Alberto Muñiz Lerma

Department of Mining and Materials Engineering

McGill University, Montreal, QC

April 2016

A thesis submitted to McGill University in partial fulfillment of the requirements of the degree of Doctorate of Philosophy.

Abstract

The possibility of recycling the Al present in end-of life (EOL) aircraft while avoiding downgrading of the alloys is addressed in this thesis. Controlling the impurities during the recycling process is viewed as the most important challenge concerning the recycling of high-value alloys. The source of impurities associated with the aircraft recycling process are related with the corrosion protection coating used in aircraft fuselages, the high amount of alloying elements present in the airframe, and the pickup of impurities such as Fe and Si during the handling of the aircraft scrap.

To study the removal of impurities associated with the corrosion protection coating, two routes were explored: thermal decoating and chemical stripping. Thermal decoating was proven to be a viable method to remove the aircraft protection coating. The optimal residence time and temperature for thermal decoating were 4 minutes holding time at 480 °C. These conditions allowed the thermal degradation of the coating with an associated energy barrier of 170 kJ/mol. After thermal decoating the concentration of Cr(VI) in the aged primer was 2.6 µg of Cr(VI)/mm2 of Al substrate. This concentration level suggests that adequate environmental controls are required to limit Cr(VI)-containing particulate matter during the thermal decoating of aircraft substrates.

The chemical stripping route is an alternative method to remove the organic aircraft coatings. The evaluation of this route was carried out using commercial stripping solutions free of dimethyl chloride; instead either dimethyl sulfoxide or N-methyl-2-pyrrolidone was the active solvent in the presence and absence of an alkaline media. The stripping efficiency was evaluated in the external and internal sections of the fuselage. The coating present in the external section of the fuselage can be effectively removed by all the tested stripping solutions. However, the coating on the internal section was only removed by the stripping solution composed of a mixture of dimethyl sulfoxide, sodium hydroxide, and activators property of Greensolv® in 2.10 h. The effectiveness of this solution was correlated to the Flory-Rehner model and attributed to a combination of factors such as molar volume of the active solvent, the degree to which the coating was aged, and the alkalinity of the solution.

The other class of impurities associated with the recycling of EOL aircraft is the high amount of alloying elements present in EOL airframes. The chemical compositions of Al scrap, after blending different Al components from a CRJ-100ER aircraft was estimated using a mass balance approach and presented in Appendix A. By commingling different aircraft sections it was found that the chemical compositions of premium aerospace alloys can be obtained. Hence, a smart dismantling process is recommended if the production of high-value alloys is targeted. However, any other material not belonging to the AA2000 and AA7000 series must be avoided in the scrap stream.

After the EOL aircraft is dismantled, sorted, and decoated, the next step in the recycling process is refining. The prediction of the refining efficiency of fractional crystallization was carried out on a representative scrap chemical composition. The combined effect of stirring and solidification velocity, was incorporated and explored in a one-dimension solidification model which included back diffusion in the solid. Using this model, it was found that the optimum solidification velocities able to yield the highest refining and recovery efficiencies was between 1×10^{-6} m/s and 1×10^{-5} m/s when medium to high stirring levels were applied. The recovery efficiency of refined Al has been estimated as 31 wt% of the initial liquid when the process is carried out at 1×10^{-6} m/s and the Fe and Si concentrations are 1 % and 2 %, respectively. If any of these impurities increase, the Al recovery is reduced.

Résumé

La possibilité de recycler certains alliages d'aluminium (AA) présents dans la composition des aéronefs en fin de vie (EOL), tout en maintenant la qualité de ces alliages, est traitée dans cette thèse. Le contrôle des impuretés au cours du recyclage devient alors un défi de taille à l'obtention d'alliages de qualité. Les sources d'impuretés sont associées aux revêtements contre la corrosion, aux hauts taux d'éléments d'alliages présents, ainsi qu'aux éléments externes présents lors de la manutention des rebuts d'aéronefs, tel que le Fe et le Si.

Deux voies ont été explorées afin d'éliminer les impuretés reliées au décapage des revêtement anticorrosion: le procédé thermique, et le procédé chimique. Le premier est reconnu comme étant une méthode efficace et viable pour enlever les revêtements de protection des aéronefs. Il a été démontré que le temps d'immersion et la température requise pour le décapage thermique des substrats d'aluminium est de 4 minutes et 480°C. Ces conditions ont permis la dégradation du revêtement associée à une barrière énergétique de 170 kJ/mol. De plus, la concentration de Cr(VI) dans l'apprêt, suite au décapage, a été évaluée à 2,6 µg de Cr(VI)/mm^2 de substrat d'aluminium. Ce niveau de concentration suggère qu'un contrôle environnemental adéquat est requis lors du procédé de décapage thermique afin de limiter la contamination au Cr(VI).

Le décapage par procédé chimique, est un procédé alternatif à l'élimination des enduits organique d'aéronefs. L'évaluation de ce procédé a été effectuée en utilisant des solutions décapantes commerciales sans dichlorométhane, remplacé par du diméthyl sulfoxyde ou par du N-méthyle-2-pyrrolidone, comme solvant actif. L'efficacité de décapage de ces solutions commerciales a été évaluée sur des sections externes et internes. Il a été démontré que le revêtement présent à l'extérieur pouvait être décapé efficacemen. Cependant le revêtement de la partie intérieure n'a été décapé uniquement que par la solution contenant un mélange de diméthyl sulfoxyde, d'hydroxyde de sodium et d'un activateur, propriété de Greensolv®, en 2h10. L'efficacité de la solution suit le modèle de Flory-Rehner, selon une combinaison de facteurs tels que le volume molaire du solvant actif, le degré de vieillissement de l'enduit, ainsi que l'alcalinité de la solution.

L'autre source d'impureté associée au recyclage d'aéronefs en EOL provient de la grande quantité d'éléments d'alliage présents. Suite au mélange des alliages rebutés provenant des différentes

composantes d'un appareil CRJ-100ER, la composition chimique finale a été estimée suivant une approche de bilan massique et est présentée à l'Annexe A. Il est cependant possible d'obtenir des alliages de qualité, respectant les tolérances requises par l'industrie aéronautique, en mélangeant certaines sections de l'aéronef. Un démantèlement précis et bien planifié est donc recommandé dans le cas où la production d'alliage recyclé de grade aéronautique est ciblée. Il est préconisé d'éviter tout matériaux n'appartenant pas aux séries AA2000 et AA7000 afin de recycler efficacement ces dernières.

Après démantèlement de l'aéronef, le décapage et le tri des matières, suit le raffinage. Un modèle de prédiction de l'efficacité a été développé avec l'utilisation de rebuts représentatifs. L'effet combiné de l'agitation et de la vitesse de solidification, a été incorporé et étudié dans un modèle de solidification à une dimension, qui inclut la rétrodiffusion dans le solide. L'utilisation de ce modèle a permis de déterminer une vitesse de solidification optimale entre 10^{-6} et 10^{-5} m/s, avec une agitation de moyenne à élevée. L'efficacité de récupération d'un AA raffiné a été estimée à 31% massique du liquide initial lorsqu'une vitesse de solidification de 10^{-6} m/s et les taux de concentration de Fe et de Si étaient respectivement de 1% et 2%. L'augmentation d'une de ces deux impuretés, viendrait par conséquent faire chuter le taux de récupération de l'aluminium.

Table of Contents

List of figures

List of tables

Acknowledgments

Firstly, I would like to acknowledge the Faculty of Engineering for the McGill Engineering Doctoral Award (MEDA) provided to support all my graduate studies, as well as the Consortium de Recherche et d'Innovation en Aérospatiale au Québec (CRIAQ), Bombardier, Bell Helicopter, Sotrem-Maltech, BFI, Nano Quebec, and Aluminerie Alouette for funding this project.

I would like to thank and express my gratitude to my two research supervisors. Prof. Mathieu Brochu and Prof. In-Ho Jung. I sincerely acknowledge all the support, guidance, advices, encouragement, patience and confidence throughout this work. I specially wish to thank Mathieu for giving me the opportunity to learn new things and to help me with anything that I needed, not only academically but also personally.

I would like to express my gratitude to all the members and alumni of the Powder Processing and Additive Manufacturing of Advanced Materials group (P^2AM^2), Masum, Phil, Abhi, Bamidele, Nesli, David Walker, Nejib, Dany, Yuan, Xianglong, Joseph, Jason D., Melissa, Rodrigo, Andrew, Gil, Sam, Justin, Sumin, Marie-Pier, Ryan, Cory, David Heard, Jason M., Lucie, Yaoyao and Javier for all the parties and scientific discussions that undoubtedly enriched my graduate studies. Javier, I will not forget all the great fishing times that we have spent together talking about tons of things but specially, trying to get the big fish! I know I know, you got a good one but I let him escape☺. I would also like to thank my friends Dong-Geun Kim and Manas, for all the helpful discussions on thermodynamics and solidification during this adventure. Also, I would like to acknowledge the administrative and technical staff in the department for all their assistance. Barbara, Terry, Monique, and Robert.

Finally, in a very special way, I would like to thank my parents and my brother who have always been encouraging me all these years. But specially, I want to express my most sincere gratitude to my wife Veronica and my little daughter Dania, which undoubtedly have made an enormous sacrifice during these last 3 years and a half. Vero, without your support, your love, your encouragement, your understanding, your company, and your incredible patience, this adventure would not be the same. Amor muchas gracias desde el fondo de mi corazón a ti y a Dania.

Contribution of Authors

This thesis has been constructed according to the guidelines of the Faculty of Graduate and Postdoctoral Studies of McGill University for a manuscript-based thesis and it contains three manuscripts either published or submitted for publication.

Chapters 4 through 6 are individual manuscripts and are formatted as such. As the first author on the three manuscripts included within this thesis, I produced all of the samples, performed the analysis, and wrote the manuscripts. Below are the contributions of the co-authors for each paper in the different chapters presented in this dissertation.

Prof. Milan Marić offered technical expertise throughout the investigation of the chemical decoating of aircraft Al alloys and creation of the manuscript in Chapter 5.

Dr. Manas Paliwal supplied technical expertise with the development of the solidification model as well as with the creation of the manuscript in Chapter 6.

Prof. In-Ho Jung co-supervised the entire project as well as supplied technical and scientific advice throughout the project.

Prof. Mathieu Brochu supervised the entire project and supplied technical and scientific advice for each manuscript.

1: Introduction and Problem Statement

Global warming and climate change caused by the emission of greenhouse gases (GHG) are one of the greatest issues that the world is currently facing. According to the United Nations (UN), the global emissions of carbon dioxide (CO_2), have increased around 50 % since 1990 [1]. If this trend continues, the UN has predicted that at the end of this century, the global temperature will increase 1.5 °C by 2065 changing the weather patterns [1.1].

In September 2015, with the aim to develop an action plan to improve the life quality of people and eradicate the main global problematics, the UN in agreement with world leaders adopted 17 sustainable development goals to be accomplished by 2030. Within these goals, two important initiatives which are: Ensure sustainable consumption and production patterns, and take an urgent action to combat climate change and its impacts, were adopted [1.2]. In this context, the aerospace sector led by the International Civil Aviation Organization (ICAO) has been committed to work and contribute to the achievement of the UN sustainable goals. In fact, the ICAO is looking to reduce the environmental footprint of aviation industry in different aerospace areas being one of this, the recycling of aircraft at the end-of-life (EOL) [1.3].

According to the Avolon report on the aircraft retirement trends and outlook [1.4], over 31,000 jet airliners have been produced since the beginning of the jet age 58 years ago. Additionally, it has been also reported that statistically, aircraft have been retired or reached the end of life when the operational and maintenance cost exceed the financial contribution that it can earn. This economic inflection point occurs approximately after 25 years of the aircraft's life. After the aircraft operation has overpass its lifespan, airplanes are parked in boneyards around the world and wait for a final disposal. Ten years ago, this final disposal was carried out in a non-controlled process downgrading the value of the aircraft components (Figure 1-1) [1.5].

In 2006, it was estimated that 12,000 aircraft would be retired in the following two decades reaching a peak of 1000 aircraft disposed annually by 2023 [1.6, 1.7]. Based on this statistics and in the sustainability vision of the aerospace sector, recycling of EOL aircraft started to get attention. Airbus and Boeing, two of the major aircraft manufacturer, separately started programs oriented to study the management of EOL aircraft. Specifically, Airbus launched the project called

"Process for Advanced Management of End-of-Life Aircraft (PAMELA)", oriented to study the dismantling and recycling of a 24-year-old A300B4 aircraft. This project was mainly focused on the improvement of the dismantling operations with the objective to increase the amount of recovered materials where purity was not the main goal. The Airbus project concluded that around 85% (in weight) of the aircraft under study can be either reused (15%) or recycled (70%); where Al components from the 2XXX and 7XXX series accounted for the highest recycling rate [1.8].

Figure 1-1.A view of grounded aircraft at the Mojave boneyard and the subsequent dismantling process [1.9].

Boeing on the other hand, launched a similar initiative than Airbus. However, they were oriented on developing safe and sustainable management of EOL aircraft and components. The result was the creation of a voluntary association known today as the *"Aircraft Fleet Recycling Association (AFRA)"*, founded with the participation of another 10 members [1.6]. In the words of Derk-Jan van Herden, president of the association, has reported that the aviation sector is currently successful in reusing parts and components of aircraft that reach the EOL. As a matter of fact, they have estimated that around 40 % to 50 % of the dismantled aircraft weight is returned to the supply chain, where engines account for the highest weight. The remaining fuselage is separated by metal type, crushed, and sent to the proper recycling channel [1.3].

Later, in 2008 the European commission launched one of the most ambitious public-private aeronautical research program called Clean Sky. The aim of Clean Sky was to accelerate the

development and market introduction of new green technologies for the aviation industry [1.10]. From this research program, the project *"Aircraft Metal Recycling (AIMERE)"* was undertaken. This project was focused on the improvement of the dismantling and materials recovery operations, and on the determination of the current recycling routes of EOL aircraft materials to find new ideas for high-value added industrial applications. The project concludes that they were able to improve the dismantling process being able to increase the materials recovery. Additionally, it also concludes that the Al alloys that are present in aircraft can be used in the automotive and construction industries and in bicycle frames. However, it does not report any Al recycling process able to obtain high-value alloys from dissembled aircraft.

From these previous aircraft recycling initiatives, PAMELA, AFRA, and AIMERE, the dismantling techniques have been improved significantly considering the old practices. Nevertheless, there is still a lack of published literature regarding to the recycling process of the remaining aircraft fuselage rich on Al, which represents approximately 80 % of the total aircraft weight [1.11]. Recycling the remaining Al from EOL aircraft into high-value alloys, represents the major challenge to both the Al and aerospace industries. It has the potential to save approximately 95 % of the embodied energy cost and emissions of GHG compared to the production of Al from bauxite [1.12]; and also the possibility to promote a closed-loop recycling process avoiding the downgrading of the alloys and closing the aircraft life cycle.

Recycling Al cans and aircraft are not exactly the same thing. Aircraft are composed of a mixture of complex engineered alloys that contains Cu and Zn as main alloying elements. Additionally, these alloys are usually covered by an organic/inorganic coating system, which contains hexavalent chromium that provides the Al substrates corrosion protection and esthetics [1.13]. Hence, the main problems associated to the recycling of EOL aircraft are first, the safe removal of the corrosion protection coating. This coating is responsible for increasing the amount of metal lost by oxidation, gaseous emissions, and salt flux disposal once Al is recycled [1.14]. The second main problem is the presence of high amount of alloying elements, such as Cu and Zn, which cannot be removed by traditional methods. The high concentration of these elements in the Al scrap, limits the production of high-value recycled alloys downgrading the alloys by a cascade recycling process. For instance, no commercial wrought alloys can be obtained if Cu concentration is above to 2.6 % wt to produce 7XXX Al alloys, or if Zn concentration is above 0.5 % wt to

produce 2XXX series Al alloys [1.15]. Thus, a casting alloy must be produced. Finally, in addition to the presence of the organic/inorganic coating and the high amount of alloying elements, the pickup of detrimental impurities such as Fe and Si during handling the EOL aircraft fuselage represents a third significant problem associated with aircraft recycling [1.16]. The presence of these impurities is detrimental to the mechanical performance of the alloys due to the formation of intermetallic compounds which decreases the fracture toughness of the recycled alloy [1.17].

The Consortium for Research and Innovation in Aerospace in Quebec (CRIAQ), a non-profit organization established in 2002 by the financial support of the Quebec government, initiated in 2011 a research program in collaboration with the aerospace, Al, and recycling industry and Quebec universities denominated *"Process for Advanced Management and Technologies of Aircraft End-of Life (CRIAQ-ENV412)"* [1.18]. The overall objective was to develop general methods and test them on an experimental platform to dispose of and/or implement recycling processes and dedicated infrastructure for EOL aircraft and helicopters.

In the frame of the CRIAQ-ENV412 program, the general objective of the research presented in this thesis is to study the recycling of aerospace Al components from a Bombardier CRJ-100ER (Shown in Figure 1-2), able to produce high-value added alloys giving particular attention to the three main problematics of Al aircraft recycling. Thus, in order to achieve this goal a comprehensive literature review pertaining to the Al recycling process, specifically that of decoating, alloy blending, and metal refining with particular attention on fractional crystallization, are presented in **chapter 2**. The fundamentals of Al recycling and critical processing parameters have been understood this way. **Chapter 3** presents the general and particular objectives of this research project. The results regarding to the removal of the aircraft corrosion protection coating are shown in **chapters 4 and 5**. Additionally, the results corresponding to the theoretical refining efficiency of fractional crystallization are elucidated in **chapter 6**. In order to evaluate the potential chemical composition obtained from blending different alloys from the aircraft under study, mass balance calculations of the aircraft alloys were carried and the results are presented in **appendix A**. Finally, the summary and future work, conclusions, and the contribution to the knowledge are depicted in **chapters 7, 8, and 9** respectively.

Figure 1-2. Frontal section of a CRJ-100ER aircraft donated by Bombardier for the development of the present project.

In summary, it has been shown that in order to increase the value of recycled Al components from aircraft at the EOL by a closed-loop recycling process, it is necessary to overcome the problematics associated to the impurities present in the Al aircraft scrap. By understanding the effect of the processing parameters in the recycling process, the recycled Al quality can be potentially improved. In this work, the recycling of aircraft Al components is studied making emphasis in the production of high-value added alloys in a closed-loop recycling process.

References

[1.1] United Nations. Goal 13: Take urgent action to combat climate change and its impacts. 2015 2016]; Available from: http://www.un.org/sustainabledevelopment/climate-change-2/.

[1.2] United Nations. A/RES/70/1 Transforming our world: The 2030 agenda for sustainable development. 2015, UN. p. 41.

[1.3] ICAO, E-Gap Seminar showcases power of partnerships, in ICAO Journal. 2015, ICAO Communications Unit: Montreal, CA. p. 14-17.

[1.4] Fosberg, D., Aircraft retirement trends and outlook. Economic life analysis reprised and expanded., AVOLON, Editor. 2012.

[1.5] Feldhusen, J., J. Pollmanns, and J. Heller, End of Life Strategies in the Aviation Industry, in Glocalized Solutions for Sustainability in Manufacturing, J. Hesselbach and C. Herrmann, Editors. 2011, Springer Berlin Heidelberg. p. 459-464.

[1.6] AFRA. Aircraft Fleet Recycling Association. 2014; Available from: http://www.afraassociation.org/.

[1.7] AFRA. Aircraft Fleet Recycling Association.: Aircraft Retirement Tsunami. A 1000 Aircraft a Year to leave Service by 2023. 2014; Available from: http://www.afraassociation.org/news.cfm?newsid=162.

[1.8] Airbus, S.A.S. Eco-efficiency and Sustainability -G9- Issue 1. Process for Advanced Management of End of Life of Aircraft Available from: http://ec.europa.eu/environment/life/project/Projects/index.cfm?fuseaction=home.showFile&rep=file&fil=ACADEMY_PAMELA.pdf.

[1.9] Mojave air and space port. Aircraft boneyard. 2016; Available from: http://www.mojaveairport.com/.

[1.10] European Commision. Final report Summary - AIMERE (Aircraft Metal Recycling). Project 323402-FP7-JTI, E. Commision, Editor. 2014.

[1.11] W.D. Menzie, J.J.B., D.I. Bleiwas, E.L. Bray, T.G. Goonan, M. Grecia The Global Flow of Aluminum From 2006 Through 2025: U.S. Geological Survey Open-File Report 2010–1256, 73 p., available at http://pubs.usgs.gov/of/2010/1256/. 2010.

[1.12] Green, J.A.S., Aluminum Recycling and Processing for Energy Conservation and Sustainability. 1-271, ASM International, 2007.

[1.13] Chattopadhyay, A.K., Zentner, M.R., 1990.

[1.14] Schlesinger, M.E., Aluminum recycling. CRC/Taylor & Francis, Boca Raton, FL, 2007.

[1.15] The Aluminum Association. International Alloy Designations and Chemical Compositions for Wrought Aluminum and Wrought Aluminum Alloys. 2009, The Aluminum Association: Arlington, VA.

[1.16] Das, S.K., J. G., Light metals., 2007: p. 1161-1166.

[1.17] Staley, J.T., Microstructure and Toughness of High-Strength Aluminum Alloys, ASTM STP 605, in Properties Related to Fracture Toughness. 1976, American Society for Testing and Materials: Montreal, CA. p. 71-103.

[1.18] Consortium for Research and Innovation in Aerospace in Quebec (CRIAQ). 2016; Available from: http://www.criaq.aero/.

2: Literature Review

2.1: Aluminum Recycling

In most extraction and process industries, recycling, resource recovery, waste management, and environmental conservation have been among the major concerns in the last half-century. It began with the environmental pollution consciousness caused by the generation of waste during industrial processes and at the product's end of service life [2.1]. Al is one of the most used metals in the world after steel [2.2], and the unique combination of its physical properties results in its use in a variety of applications in the construction, packing, and transport sectors [2.3].

The main natural Al -producing ore is Bauxite, a mineral that consists primarily of hydrated Al oxides [2.4]. Al is recovered from bauxite by the Bayer process [2.5], a leaching process that selectively dissolves the Al from the ore using sodium hydroxide in a high temperature solution leaving the impurities behind. The leached solution is cooled down and seeded with aluminum hydroxide crystals to promote the growth of these crystals. Further heating and drying of the aluminum hydroxide crystals produces alumina, which is then electrolytically reduced by the Hall-Hèroult electrolytic process to produce pure Al [2.6]. However, obtaining primary Al from bauxite ore is one of the most energy-intensive and GHG emitting processes on a per weight basis, consuming around 45.21 kWh/kg tf [1] of Al and emitting approximately 12kg of CO_2/kg of Al produced [2.7, 2.8].

In recent decades, an increasing fraction of the Al supply has come from a different ore source as shown in Figure 2-1 [2.9]. This ore source is *"Al scrap",* which is mainly recovered from industrial wastes and EOL products. The processing of this source to produce new Al and aluminum alloys is known as *"recycling"* and the products obtained by this process are termed *"secondary"* [2.10]. Thus, by definition, the Al produced from scrap is denominated "*secondary Al*".

[1] The "tf" superscript (tactic-feedstock energy) is a measure of energy that includes the energy used to produce and transmit the energy consumed within a facility and raw material feedstock energy.

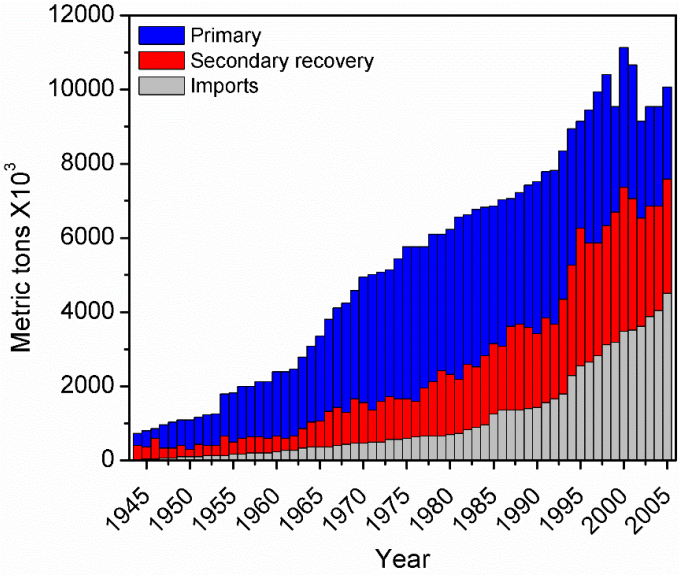

Figure 2-1. U.S. aluminum supply [2.8]

Nowadays, the best Al recycling practices are found in the automotive and beverage can industries, which account for the highest recycling rates of Al in the world [2.11]. Derived from these good practices, the general recycling process to obtain secondary Al from scrap is schematized in Figure 2-2. This process is divided in two main important steps: scrap pre-treatment and scrap refining. The scrap pre-treatment operations include sorting, shredding, and cleaning scrap prior to smelting and refining. These steps are carried out to reduce the amount of impurities present in the Al scrap such as wood, plastics, oils, organic coatings, and other non- Al metals. The mitigation of impurities minimizes the Al loss within the furnace, the emissions of hazardous pollutants, and the dilution with primary Al. After the Al scrap is pre-treated, it is sent to the scrap refining process which includes operations for re-melting, fluxing, degassing, alloying, skimming, and pouring. These operations are aimed to eliminate or reduce the remaining impurities that were not removed in the pre-treatment step [2.12].

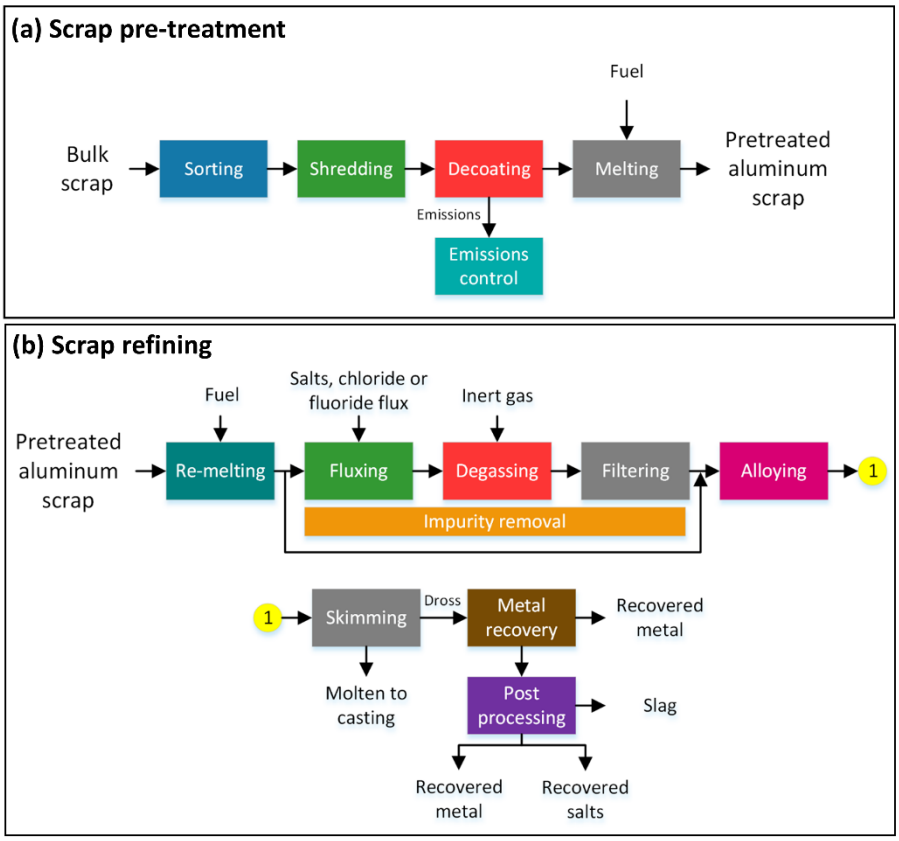

Figure 2-2. General flowchart of the aluminum recycling process showing both the (a) scrap pre-treatment, and (b) scrap refining steps [2.12].

The recycling process of aircraft Al components cannot be considered similar to the automotive and beverage can recycling. It differs in the complexity of the scrap stream and the difficulty to remove impurities by conventional methods such as fluxing, degassing, or filtering [2.13]. For instance, Al aircraft components contain high temperature resistant coatings with hexavalent chromium compounds for corrosion protection which do not exist in beverage cans or automotive parts. Additionally, aircraft scrap is also rich in certain alloying elements such as Cu and Zn from the 2XXX and 7XXX series respectively. Finally, the pick-up of detrimental impurities like Fe and Si during handling of the EOL fuselage diminishes the opportunity to obtain a closed-loop recycling process. In the following sections, the processes of sorting and blending, decoating, and refining that are used in the general Al recycling industry will be briefly described.

2.2: Aluminum Scrap Sorting

Usually Al scrap comes from different sources in a wide variety of sizes and is commonly contaminated with non- Al materials. The first step in the general recycling process is scrap sorting. This process is sometimes carried out before and/or after shredding by different techniques in order to separate the Al scrap from non- Al components. One of these techniques is called air classification. This technique, illustrated in Figure 2-3a, employs the injection of air to separate light-weight materials such as wood, paper, plastic, rubber, foam, etc., from the scrap stream. As a result, the heavy material, usually a mostly metallic scrap stream, is collected in the section contrary to the air flow while the light fraction is collected in the direction of the air flow to be further disposed [2.10].

Another sorting technique used in the Al recycling industry is magnetic separation schematized in Figure 2-3b. By this technique Al is separated from the magnetic ferrous components present in the scrap stream. It consists on a conveyor that is used to transport the bulk scrap and a magnetic drum or overhead-belt that is employed to collect the magnetic materials and separate them from the bulk scrap [2.10].

After the Al scrap has been passed through air and magnetic separators, it may contain other non-ferrous materials in addition to Al such as Zn, Sn, Pb, etc., or non-magnetic ferrous materials such as austenitic stainless steel. Hence a third process called eddy current separation, illustrated in Figure 2-3c, is carried out to further sort the scrap stream. In this technique, a rotor is covered with magnets with alternating polarities. The primary magnetic field generated by the rotating magnets causes an electric current to flow in a conductive particle which is known as eddy current. Hence, the field repels the nonmagnetic electrically conductive metals resulting in their expulsion from the scrap stream. The most significant factor to determine if a material will be ejected from the scrap stream is the ratio of the electrical conductivity and density of the material. For instance, Al has high conductivity and low density giving a ratio of 14 ($m^2/\Omega kg \cdot 10^3$) compared to stainless steel which also has high conductivity but higher density giving a ratio of 0.18 ($m^2/\Omega kg \cdot 10^3$). This means that Al will be ejected from the bulk of scrap with more ease than austenitic stainless steel, thus permitting its separation [2.10].

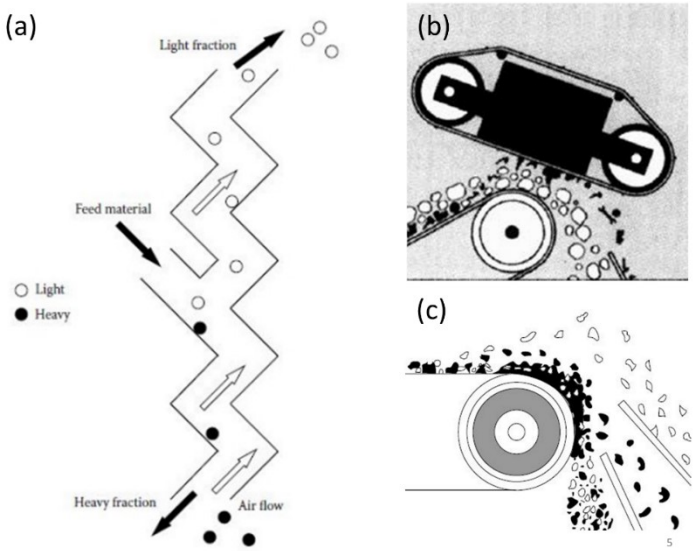

Figure 2-3. Different physical sorting techniques employed in the aluminum recycling industry: (a) a zig zag air separator, (b) an overhead-belt magnetic separators, and (c) a conveyor-type eddy current separator [2.10].

In addition to eddy current, the separation of non-ferrous materials can also be performed by heavy media separation and by color sorting. The heavy media technique uses a fluid with a known density usually between that of Al and the contaminant to separate. Hence, the materials with lower density than Al will float, while the denser materials will sink. On the other hand, color sorting which can be carried out by hand or automatically takes advantage of the color difference between scraps to sort Zn, Cu, brass, and stainless steel from Al.

Once the scrap stream has been separated from non- Al components, the remaining Al scrap can be sorted into wrought and cast alloys to increase the scrap quality. Nevertheless, due to the difficulty of distinguishing between cast and wrought alloys, the separation of Al alloy families is usually avoided resulting in the production of cast alloys, in particular A380, which has greater tolerance to impurities than wrought alloys.

In particular, in the recycling of aircraft Al alloys, the majority of the Al aircraft scrap is pre-sorted during the aircraft dismantling. Through this operation, most of the non- Al components such as the engines, the landing gear, the electronics, and the interiors are removed from the aircraft. Following dismantling, a partially empty air frame is left which is mainly composed of wrought

Al alloys from the 2XXX and 7XXX series. The typical aerospace alloy compositions are depicted in Table 2-1 [2.14]. The remaining non- Al components attached to the fuselage can then be removed by the previously mentioned sorting techniques. Nevertheless, in order to avoid the downgrading of the aircraft scrap and the production of cast alloys, the aircraft fuselage has to be either (a) sorted by alloy type or (b) wisely disassembled and blended to match the chemical composition of an existing high-value wrought alloy. Attempts to achieve the first goal will be described in this section while the work done regarding the second goal will be described in the following section.

Table 2-1. Chemical composition of typical Al alloys found in old aircraft [2.15].

Alloy	Chemical composition (wt %)								
	Cu	Mg	Mn	Cr	Fe	Si	Zn	Ti	Al
2014	3.9-5	0.2-0.8	0.4-1.2	0.1 max	0.7 max	0.5-1.2	0.25 max	0.15 max	Balance
2214	3.9-5	0.2-0.8	0.4-1.2	0.1 max	0.3 max	0.5-1.2	0.25 max	0.15 max	
2024	3.8-4.9	1.2-1.8	0.3-0.9	0.10 max	0.5 max	0.5 max	0.24 max	0.15 max	
2324	3.8-4.4	1.2-1.6	0.3-0.9	0.1 max	0.12 max	0.1 max	0.25 max	0.15 max	
7050	2-2.6	1.9-2.6	0.1 max	0.04 max	0.15 max	0.12 max	5.7-6.7	0.06 max	
7075	1.2-2.0	2.1-2.9	0.3 max	0.18-0.28	0.5 max	0.4 max	5.1-6.1	0.2 max	
7475	1.2-1.9	1.9-2.6	0.06 max	0.18-0.25	0.12 max	01 max	5.2-6.2	0.06 max	
7178	1.6-2.4	2.4-3.1	03 max	0.18-0.28	0.5 max	0.4 max	6.3-7.3	0.2 max	
7150	1.9-2.5	2-2.7	0.1 max	0.04 max	0.15 max	0.12 max	5.9-6.9	0.06 max	

The former research efforts oriented to separate the Al scrap by specific alloys were motivated by the incapability of the secondary Al industry to produce wrought Al products. Montagna and Makar [2.16] developed a technique called “hot-crush” to separate wrought and cast Al alloys from a scrap stream containing a mixture of both alloy classes. This technique relies on the difference in the thermo-mechanical behavior among cast and wrought alloys. The scrap stream is heated to a temperature ranging between 550 – 580 °C where the cast alloys suffer a loss of ductility denominated hot-shortness. After a determined time within this temperature range, the scrap mixture is transferred to an impact device and hot crushed. The hot crushing of the alloys will cause the cast alloys to fragmentize into small pieces while the wrought products are only flattened. Hence after crushing and further sieving, cast alloys are effectively separated from the wrought alloys. This separation method has been tested and validated to upgrade mixed Al scrap [2.17].

However, the process is only capable of distinguishing cast from wrought alloys, and not between alloy families of the same class. That is to say, the process cannot be applied to separate the wrought alloys from each other, which is indispensable in order to produce high-value alloys from aircraft scrap.

In recent years, the use of sensor-based techniques have become widely used for the identification and separation of materials due to the development of fast computerized digital processing techniques [2.18]. The working principle of these techniques is illustrated in Figure 2-4. First, (1) the scrap is sieved to obtain a homogeneous particle size distribution, then (2) it is isolated in a conveyor belt to be (3) further characterized piece by piece using a specific technique. (4) The material is then recognized and (5) electronically analyzed in order to obtain (6) a rejection or acceptance decision which actuates a (7) mechanical separation device. Finally, the scrap pieces are separated into (8) "rejected" or (9) "accepted" materials. This kind of sorter can be (10) remotely controlled by intra and internet connections.

Gaustad et al. [2.19], summarized the two main sensor-based techniques, i.e., X-ray fluorescence (XRF) and laser induced breakdown spectroscopy (LIBS), employed in the Al recycling industry to separate wrought alloys. The X-ray fluorescence technique uses X-ray radiation energy to eject electrons from the *K* orbital shell of determined elements present in the Al scrap. The electron vacancy created by the ejection of this electron is filled by an electron from the *L* orbital shell and at the same time it releases fluorescence energy which is captured and sensed by the XRF device. Each element has its unique characteristic fluorescence spectrum. Hence, the emitted fluorescent X-rays are directly linked to specific elements present in the Al scrap [2.20]. The main drawback of this technique is that the scrap surface has to be free of paint to obtain an accurate analysis. As a consequence, in the aircraft recycling process this technique is mainly used to pre-sort the different metals present in the air frame prior to shredding, where the sample preparation is performed manually.

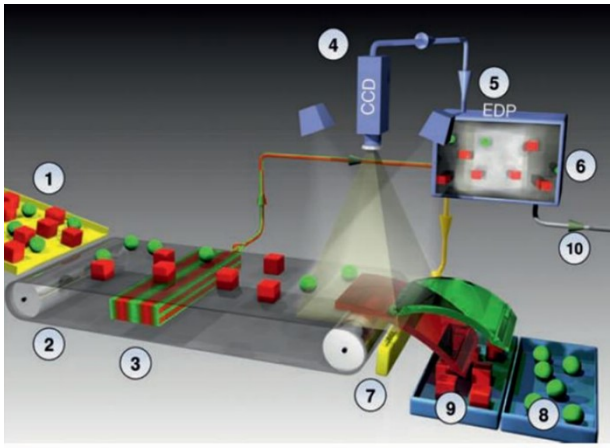

Figure 2-4. General working principle of a belt-type sensor-based sorting technique [2.18].

The highest degree of metal separation that can be currently achieved is carried out using the laser induced breakdown spectroscopy (LIBS) technique first developed by Los Alamos National Laboratory [2.19], and commissioned by Huron Valley Steel Corp for industrial scrap sorting purposes [2.10]. This technique make use of a pulsed laser as energy source to create a light emission plasma after hitting the Al scrap. The photons emitted by the plasma are measured by an optical emission spectrometer to quantify the elements present in the alloys. As a result, the Al scrap can be sorted by wrought alloys. As in the case of the XRF technique, the main disadvantage of LIBS is that the sample surface has to be free of coatings. Nevertheless, through the use of pulsed lasers the paint can be removed in one laser shot while the measurement can be carried out at the second shot, increasing the attractiveness of this process for use in aircraft recycling.

2.3: Aluminum Scrap Blending

The difficulty in producing high-value alloys from aircraft Al scrap coming from end-of-life vehicles has been previously stated. The challenge lies in the achievement of a tightly controlled chemical composition of high strength aerospace alloys with the minimum addition of primary Al and alloying elements. Technically, the problem is attributed to the lack of technology present for removing the concentration of critical alloying elements and impurities even though technological

progress has provided some sophisticated scrap sorting techniques. Unfortunately, these sorting techniques have not yet been applied to sort mixtures of shredded aircraft Al scrap [2.21].

A potential technical solution to the difficulty of producing high-value alloys from aircraft scrap is to avoid incorrect melt composition, ensuring the chemical composition of the batch in the disassembly process. Hussain and Soon [2.22] as well as Hussain and Hakim [2.23] employed a mass balance approach to formulate A360.0, A380.0, and A413.0 cast alloys from different Al scrap sources such as soft drink cans, Al engine components, and computer disks. In these studies, the authors used the X-ray fluorescence technique to individually determine the chemical composition of the scrap. Then, after a mass balance calculation and a precise combination of different scrap percentages, the determined cast alloys were successfully produced with a minimum dilution of primary Al.

With automotive recycling in mind, Das et al. [2.24], emphasized the importance of adopting disassembly and pre-sorting techniques to optimize the recycling of wrought and cast alloys. In the aircraft recycling field, this approach might be reasonable if the production of high-value alloys is desired. A “smart disassembly” of the Al air frame can provide a commingled scrap able to fit in a specific commercial wrought alloy classification with minimal dilution [2.13]. Hence, a mass balance approach prior to aircraft dismantling and shredding can be adequate for the production of high-value alloys from aircraft Al scrap.

To the best of our knowledge, Das et al. [2.13] were the pioneers in addressing the concept of “aircraft smart dismantling”. The authors proposed to dismantle the aircraft into specific sections where the components are made of similar alloys of the same series. Conceptually, they studied the potential aircraft scrap composition that could be obtained if sorting of the 2XXX and 7XXX series alloys is carried out or not. The results of their analysis are summarized in Table 2-2. The authors stated that if the scrap generated by a pre-sorted aircraft is similar to that predicted in Table 2-2, the scrap might be suitable to produce a 2024 or 7075 alloy. Nevertheless, the properties of these recycled alloys must be deeply analyzed to determine the possible applications. On the other hand, if the aircraft is not pre-sorted and a commingled aircraft scrap is obtained, the resulting composition is not suitable for any commercial alloy.

From the previous studies it can be concluded that wrought alloys either from the 2XXX or 7XXX series could be obtained by carrying out an intelligent aircraft dismantling. However, the area of opportunity for producing high-value alloys from aircraft scrap is to determine the accurate distribution and weight fraction of the alloys present in the aircraft. With knowledge of the aircraft alloy distribution and weight fractions, accurate mass balances can be obtained. The resulting information can be used as a factor to determine the dismantling criteria.

Table 2-2. Potential composition of aircraft Al scrap assuming either pre-sorting and no pre-sorting of 2XXX and 7XXX series alloys [2.13].

Alloy	Chemical composition (wt %)						
	Cu	Mg	Mn	Fe	Si	Zn	Al
Pre-sorted 2XXX	4.4	1.0	0.7	0.5	0.5	0.1	~ 93
Pre-sorted 7XXX	2.0	2.5	0.2	0.4	0.2	6.0	~ 90
Not pre-sorted R2 + R7XXX	3.0	1.8	0.4	0.4	0.4	3.0	~ 92

2.4: Scrap Decoating

Some of the main impurities found in Al scrap are the organic or organic/inorganic coatings which provide the Al substrates with corrosion protection and added aesthetics. If these impurities are not removed prior to recycling, environmental and economic problems might be encountered. For instance, the organic coating would burn upon being charged to the melting furnace releasing smoke and soot to the atmosphere, creating at the same time a health hazard in the workplace. Additionally, burning the coating at the melting conditions promotes the oxidation of the metal thus decreasing the metal yield [2.10]. This effect was observed by McAvoy et al. [2.25], and is summarized in Figure 2-5. They concluded that painted or lacquered scrap oxidizes more readily than bare scrap regardless of the alloy type. Moreover, they found that melting under a salt flux helps to reduce melt loss at the expense of increasing the salt flux disposal. Thus, a scrap pre-treatment oriented towards removing the organic coatings from the metal substrates prior to metal refining is imperative in the Al recycling process.

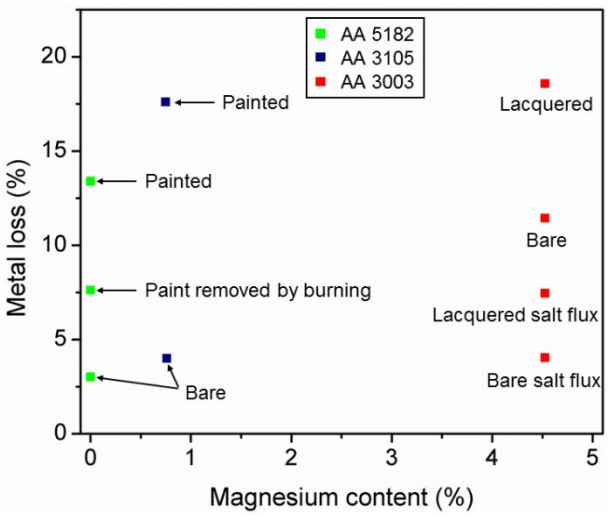

Figure 2-5. Effect of alloy type and coating on melt loss in fluxed and flux-free re-melting [2.3]

Specifically, in the aerospace industry, a three-layered coating system as the one schematized in Figure 2-6 is used for corrosion protection and aesthetics in aircraft Al alloys [2.26]. This coating system is mainly made up of a chromate conversion coating, a primer, and a topcoat. The chromate conversion coating is made of an amorphous layer of a mixed hydrated Cr(III)/Cr(VI) oxide with a ratio of about 3:1 [2.27, 2.28]. Additionally, the primer layer consists of an epoxy-polyamide matrix containing mainly chromate pigments such as barium chromate ($BaCrO_4$) or strontium chromate ($SrCrO_4$) to inhibit corrosion of the Al substrate [2.29]. Finally, the topcoat is a polyurethane layer with embedded inorganic pigments to proportionate coating color and protection against environmental erosion and mechanical abrasion [2.30]. At the aircraft end of life, these coatings remain in the 65 % to 75 % of the metallic fuselage that is sent to graveyards representing an important impurity that needs to be removed prior to the valorisation of the aircraft Al [2.9].

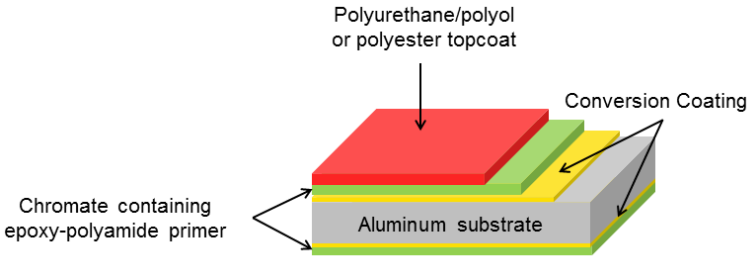

Figure 2-6. General aircraft corrosion protection system [2.26]

Different techniques have been developed to remove paints from metallic structures. In Table 2-3, the advantages and disadvantages of these techniques are presented and classified according to their main removal mechanism such as mechanical, physical, thermochemical, and chemical. Most of the listed techniques are employed only for maintenance purposes in the aerospace industry. In fact, pyrolytic stripping is the only technique that is not used for maintenance purposes though it has been used to remove organic materials from Al substrates in the Al recycling industry [2.10].

The inorganic compounds present in the aircraft coatings are characterized to be highly toxic, since they contain Cr(VI) particles [2.31]. Thus, during decoating, it is important to mitigate the emission of these particles to the atmosphere. The emission reduction of these particles can be achieved by the most widely used stripping method, chemical stripping. This method has the advantage of keeping hazardous wastes in a damp state where the risk of emitting Cr(VI) particles to the atmosphere can be decreased [2.32]. In the scope of this project, pyrolytic and chemical stripping were selected as decoating methods due to their broad use in the Al recycling industry and the capability of retaining toxic particles in liquid solution respectively. In the following two sections, these techniques will be discussed.

Table 2-3. Advantages and disadvantages of different paint removal techniques.

Category	Techniques	Advantages	Disadvantages	Ref.
Mechanical	• Plastic media blasting (PMB) • Starch media blasting • Cryogenic-mechanical	• Cheap • Free of toxic solvents	• Dust generation • Release toxic materials • Small area • Time consuming • Surface damage • Worker safety	[2.33-2.35]
	• Dry ice stripping	• No waste from blasting media • Free of toxic solvents	• Dust generation • Release toxic materials • Worker safety	
	• High-pressure water jet blasting	• Free of toxic solvents	• Control and reliability • Small area • Time consuming • Surface damage • Worker safety	
Physical	• Laser stripping • Xenon flash lamp stripping	• Free of toxic solvents • Combustion suppression • Coating selectivity	• Expensive • Small area • Toxicity of breakdown products	[2.36-2.39]
	• Thermal stripping • Hot fluidized-Bed	• Free of toxic solvents • Combustion gases burned in melting process • High volume • Widely used for metal recycling • Removes most of coatings	• Substrate oxidation • Release of toxic particle matter • Release of VOC's if process is not controlled • High capital investment	[2.10, 2.40, 2.41]
Thermochemical	• Molten salt bath	• Fast process • No secondary cleaning required • Inorganic materials retained in sludge • Effective in most coatings • Not geometry dependant	• Generation of hazardous waste • Expensive • Release high amount of CO_2 in batch processes	[2.42, 2.43]
Chemical	• Cold strippers • Hot strippers	• Keeps hazardous wastes in a damp state • Effective in most coatings • Not geometry dependant • Low investment cost • Works in any substrate shape	• Health hazards • Slow process • Substrate damage	[2.32, 2.41]

2.4.1: Thermal Decoating

Research on thermal decoating was driven by the growing demand of Al beverage cans and the need to efficiently remove their coating prior to recycling in order to increase the Al yield. Generally, the thermal decoating process consists of the application of heat to promote the volatilization, pyrolysis, and oxidation of organic coatings attached to Al substrates [2.44]. Different technological developments concerning the processes to remove organic materials attached to metallic substrates have been reported in the literature. One such technology, shown in Figure 2-7, was developed by ALCOA three decades ago [2.45]. The process consisted of the controlled feeding of coated Al scrap into the surface of a molten metal stream. During the process, the scrap was allowed to float over the molten stream for a sufficient time permitting the pyrolysis of the organic materials by heat conduction from the molten bath. Then, after the organic material was removed from the Al, the scrap was mechanically immersed into the molten metal pool.

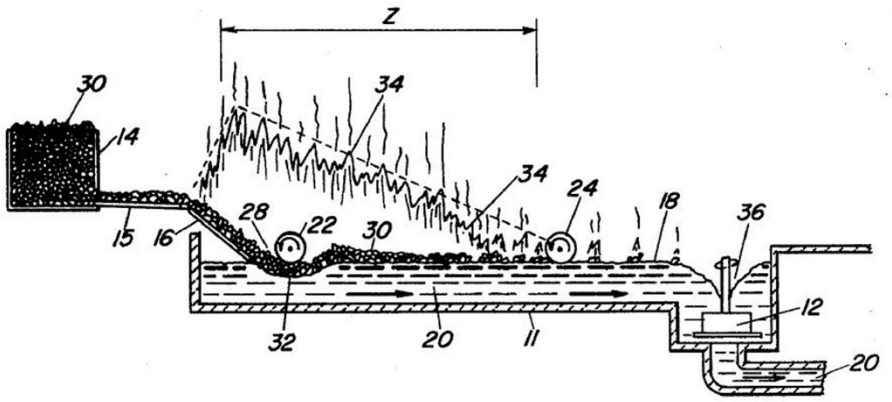

Figure 2-7. Floating-scrap thermal decoating process developed by ALCOA[2]. [2.45]

Since the previous decoating process is done in the same melting furnace, the main disadvantages are the increase of skim and the introduction of inorganic particles from the coated scrap to the molten Al stream. In order to improve the thermal removal of organic materials from Al scrap, the Al recycling industry developed more efficient processes in terms of waste management and

[2] The number details of the figure can be found in the corresponding reference number.

energy conservation. In this sense, at least three types of furnaces have been reported in the literature categorized according to the furnace arrangement: rotary-kiln [42.6, 2.47], belt-type [2.48, 2.49], and fluidized-bed [2.50-2.52]. The first type of furnace arrangement, schematized in Figure 2-8, consists of an inclined rotating drum equipped with longitudinal bars to lift and agitate the scrap during the heating process. The coated scrap in these kinds of furnaces is fed at the highest end of the rotating drum while the hot gas responsible for the coating pyrolysis is injected either in a counter-current or co-current.

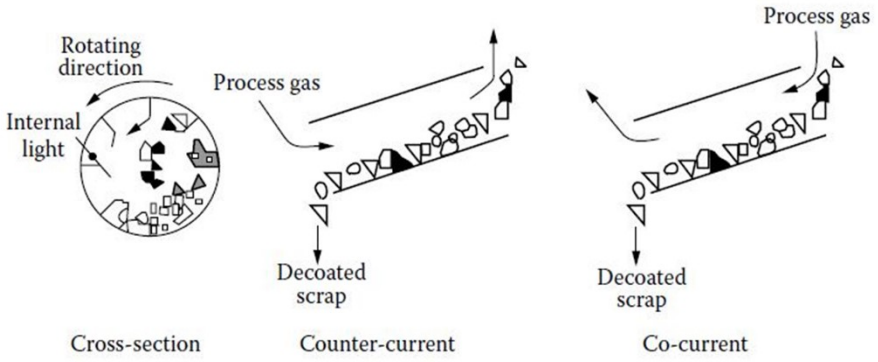

Figure 2-8. Typical rotary-kiln type decoating furnace [2.10]

The belt-type thermal decoating furnace is illustrated in its basic form in Figure 2-9. The scrap in these kind of furnaces is packed in a bed of about 4 to 40 cm thick and transported through a pyrolysis zone using a gas-permeable conveyor which can be vibrated to promote homogeneous heating. In the pyrolysis zone, an oxygen-containing hot gas is passed downwardly through the moving scrap bed causing the scrap temperature to raise up to 500-600 °C. As a result, the organic materials attached to the scrap are thermally decomposed. Additionally, since the decomposition reaction is exothermic in nature, the exhaust gases can be recirculated into the process in order to optimize the energy consumption or they can be released to the atmosphere after a proper gas treatment [2.10, 2.49].

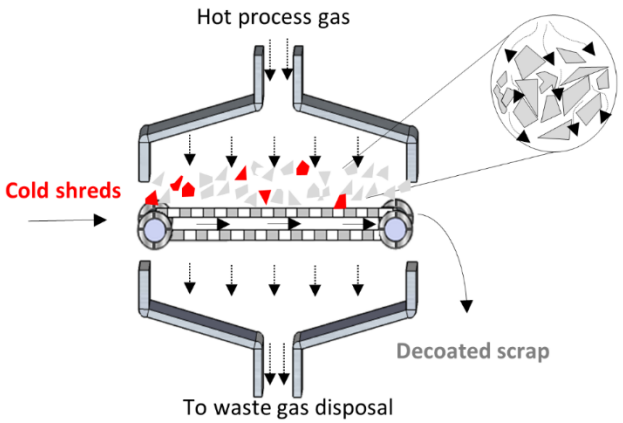

Figure 2-9. Basic design of a belt-type decoating furnace [2.10]

The third kind of thermal decoating furnaces are the denominated fluidized-bed type. An example of this type of furnace is that developed by ALCAN in the 90's and schematized in Figure 2-10 [2.52]. This process involves heating the coated scrap in a bed of inert solid particles such as sand, salts, alumina, or mixtures of these materials with diameters in the range of 20 to 2 mm, fluidized by an oxygen-containing hot gas injected from the bottom of the bed. During the process, the fluidized bed is maintained at a temperature of 400 – 650 °C depending on the melting point of the scrap and the contaminants present. The scrap is transported through the fluidized bed using a porous belt conveyor, forcing the metal to pass through the hot fluidized solid particles. The contact between the hot particles and the scrap improves the heat transfer in comparison with the belt-type furnace. After the scrap has been passed through the hot fluidized bed, it is transferred to a particle removal chamber. In this chamber, the Al scrap is cleaned from any fluidized bed particle remaining attached to the metal using a vibratory belt conveyor in combination with air jet cleaning and vacuum processing.

A special advantage of the fluidized bed treatment in addition to the improved heat transfer, is the ability to incorporate protective materials to the process such as fluoride compounds. These materials can be added either in a solid state or in gas form. If the protective material is added as a solid such as AlF_3, it generally forms part of the fluidized bed as a constituent in amounts of about 5 - 10 wt. % of the fluidized bed. On the other hand, if the protective material is added in gas form such as SF_6, it may be introduced to the system through the hot gas inlet in an amount of a few volume percent of the fluidizing gas ranging from 0.1 - 1.0 % by volume.

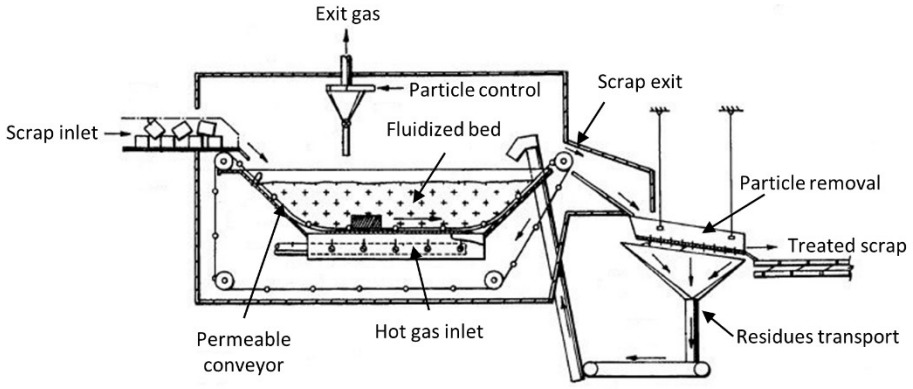

Figure 2-10. ALCAN Fluidized-bed decoating furnace [2.52]

Independently of the thermal decoating process employed to eliminate organic materials from Al scrap, four essential processing parameters (temperature, oxygen levels, residence time, and gas/metal contact) must be controlled to obtain optimum results [2.44]. The temperature has to be high enough to optimize residence time but low enough to avoid metal melting. The second process parameter is the oxygen level in the hot gas. This parameter is essential for the reduction of char to produce CO_2 gas. If there is not sufficient oxygen present at the pyrolysis step, partially decoated scrap can be obtained. Additionally, during the combustion of the char, oxygen is consumed. Hence, if the processing gas is recirculated, the oxygen content must be adjusted by a secondary injection of air. The third important processing parameter corresponds to the residence time of the scrap inside the furnace. This residence time depends on the organic material to be removed and it is controlled either by the inclination and rotation speed of a rotary-kiln type furnace or by the speed of the porous belt conveyor in the belt-type and fluidized-type furnaces. Finally, the gas/metal contact is the fourth important parameter to control during thermal decoating. Usually, a large surface area is necessary to maximize the gas/metal contact and hence minimize the heating rate and reaction time. The gas/metal contact is mainly controlled by the scrap presentation form and its flow inside the furnace. Ideally, the scrap should be present with a particle size ranging from 25 – 50 mm in a square morphology. These scrap conditions facilitate its transport through the furnace without bridging or sticking. An alternative method for improving the gas/metal contact is by controlling the conditions of scrap flow inside the furnace. In the rotary-kiln furnace, the scrap flow is controlled by the presence of longitudinal bars within the rotary drum. These bars

allow the scrap to be lifted thus mixing the scrap with the hot processing gas. In the belt-type furnaces, the gas/metal contact is usually improved by vibrating the conveyor belt.

In order to understand and optimize the decoating process, kinetic and thermal studies have been carried out on polyester coated Al substrates, as well as on used beverage cans, and painted Mg alloys in automotive objects [2.7-2.11]. Nevertheless, no fundamental studies have been found in the literature corresponding to the thermal decoating of aircraft Al scrap for recycling, which is currently a topic of interest in the aerospace industry.

2.4.2: Chemical Decoating

Aside from sanding, chemical paint stripping, defined as the use of chemicals to remove paint from a surface, is one of the oldest and most common and effective paint removal methods that exist nowadays [2.53]. In this process, the chemical paint stripping solution is applied to coated substrates either by brushing, spraying, or immersing. After a determined reaction time, the paint is lifted, and then cleaned with high pressure water to obtain a substrate free of organic coatings. According to the World Intellectual Property Organization, chemical paint stripping dates from the nineteenth century, where one of the first paint remover solutions containing a mixture of potash alum, burnt umber, wheat-flour, phenol, and water was patented by Frank P. Foster in 1888 [2.54]. However, it was not until the introduction of chlorinated compounds such as methylene chloride at the beginning of the twentieth century that this method became popular due to its effectiveness on a variety of paints [2.55, 2.56].

The ingredients of chemical strippers have been modified over time to fulfill the paint stripping requirements of new paints. Nevertheless, the main structure of the components have remained the same. According to Wollbrinck [2.57], the formulation of stripping solutions range in complexity from two-component to multicomponent systems that contain primary and co-solvents, activators, thickeners, surfactants, sequestering agents, corrosion inhibitors, and colorants which have different functions as those described in Table 2-4.

Chemical strippers are generally classified in hot and cold solutions. The hot stripping solutions are characterized to work at temperatures between 50 °C to 90 °C while cold strippers work at

room temperature. Additionally, the solutions can also be either alkaline or alkali-solvent based where the alkalinity is given by alkali-metal hydroxides, organic amines, or hydroxyl compounds. The main action of alkaline stripping solutions is the hydrolyzation of the paint binders to promote swelling and lifting of the organic coatings [2.41]. However, coatings such as epoxy, high solid coatings, and waterborne coatings, similar to those employed for aerospace applications, show a resistance to strippers composed primarily of alkali [2.58].

Table 2-4. Main components and activity of commercial stripping solutions [2.57]

Component	Primary functions
Primary solvent	• The most active ingredient • Penetrates and swells the organic coating
Co-solvents	• Incorporated at levels of 5 - 10 % • Helps to attack coatings resistant to primary solvents • At higher concentrations they serve as diluents and may lower the flashpoint of the composition
Activators	• Increase the penetration rate of the solvent into the organic coating
Thickeners	• Employed in thixotropic formulas to allow the paint to remain in place on vertical surfaces • Reduces evaporation • Prolongs the contact time of the solvent with the coating
Surfactants	• Assists solvents by wetting the surface of the paint • Increases the contact area between the solvent and the coating • Helps to clear the surface on washing
Sequestering agents	• Ties up the hard water salts in aqueous-based stripping solutions • Assists in the clearance of inorganic materials
Corrosion inhibitors	• Protects the metal substrates and the stripping baths from corrosion
Colorants	• Added for marketing purposes • Identifies the areas where the remover has been already applied

Methylene chloride-based stripping solutions have been the most effective formulations to remove aircraft paint systems [2.59]. Nevertheless, the high toxicity of methylene chloride lead it to be included in the list of hazardous air pollutants (HAP) by the US Environmental Protection Agency (EPA) in 1990, restricting its use in stripping formulations [2.60]. Due to such regulation, research was primarily devoted towards the understanding of the paint stripping mechanism to develop

alternative solutions as efficient as the methylene chloride based paint removers [2.59, 2.61-2.63]. The resulting research efforts, gave rise to a well-accepted chemical stripping mechanism schematized in Figure 2-11.

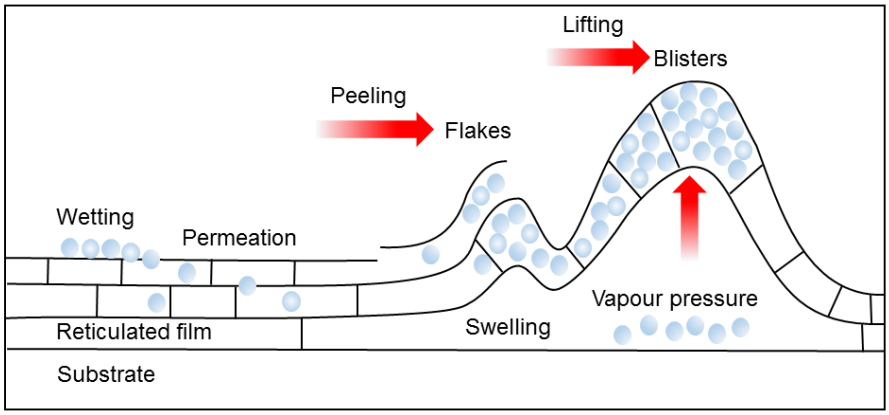

Figure 2-11. Chemical stripping mechanism of a cross-link polymer [2.61].

First, the stripping solution has to be attached to the coating surface by wetting. The degree of wetting depends on the cohesive forces between the liquid molecules and the adhesive forces between the liquid and the coating surface. If the adhesive forces are stronger than the cohesive forces, a high wettability is expected. In stripping solution formulations, wetting is controlled by the addition of surfactants to reduce the surface tension of the solution and/or by increasing the working temperature [2.57]. Once the stripping solution has wetted the coating surface, permeation of the solution through the paint takes place.

Permeation is the transport of matter through a membrane in response to an activity gradient. It is described by Equation 2-1, where P represents the permeability coefficient defined as the product of the diffusion constant D and the equilibrium solubility coefficient K, Δc is the concentration gradient between the external and the internal section of the coating, and h corresponds to the coating thickness [2.64, 2.65].

$$J = \frac{P * \Delta c}{\mathrm{h}} \qquad \text{Equation 2-1}$$

It can be seen from this equation that permeation strongly depends on the solubility between the primary solvent in the stripping solution and the coating. The solubility is usually evaluated in terms of Hansen solubility parameters (HSP), proposed by Hansen in his PhD studies in 1967 [2.66]. These parameters are based in the assumption that the total energy of vaporization, E, i.e., the total cohesive energy that holds a liquid together, is the sum of the three individual energy contributions: (1) dispersion E_d, (2) permanent dipole-permanent dipole E_p, and (3) hydrogen-bonding forces E_h. Dividing each contribution by the molar volume of a solvent, and using the definition of the Hildebrand solubility parameter, $\delta = (E/V)^{1/2}$, the square of the total (or Hildebrand) solubility parameter is obtained as the sum of the squares of the Hansen d, p, and h components as shown in Equation 2-2 [2.67].

$$\delta^2 = \delta_d^2 + \delta_p^2 + \delta_h^2 \qquad \text{Equation 2-2}$$

Materials with similar HSPs will present higher affinity compared with those materials where the HSPs are not similar. Hence, if the HSPs between the primary solvent and the coating are similar, the mass transport by permeation will be enhanced thus promoting swelling of the coating [2.65].

After the polymer coating has swollen by the active solvent in stripping formulations, high shearing stresses along the interface between the polymeric coating and the dimensionally stable substrate are produced. These stresses lead to wrinkling of the film followed by the rupture of the adhesive linkages between the coating and the substrate giving rise to removal of the paint [2.68-2.70]. Additionally, the solvent vapour pressure or any reaction occurring between the stripping solution and the substrate might enhance the lifting of the coating [2.69].

Chemical stripping solutions in the aerospace industry have been mainly designed to remove the paint from the external section of the fuselage since the internal coating facing the aircraft cabin is not usually removed and remains intact during the entire aircraft life. Nevertheless, it has been observed by Ebenezer and Graham [2.71] that the primer coating usually located in both, the external and internal sections, is difficult to remove using the most aggressive stripping solution, i.e., methylene chloride. Hence, research has to be done to evaluate the performance of newer solvents such as N-methyl-2-pyrrolidone (NMP) and dimethyl sulfoxide (DMSO), which have

been proposed to be possible replacements of methylene chloride [2.59, 2.61]. Such evaluation must be carried out with Al recycling applications in mind where the external and internal aircraft coatings must be removed.

2.5: Aluminum Refining

In order to fulfill the quality requirements of secondary Al, the removal of impurity elements and inclusions that are not otherwise removed by physical methods is carried out by aluminum refining. Secondary smelters usually employ methods such as fluxing, degassing, and filtering to remove the remaining impurities from Al scrap following the sequence shown in Figure 2-12. First, the molten metal is held in a melting furnace for a pre-determined time to carry out fluxing and sedimentation, followed by degassing and filtering to further cast the clean ingot. The objective of each technique will be briefly described in the following sections [2.72].

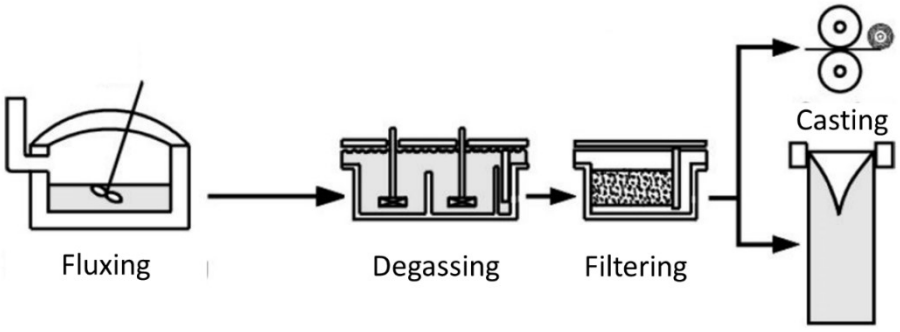

Figure 2-12.Sequence of the main refining processes practiced by secondary smelters [2.72]

2.5.1: Fluxing

Fluxing is a technique that is mainly used to reduce oxidation of the Al stream. However, it also helps to separate inclusions, remove hydrogen, and to promote certain elements to migrate into the dross, or top layer of the melt [2.19]. It is carried out by the addition of molten salt fluxes based

on equimolar mixtures of sodium and potassium chlorides [2.73, 2.74]. The addition of additives can be done to modify different properties such as fluidity, wettability, and reactivity [2.74].

Utigard et al. [2.74], calculated the standard Gibbs energy of formation of different elements exposed to reactive additives used in fluxes as shown in Figure 2-13. According to their results, the thermodynamic stability is higher for fluorides, followed by chlorides, oxides, and sulphides. The removal of metallic impurities will occur when the standard Gibbs energy of formation is lower than the formation of Al-flux compounds (for instance, lower than the energy of formation of $AlCl_3$ in the case of chlorinated fluxes, or lower than the energy of formation of AlF_3 in the case of fluorinated compounds). Thus, Li, Na, Ca, Mg, Ba, K and Sr, which are more stable than Al, can be removed by the addition of fluxes containing Cl_2, F_2, C_2Cl_6, or SF_6.

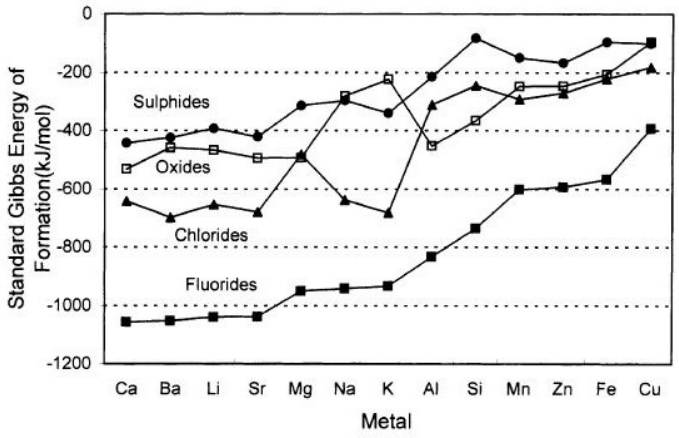

Figure 2-13. Standard Gibbs energies of formation of several sulfides, oxides, chlorides, and, fluorides obtained at 723°C per mole of S, O, Cl_2, and F_2 respectively [2.75].

Nakajima K. et al [2.76] also carried out a thermodynamic assessment to determine the removability of the main alloying elements from Al, either by transferring them into the slag or the gas phase. Their thermodynamic calculations predicted that only Mg and Zn can be removed from molten Al, Mg being distributed in the slag as oxide and Zn into the gas phase by the application of vacuum. The rest of the main alloying elements such as Cu, Mn, Fe, and Si remain as tramp elements in Al.

Combining the results of Utigard et al. [2.74] and Nakajima et al. [2.76], the element radar chart for the removal of alloying elements from Al is schematized in Figure 2-14. It is worth noting that Cu, one of the main alloying element present in the aircraft scrap, and the detrimental impurities Fe and Si, are thermodynamically impossible to remove. Nevertheless, the concentration of Zn can be decreased by reducing its gas partial pressure either using argon or vacuum, transferring Zn into the gas phase. Boeree C.R. [2.77] experimentally tested the removal of Zn by injecting argon at a flow rate 3.2 cm^3/s for 30 min to an Al melt held at 900 °C, obtaining a Zn removal efficiency of ~9%. Wei et al. [2.78], on the other hand, studied the Zn removal from Al by a non-conventional refining process called vacuum distillation. They reported that Zn in Al can be removed easily by this technique with a removal efficiency of 98%. However, in order to achieve such efficiency, high vacuum levels exceeding 10 Pa at 800 °C for a period of 30 min were required. As a consequence, the conditions for Zn removal and the lack of reduction of Cu, Fe, and Si concentrations from molten Al complicate the recycling of aerospace Al alloys from EOL aircraft. In the section 2.6, previous studies carried out to remove of Fe and Si from Al will be presented.

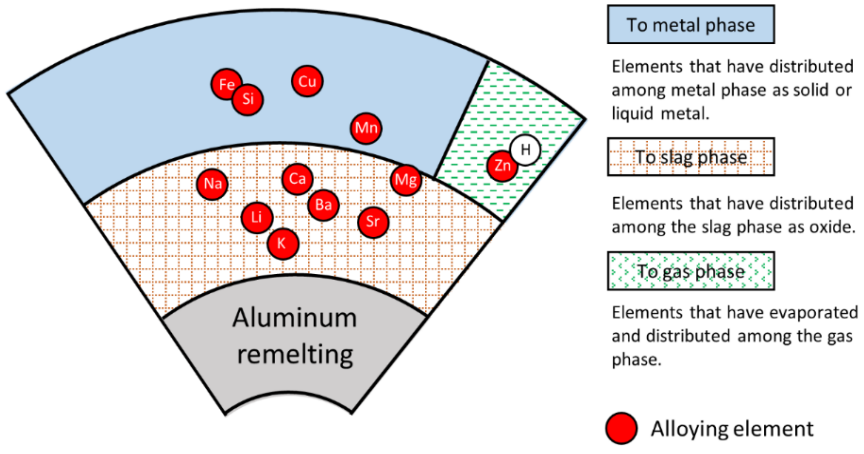

Figure 2-14. Element radar chart for the removal of alloying elements from Al. [2.74, 2.76].

2.5.1: Degassing

Hydrogen can be dissolved by Al at high temperatures, creating porosity in the final cast products. The main sources of this impurity are the humidity present in the scrap and the water vapor generated by the combustion of fossil fuels [2.10]. Degassing is often employed by secondary smelters to reduce the concentration of dissolved hydrogen from Al. This process consists of the injection of a non-reacting purging gas or a mixture of chlorine and argon gases through a tube, pipe, lance, or porous plug to generate bubbles inside the melt [2.74]. The partial pressure of hydrogen in the formed bubbles is very low, allowing the diffusion of hydrogen atoms to the bubble surface while it is rising to form hydrogen gas. When the bubble reaches the melt surface, the hydrogen gas is released [2.79]. The hydrogen removal effectiveness is affected by the bubble size which is controlled by the type of diffuser used to inject the gas. In Figure 2-15, lance, porous plug, and impeller diffusers are compared. The use of a lance produces large spherical cap bubbles resulting in inefficient degassing. A porous plug significantly improves the hydrogen removal due to a reduction of the bubble size. However, the bubbles rise as a plume above the plug that tend to coalesce and grow. The best results for the removal of hydrogen were observed by an impeller diffuser which produces fine bubbles homogeneously distributed through the molten scrap [2.80].

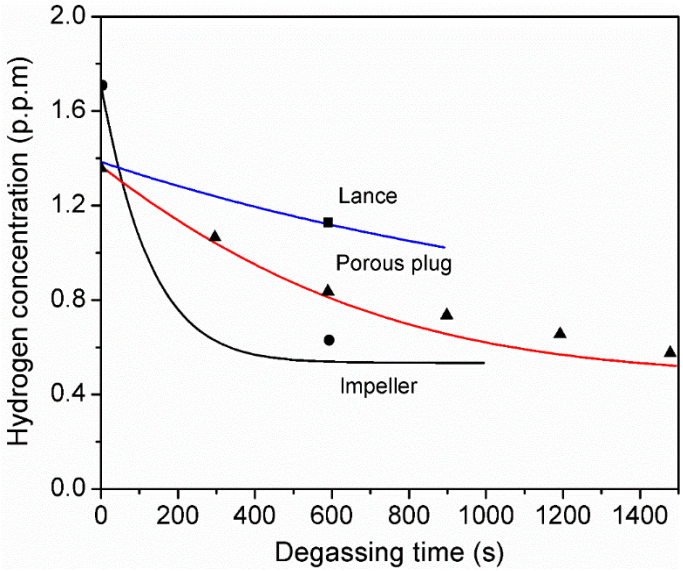

Figure 2-15. Hydrogen removal rate from Al-7Si-0.6Mg (wt%) by three different diffusers [2.80]

2.5.2: Filtering

Inclusions are suspended particles in molten Al that are classified in two classes: exogenous and endogenous. The former are particles already existing as a separate phase such as alumina, silica, silicon carbide, etc., which are picked up by the molten Al as a result of wear and erosion of the vessel materials used in the recycling process. On the other hand, endogenous particles are inclusions formed by chemical reactions during melting. For instance, alumina or spinel, which result from the oxidation of molten Al combined with the presence of alloying elements like Mg. Another example are titanium and Al diborides, originating from grain refinement additions to the melt before casting [2.81]. The presence of these inclusions reduces the fluidity of molten Al, increases the internal porosity in castings, and reduces the strength, the ductility, and the fatigue resistance of secondary products. In general, the larger the inclusions, the greater their deleterious effects [2.82].

The removal of non-metallic and intermetallic particulate suspensions can be accomplished by different processes such as sedimentation, bubble flotation, electromagnetic force, and melt filtration before casting. Nevertheless, filtration systems are relatively cheap, and hence are one of the most used processes for inclusion removal [2.83]. Filtration is defined as the process of removing inclusions by forcing the molten metal to pass through a porous material. The filtration efficiency η, which determines the quality of the filtered metal, can be expressed by the Equation 2-3 where C_i and C_o are the volume fraction of inclusions in the melt before and after filtration [2.84]:

$$n = \frac{(C_i - C_o)}{(C_i)} \cdot 100\% \qquad \text{Equation 2-3}$$

The effectiveness of a filtration process can be affected by (1) the *filter parameters*, i.e., geometrical dimension, size of structural units, distribution and arrangement in the filter, porosity, and chemistry; (2) the *inclusion parameters*, such as nature, size, and number; and (3) the *fluid and process parameters*, such as filtration speed, and upstream treatment [2.83]. These parameters are affected during filtration due to the transient nature of the process. For instance, the filter

porosity and the specific surface area decrease with time due to the accumulation or deposition of suspended particles within the filter giving rise to an increase of the pressure needed to pass the molten metal through the filter [2.79].

The main mechanisms that contribute to the removal of inclusions are cake and deep-bed filtration schematized in Figure 2-16. If filtering occurs by cake filtration, the particles are sieved at the surface forming a cake rich of inclusions larger than the size of the filter pores. This filtering process is effective for removal of larger inclusions, but impractical from the operational point of view due to the increase of the operational pressures to allow the molten metal pass through the filter [2.82]. On the other hand, if filtering occurs using a deep-bed filter, the removal of the suspended particles rely on the torturous route that the molten metal has to travel through the filter. During the molten travel, the inclusions are deposited in the filter walls by the effect of the interfacial energies between the inclusion/filter, metal/filter, and metal/inclusion. Therefore, in order for the inclusion to remain trapped at the filter walls, the interfacial energy between the inclusion/filter has to be lower than the interfacial energy between the metal/filter and metal/inclusion. The main advantage of this kind of filtration is the presence of a large surface able to trap particles smaller than the pore size. As a result, deep-bed filters are among the most used by smelters [2.82, 2.85].

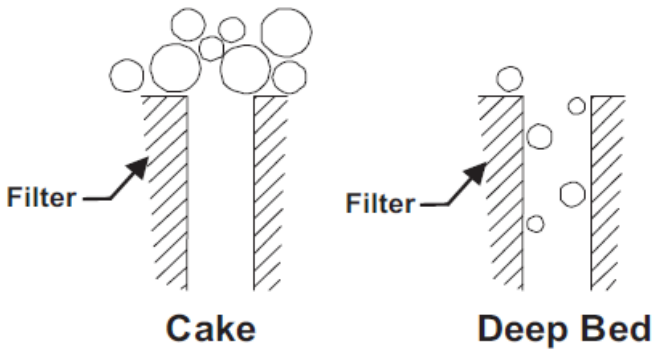

Figure 2-16. Two main modes of filtration used by Al smelters [2.85].

The particle concentration (C_z) through a depth (z) of a ceramic foam filter (CFF) using a deep-bed mechanism, can be calculated as a function of filter pore size, melt velocity, filter thickness, and inclusion particle size according to Equation 2-4 [2.85]:

$$C_z = C_o \cdot \exp - \frac{3n_t(1-\varepsilon)z}{4\varepsilon R_c} \qquad \text{Equation 2-4}$$

where C_o corresponds to the incoming concentration of inclusions, n_t is the total filter collection efficiency, ε the filter bed porosity, and R_c the filter particle radius. Manipulating the previous equation, the removal efficiency can be computed as a function of filter pore size, melt velocity, filter thickness, and inclusion particle size. In general, the removal efficiency tends to increase as filter pore size decreases, and inclusion particle size increases as it is shown in Figure 2-17 [2.85].

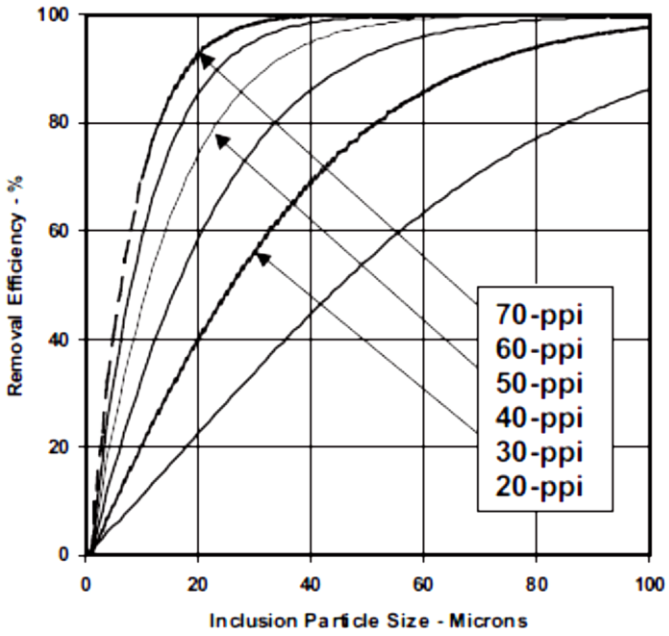

Figure 2-17. Effect of pore size on filtration efficiency [2.85].

Selection of the filter pore size is critical. Pore size selection is a function of incoming metal quality and final product requirements. Moreover, it also has an influence on both the flow rate of Al through the filter and the pressure required to prime the filter [2.85].

2.5.3: Summary of Aluminum Refining

In summary, the accumulation of unwanted impurities is an important problem that recyclers face in order to produce secondary Al products with acceptable quality. These impurities are strongly dependant on the scrap quality and are mainly classified in three classes such as unwanted elements, dissolved gas, and inclusions. The source of the unwanted elements is primarily the alloying elements that are present in the scrap stream and the conditions in which the scrap is handled. For instance, Cu, Zn, and Mg are present as alloying elements in Al alloys used in the aerospace industry. Fe and Si are present as tramp elements from the production of primary Al from bauxite. Fe accumulates in the scrap Al due to the steel tools used in the shredding operations while Si builds up due to the exposition of Al to SiO_2 from the environment and to the scrap contaminated with high Si-content alloys if no alloy sorting exists [2.86]. The dissolved gas, mainly hydrogen, is associated with the humidity of the scrap and the water vapor generated by the combustion of fossil fuels. Finally, inclusions such as alumina, silica, silicon carbide, and intermetallics are incorporated to secondary molten Al by the wear and erosion of the vessel materials used in the recycling process and the chemical reactions occurring in the melt [2.79]. The main processes employed by secondary smelters and the feasible concentration reduction of these impurities are summarised in Table 2-5.

Table 2-5. Summary of the main refining methods used by secondary smelters [2.10, 2.72]

	Fluxing	**Degassing**	**Filtering**
Main purpose	Removes alkalines & inclusions	Removes hydrogen	Removes inclusions
Secondary purpose	Stir	Removes inclusions	N/A
Placement	In holding furnace	Between holder & filter	Between degasser and Casting pit
Typical levels (ppm)	Entry: Na <10 ppm Ca < 40 ppm	Entry: 0.40–0.60 H_2	Entry: 0.5<5 mm^2/kg
	Exit: Na < 1 Ca < 4 ppm	Exit: 0.10-0.20 (at equilibrium)	Exit: <0.1 mm^2/kg PoDFA
Inclusion removal	PoDFA: 0.01-0.6 mm^2/kg depending on alloy	+ 70% (chlorine) 0 % (non-chlorine)	CFF: 40-90% DBF: 90%

It is worth noticing that the Al refining techniques, fluxing, degassing, and filtering, do not remove the main impurities found in aircraft scrap such as Cu, Zn, Fe, and Si. Thus, developing a processing approach to produce high value-added alloys from aircraft scrap in a closed-loop recycling process remains to be achieved.

2.6: Removal of Detrimental Impurities from Molten Aluminum

The reduction or removal of detrimental impurities such as Fe and Si is one of the most challenging tasks in the recycling of aircraft Al components when the primary objective is to produce premium aerospace alloys which are usually restricted to 0.5 wt% in both Fe and Si composition [2.10]. However, if the main objective of aircraft recycling is not to produce high-value alloys such as those from the 7xxx series, the aircraft Al scrap is downgraded to Al cast products, commonly from the 3xx.x family, which are characterized to allow higher content of alloying elements. As a case in point, the Al alloy 364.0 can tolerate up to 9.5 wt% of Si and 1.5 wt% of Fe, and the alloy 380.0 can permits up to 9.5 wt% of Si, 2 wt% of Fe, 4 wt% of Cu, and 3 wt% of Zn [2.10, 2.87].

One of the main processes employed by the Al industry to produce ultra-pure Al is the three-layer electrolytic refining method. In this process, pure Al is produced in an electrolytic cell having three layers as schematized in Figure 2-18. The bottom layer in the cell consists of impure Al smelted with 30 – 35 wt% Cu forming the anode. The middle layer is made up of molten salts – electrolytes of fluorine salts or mixtures of fluorine ($NaF + AlF_3$) and chlorine ($BaCl_2 + NaCl$) salts. The contaminated Al is electrolytically purified by transferring Al through the molten salts layer, giving rise to an upper layer serving as cathode consisting of 99.999% aluminum [2.88]. Nevertheless, the three-layer electrolytic process is very energy intensive consuming approximately 17 – 18 kWh/kg of Al, limiting its applications only to the production of extremely high purity Al [2.89].

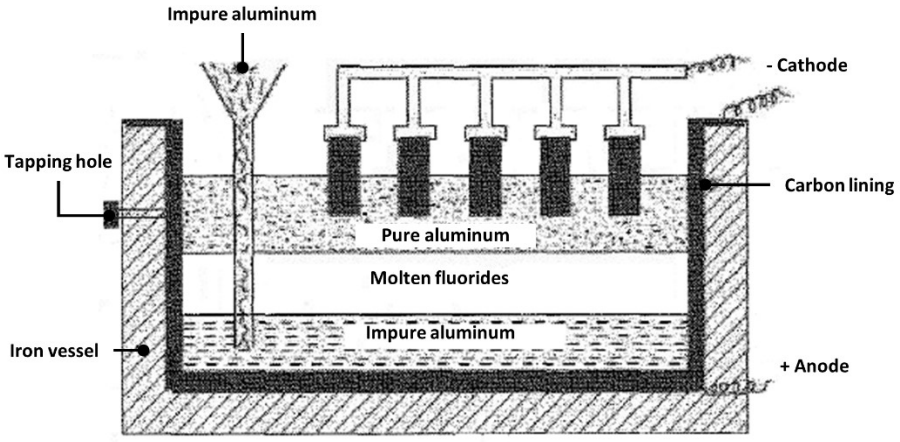

Figure 2-18. Purification of Al by Hoopes cell [2.90].

For decades, the Al recycling industry which typically produces cast alloys, has been interested in finding new methods to remove, decrease, or control the deleterious effect of detrimental impurities in Al alloys. Nevertheless, most of the research has been devoted to controlling Fe from Al scrap due to the low tolerances of this element in cast alloys, restricted to a maximum of 1.3 wt% compared with those of Si which can be as high as 11 wt% [2.91].

The equilibrium solid solubility of Fe in Al is negligible, less than 0.05 wt% at the eutectic temperature of 654 °C. Thus, in alloys containing Fe and Si, the binary Al-Fe and ternary Al-Fe-Si represent the main Fe-rich phases present in Al alloys [2.92]. The liquidus projection at the aluminum rich corner of the Al-Fe-Si system is presented in Figure 2-19. During equilibrium solidification of commercial Al alloys, the primary phase to form is usually FCC-Al followed by the binary Fe-rich phase Al_3Fe, and the ternary α-Al_8Fe_2Si, and β-Al_5FeSi phases [2.93]. Nonetheless, if contamination of Fe and Si is high enough, the solidification pattern changes with the formation of Fe-containing phases before the crystallization of Al grains. Formed before FCC-Al, the Fe-rich constituents present the possibility of free growth generating coarse crystals in the liquid phase which are detrimental in the solidified material [2.91].

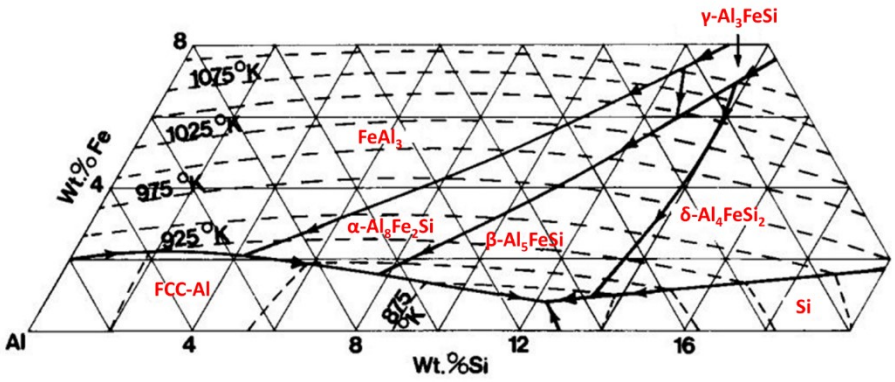

Figure 2-19. Liquidus projection of the Al rich corner in the ternary Al-Fe-Si phase diagram [2.93]

Precipitation is one of the well stablished techniques by secondary smelters to decrease the Fe concentration from cast alloys. The process consists of three main steps; first, elements such as Mn or the combination of Mn and Cr are added to molten Al to form Fe-rich intermetallic particles. Subsequently, the melt is held at temperatures between 600 °C and 650 °C to promote the formation and growth of intermetallics. Finally, the formed intermetallics are removed from the molten metal either by gravity separation, centrifuge separation, filtration separation, or electromagnetic separation [2.94-2.97]. The removal efficiency of each method is summarized in Table 2-6.

Flores et al. [2.98] studied the crystallization of $Al_8FeMnSi_2$ intermetallic particles formed during the refining of Al-9.5 wt% Si with different concentrations of Fe and Mn. In their discussion they stated that increasing the amount of Mn to 2.2 wt% can effectively remove Fe from Al by the formation of $Al_8FeMnSi_2$ phase. In their observations, they found that the intermetallic $Al_8FeMnSi_2$ nucleates, forming small individual rounded particles, after 10 minutes of holding the molten Al at 604 °C. At longer holding times, the intermetallic particles grew in a polyhedral morphology forming agglomerates with sizes up to 200 µm, settling down to the bottom of the melt. Hence, due to the intermetallic phase precipitation, the concentration of Fe and Mn in molten Al decreases from 1.6 to 0.4 wt% in the case of Fe and from 2.2 to 0.5 wt% for Mn as shown in Figure 2-20.

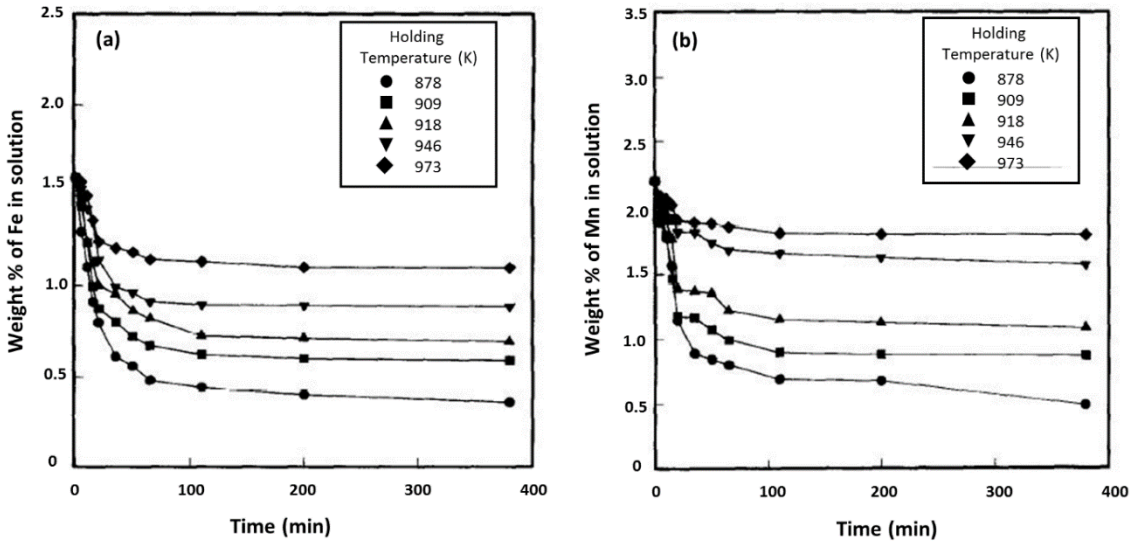

Figure 2-20. Concentration of dissolved (a) Fe and (b) Mn in an Al alloy Al-9.5Si-2.2Mn-1.6Fe (wt%) at different holding temperature and time [2.98].

Similarly to Flores et al. [2.98], Cao and Campbell [2.94] studied the possibility to increase the quality of Al by removing primary intermetallics from Al melts. In their work, the authors investigated the sedimentation of primary $Al_{15}(FeMn)_3Si_2$ particles by holding the melt at 600 °C. Particles with an equivalent diameter ranging from 100 to 170 μm were obtained at holding times between 1 and 4 h. After selected sedimentation times, the authors decanted the Al melt leaving approximately 36 wt% of the melt located at the base of the crucible which they called *"precipitate-rich melt"*. The remaining 64 wt% of the melt was denominated *"clean melt"*. The concentration variation of Fe and Mn were reduced from 1.14 to 0.3 % for Fe and from 1.09 to 0.6 % for Mn as depicted in Figure 2-21. Nevertheless, it is worth noticing that after decantation, no significate difference between the purified and rich precipitate melt was observed. Thus, it suggests that the nucleation and sedimentation of Fe rich precipitates containing Mn allows the effective removal of impurities. Nevertheless, the decantation process was not effective enough to separate the intermetallic particles giving rise to a similar impurities' concentration. A possible reason for the lack of intermetallic separation might be the result of fluid flow in the melt during decantation.

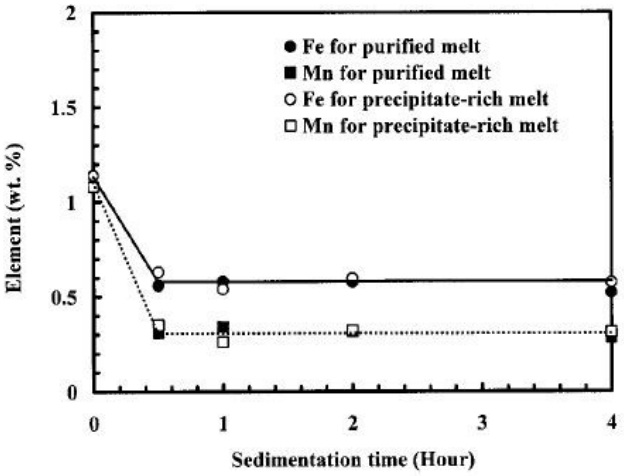

Figure 2-21. Concentration of Fe and Mn in the *"purified"* and *"precipitate-rich"* melts prior filtration [2.94].

The combination of Mn and Cr in Fe-containing molten Al, has been also used to decrease the concentration of Fe from contaminated Al alloys. In the study of Shabestari and Gruzleski [2.99] the addition of 0.3 wt% Mn and 0.10 wt% Cr to an Al-12.5 wt% Si-1.21 wt% Fe alloy was reported. The authors stated that at around 630 °C, the intermetallic $Al_{12}(Fe,Mn,Cr)_3Si_2$ phase formed having a polyhedral morphology with an average size of 50 μm after a period of 180 minutes. Additionally, they observed that the presence of intermetallic compounds increased from the top to the bottom of the melt due to sedimentation by gravity. As a consequence, the concentration of Fe, Mn, and Si decreased substantially.

Research studies have also demonstrated the removal of Fe-rich particles through forced sedimentation promoted by a centrifugal force [2.96, 2.100]. Matsubara et al. [2.96], studied the effect centrifugation on an Al-11 wt% Si containing 2 wt% of Fe and different amounts of Mn using a vertical centrifugal casting apparatus with a crucible diameter of 90 mm. According to the authors, both the centrifugal force caused by different rotation speeds and the Mn/Fe ratio have a great influence on the refining ratio of Fe as illustrated in Figure 2-22 (a) and (b), respectively. At a rotation speed of 8.3 s^{-1}, the Fe-containing particles are unable to be expelled from the central region of the melt, avoiding the cleaning of the alloy. Nonetheless, as the rotation speed is increased up to 41.8 s^{-1}, the reduction of Fe and Si is evident. Additionally, the refining ratio obtained at higher rotational speeds can be improved by controlling the Mn/Fe ratio as depicted in

Figure 2-22b. By increasing the Mn/Fe ratio up to 1.5, the Fe removal fraction increases to a maximum of ~86 %. However, at ratios higher than 1.5, the Fe removal efficiency decreased slightly. The authors concluded that the formation and growth of Fe-rich particles is the main cause of Fe removal in Al-Si alloys. Additionally, they remarked that the Mn/Fe ratio is an important process parameter to obtain a high reduction of Fe.

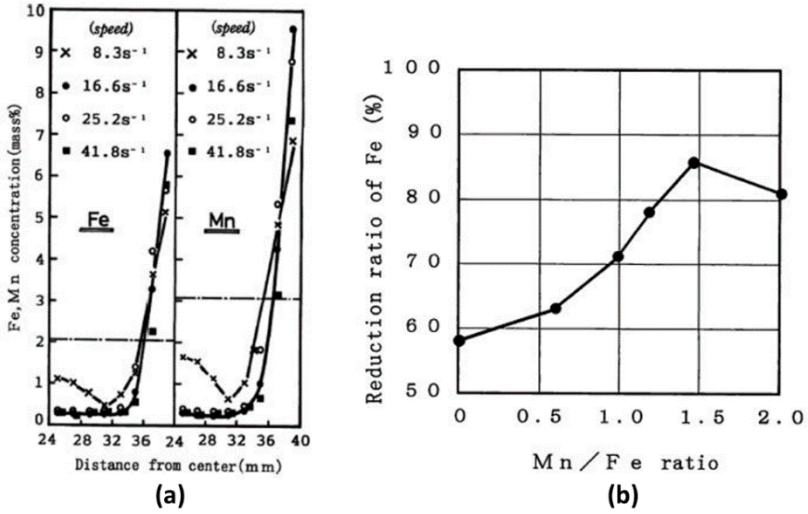

Figure 2-22.Effect of the (a) rotation speed and the (b) Mn/Fe ratio on the refining ratio of Al-Si-Fe-Mn alloys [2.96]

In addition to sedimentation techniques, Fe-rich intermetallic particles can also be removed from molten scrap by filtration following the steps depicted in Figure 2-23 [2.97, 2.101]. In this process, the formation of Fe-rich compounds is also promoted by the addition of Mn to Al-Si alloys. After holding the melt from 10 - 20 minutes at a specific nucleation and growth temperature, the melt containing the intermetallic compounds is filtrated using either a 20 or 30 ppi ceramic foam-type filter. Moraes et al. [2.97] studied the removal of Fe from recycled Al-Si alloys through filtration, analyzing the effect of Cu, Si, Fe, and Mn concentration on the Fe removal efficiency. In the same way as Cao and Campbell [94], they also observed that the presence of Mn promotes the formation of the $Al_{15}(Fe,Mn)_3Si_2$ phase. In fact, the growth and coarsening of the intermetallic phase is enhanced by increasing the Mn concentration and efficiencies of 83 % were also obtained at Mn/Fe ratios of 1.5.

Brun et al. [2.101] analyzed the removal of Fe-rich intermetallic from hyper-eutectic Al-Fe-Mn melts through filtration using ceramic foam filters and active filters. The main intermetallic particles observed in their study were $Al_6(Fe,Mn)$ and $Al_{13}Fe_4$. According to the authors, these intermetallic particles were removed from molten Al by filtering the molten Al at 600 °C reducing the Fe and Mn concentration from 2.5 to 0.4 wt% and 1.5 to 0.44 wt% respectively. In their filtration experiments using surface modified active filters which are ceramic foam filters coated with a salt, the Fe removal efficiency was not successful due to the lack of entrapment of large $Al_6(Fe.Mn)$ particles.

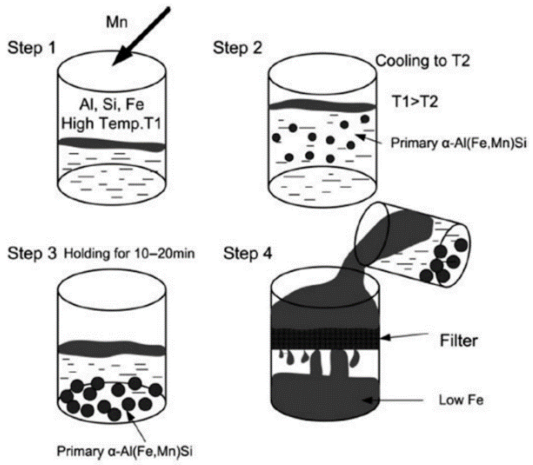

Figure 2-23. Schematic of the filtration process of Fe-rich intermetallic particles where T1 and T2 are the melting and the holding temperatures respectively [2.97].

Electromagnetic separation has also received attention by researchers in order to find alternatives to reduce Fe from Al melts. The principle of this process relies on the application of an electromagnetic field to Al melts to separate Fe-rich intermetallics as illustrated in Figure 2-24. The induced electromagnetic force, *F*, which is the product of the imposed electric current, *J*, and magnetic flux, *B,* compress the molten metal in the direction of the electromagnetic field creating a pressure gradient. Due to the low conductivity of the Fe-rich particles, these suspended particles do not experience the electromagnetic force. Hence, the particles are forced to move in the opposite direction of the electromagnetic force separating them from bulk of the melt [2.95, 2.102, 2.103].

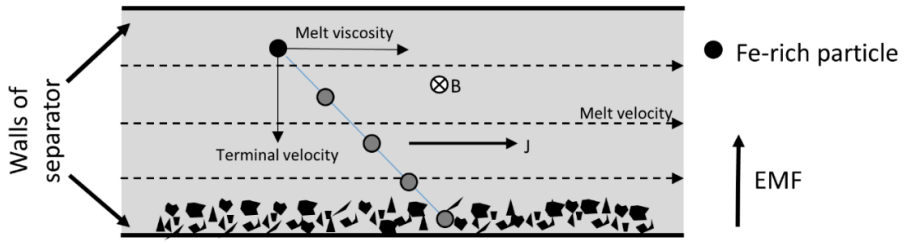

Figure 2-24. Principle of electromagnetic separation of Fe-rich particles suspended on molten Al [2.102].

Kim and Yoon [2.103] and Xu et al. [2.95] studied the electromagnetic separation of Fe-rich particles from Al-Si alloys at different Mn/Fe ratios. Both studies obtained the highest Fe removal efficiency ranging between 65 and 73 % in approximately 20 to 40 minutes of treatment when the Mn/Fe was higher than 1. As with Cao and Campbell [2.94] and Matsubara et al. [2.96] in their studies of filtration and centrifugal separation, the authors attributed the high efficiencies to the formation and growth of $Al_{15}(Fe,Mn)_3Si_2$ intermetallic particles that change their morphology from needle-like to polyhedral particles when the Mn/Fe increases.

In summary, a crucial technical subject in the recycling of aircraft Al components is how to remove the detrimental elements which are harmful to the mechanical properties and difficult to remove from molten Al, i.e., Fe and Si. Research results suggest that processes such as sedimentation, centrifugation, filtration, or electromagnetic separation, compiled in Table 2-6, help to decrease the concentration of Fe from Al alloys but not the Si concentration. In essence, researchers in these previous studies were only focused on the removal of Fe from Al because the primary objective was to recycle Al scrap into Si-rich cast alloys. Hence, Si was not a problem; in fact, it was beneficial since the presence of more than 3 wt% Si with additions of Mn, helps to form intermetallic phases containing Fe such as α-$Al_{15}(Fe,Mn)_3Si_2$ as shown in Figure 2-25, which tend to settle to the bottom of the melt permitting its separation. Nevertheless, the previously mentioned methods have a significant disadvantage to be used in the recycling of aircraft Al components into high value products from the 7000 series. The disadvantage is the addition of Si and Mn to the aircraft scrap to promote the formation of Fe-rich intermetallics. The non-reacted Si and Mn will

remain as impurities above the concentration limit of AA7000 series alloys making impossible the recycling of aircraft Al scrap into high value products. Fractional crystallization, which is a refining process employed to produce pure Al, could be potentially used to obtain aerospace grade Al alloys without the addition of extra elements. Therefore, this process will be the main topic to discuss in the following section.

Table 2-6. Summary of Fe removal techniques and their higest efficiencies reported in the literature.

Authors	**Composition (wt% Al balance)**	**Mn/Fe**	**Holding**		**After Holding (wt%)**		**Fe removal (%)**	**Technique**
			Temp (°C)	Time (min)	Mn	Fe		
Flores [2.98]	9.5Si-1.6Fe-2.2Mn	1.37	604	380	0.5	0.4	75	Gravitational separation
Cao [2.94]	11.1Si-1.1Fe-1.091	0.95	600	20	0.6	0.3	73	
Shabestari [2.99]	12.4Si-1.2Fe-0.3Mn	0.23	630	180	0.25	1.1	9*	
Van der Donk [2.104]	12Si-2Fe-1.5Mn-0.2Cr	0.75	600	180	0.27	0.69	65	
Matsubara [2.96]	11Si-2Fe-2Mn	1	NA	NA	0.3	0.36	82	Centrifuge separation
	11Si-2Fe-2.5Mn	1.22			0.2	0.23	89	
	11Si-2Fe-3Mn	1.45			0.12	0.15	92	
	11Si-2Fe-4.15Mn	2			0.1	0.13	93	
Van der Donk [2.104]	12Si-2Fe-1.5Mn-0.2Cr	0.23	600	45	0.3	0.7	65	Filtration separation
Moraes [2.97]	12Si-1.32Fe-1Mn	0.75	605	30	NA	0.4	69	
	12Si-1.30Fe-1Mn	0.77	625	30		0.48	63	
	12Si-1.34Fe-1.5Mn	1.1	605	30		0.25	81	
	12Si-1.14Fe-1.5Mn	1.4	610	30		0.41	64	
	12Si-0.98Fe-1.5Mn	1.5	605	30		0.18	82	
Brun [2.101]	2.5Fe-1.5Mn	0.6	600		0.44	0.4	84	
Kim [2.103]	6.4Si-1.7Fe-1.6Mn	0.94	690	20	NA	0.45	73	EM separation
Xu [2.95]	12Si-1.1Fe-1.2Mn	1.1	640	30	0.26	0.41	63	

* Efficiency measured at the middle of the crucible.

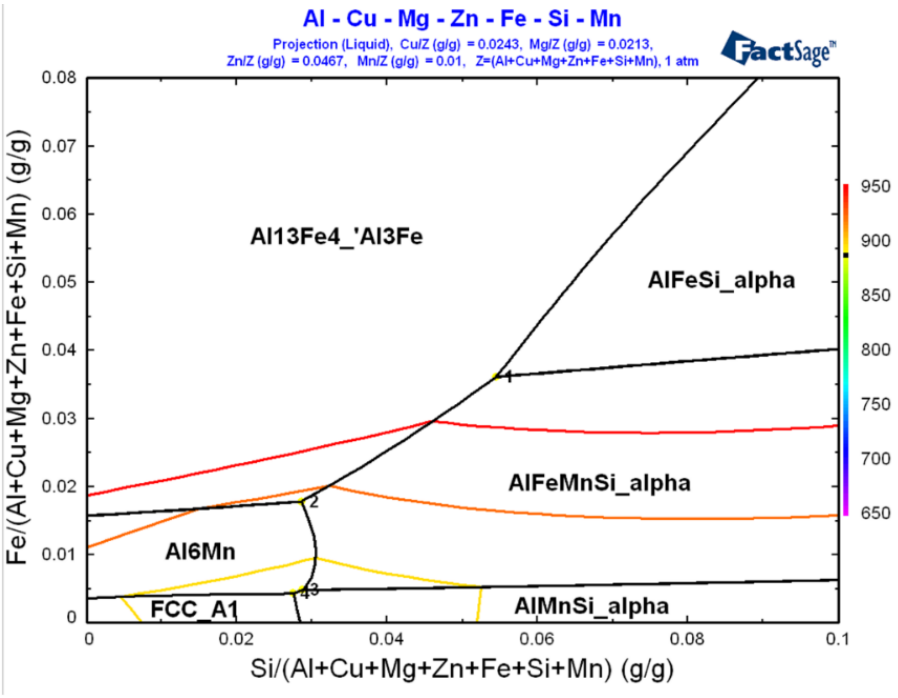

Figure 2-25. Liquidus projection of the multicomponent Al-2.43Cu-2.13Mg-4.67Zn-1Mn-xSi-yFe (wt%) system.

2.6.1: Fractional Crystallization

Fractional crystallization is a separation process that is applied to purify organic melts and metals [2.105]. Industrially, this process can be carried out either by growing crystals freely in the melt (suspension-based methods), or in a layer formed on a cool surface (layer-based methods) as illustrated in Figure 2-26. An advantage of suspension-based methods is that the solid/liquid interface is relatively large which favours crystal purity and production rate. Nevertheless, the separation of crystals from the mother liquor is a difficult task that has to be done in a dedicated equipment. On the other hand, the layer-based crystallization technique does not need special processes to separate the crystals from the melt since the solid/liquid separation is easily performed by gravity and draining the residual melt. Additionally, the melt can be mechanically mixed improving the cleanliness of the fraction of solid formed [2.105, 2.106].

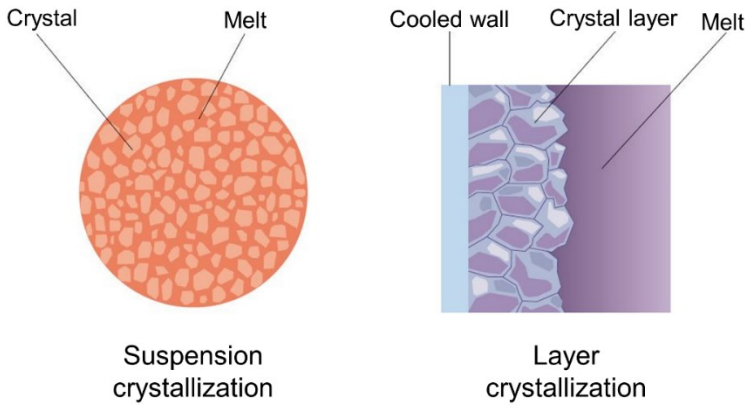

Figure 2-26. Suspension and layer fractional crystallization methods [2.107].

In both fractional crystallization methods, the impure material is always processed between the solidus and liquidus temperatures where solid and liquid fractions co-exist as schematized in Figure 2-27. A controlled cooling in this region allows the molten material to slowly solidify. During solidification, the lattice structure of the primary phase crystals as they begin to grow cannot easily accommodate impurities and the unwanted impurities tend to segregate at the moving solid/liquid interface. This impurity segregation generates a gradient of concentration through the solidified material that is affected by the thermodynamic partitioning of impurities, diffusion, solidification velocity, and degree of melt stirring. As a consequence, the section where the high impurity concentration is obtained is rejected and the process is repeated until the desired purity is achieved [2.108, 2.109].

The thermodynamic partitioning of impurities (solutes), which mainly provides the gradient of concentration within the solidified material, can be predicted through the analysis of the corresponding phase diagram assuming that the local solid/liquid interface is in equilibrium. This assumption permits the determination of the equilibrium solid and liquid concentrations during cooling if the solid/liquid interface temperature is known as illustrated in the hypothetical binary phase diagram shown in Figure 2-27. Thus, the ratio of the composition of solute in the solid in equilibrium with liquid, C_s, and the composition of solute in liquid in equilibrium with solid, C_l, describes the thermodynamic partition of impurities, k, as in Equation 2-5 [2.110]. Knowing the equilibrium partition coefficient of the system, the solute concentration in the solid fraction during solidification can be estimated.

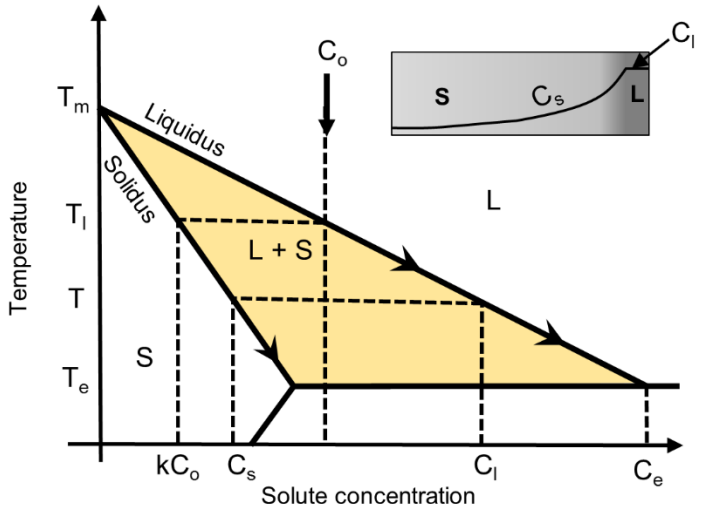

Figure 2-27. Hypothetical binary phase diagram illustrating the equilibrium of solid and liquid compositions and the concentration gradient in the solidified material.

$$k = \frac{C_s}{C_l} \qquad \text{Equation 2-5}$$

Industrially, different patents can be found in the literature describing different fractional crystallization devices for the production of high-purity Al [111-113], or to recycle aluminum scrap [2.114-2.117]. Nevertheless, the main question that has to be considered when selecting fractional crystallization to remove impurities from Al is to what extent the impurities can be theoretically separated from the base metal by this principle. In this sense, only a few studies have been reported in the literature oriented to study the effect of the scrap composition and the processing parameters on the theoretical refining efficiency of fractional crystallization.

Sillekens et al. [2.118] estimated the theoretical purification efficiency for the binary Al-X where X represents an specific alloying element. The purification efficiency was obtained assuming no concentration gradients in the solid or liquid phases. In other words, the "equilibrium" or lever rule principle was applied; hence, the concentrations of solute in the solid and liquid provided by the equilibrium phase diagram were directly used. According to the authors, the purification efficiency η, is represented by Equation 2-6:

$$\eta = 1 - \frac{C_{B,S}}{C_{B,o}} \qquad \text{Equation 2-6}$$

where $C_{B,S}$ is the concentration of the solute B in the solid phase and $C_{B,o}$, represents the initial solute concentration obtained by Equation 2-7 in which P represents the solid fraction in the semi-solid state. Then, by combination of Equation 2-6 and Equation 2-7, the isothermal refining efficiency can be estimated.

$$C_{B,o} = C_{B,L} - P\left(C_{B,L} - C_{B,S}\right) \qquad \text{Equation 2-7}$$

Boender et al. [2.119] studied the thermodynamic capabilities of fractional crystallization for the binary system Al-Si, and the ternary systems Al-Si-Fe, Al-Si-Mn, and Al-Cu-Mg. The capabilities of the process were studied employing the Scheil-Gulliver model implemented on the thermomechanical software ThermoCalc. The Scheil-Gulliver model describes the solute redistribution within the solid during solidification of an alloy as a function of solid fraction (see Equation 2-8). This approach, unlike equilibrium solidification, assumes that during solidification the solute does not diffuse back into the solid; it is completely rejected into the liquid which is considered to be completely mixed. Additionally, the Scheil-Gulliver model also assumes local equilibrium at the advancing solid-liquid interface allowing the use of equilibrium phase diagrams in the solidification analysis.

$$C_S = kC_o(1 - f_S)^{(k-1)} \qquad \text{Equation 2-8}$$

The Scheil-Gulliver computation carried out by Boender et al. [2.119] provided the composition of the melt and the solidified fraction using a temperature increment of 1 K. Their results indicate that Si, Fe, and Cu can be removed by fractional crystallization from molten Al with an efficiency of 80 to 90 % by solidifying 20 to 40 % of the melt. Additionally, they stated that Mn and Mg can be removed with a lower efficiency, i.e., 40 to 60 % by solidifying the same amount of mass from

the original liquid. Finally they concluded that a higher concentration of one element in the melt may influence the removal efficiency of other elements negatively.

Even though the studies carried out by Sillekens et al. [2.118] and Boender et al. [2.119] provide to some extent the refining efficiency of Al from impurities such as Si, Fe, Mn, or Cu, the refining efficiencies are obtained by considering only binary or ternary systems. Additionally, such studies did not take into account the effect of back diffusion during solidification which might have a negative impact on the refining efficiency due to the low growth rates achieved in fractional crystallization. Furthermore, the previous studies were not able to provide the working solidification velocity which is one of the most important parameters in fractional crystallization. This parameter, in addition to providing the processing time, can affect the distribution of solutes within the solid.

According to the equilibrium solidification conditions previously mentioned, if solidification occurs slowly the solute concentration in the liquid is uniform and the concentration of the solidified material is k_o times that in the liquid. If solidification does not occur slowly, this is no longer true and the melt solidifies under non-equilibrium conditions. The solute is rejected from the growing solid more rapidly than it can diffuse into the main body of liquid. As a result, an enriched layer of solute builds up ahead of the solid/liquid interface known as the diffusion boundary layer. The solute concentration in this zone, rather than the concentration in the main body of liquid, determines the effective solute incorporation into the growing solid [2.120].

Burton et al. [2.121] proposed a steady-state equation to describe the effective distribution of solute in crystals grown from a melt considering the buildup of impurities in a denominated boundary layer, δ. The authors assumed that beyond this layer, the fluid flow keeps the concentration uniformly equal to C_l. However within δ, the growth velocity and diffusion contribute to transporting the excess solute away from the growing crystal. Their mathematical analysis led them to derive the well-known effective distribution coefficient k_{eff}, depicted in Equation 2-9:

$$k_{eff} = \frac{k_o}{k_o + (1 - k_o)e^{\frac{V \cdot \delta}{D_l}}} \qquad \text{Equation 2-9}$$

where V is the solidification velocity, δ the thickness of the diffusion boundary layer ahead the solidification front, and D_l corresponds to the diffusivity of the solute in the liquid. The effect of the exponential term in Equation 2-9 is shown in Figure 2-28. Since the diffusivity of solute in liquid is constant due to the steady-state condition, and the diffusion boundary layer depends on the fluid flow ahead of the interface, the effective partition coefficient will mainly depend on the solidification growth velocity. Hence, as the solidification velocity increases, the exponential term will also increase giving rise to higher effective partitioning coefficients.

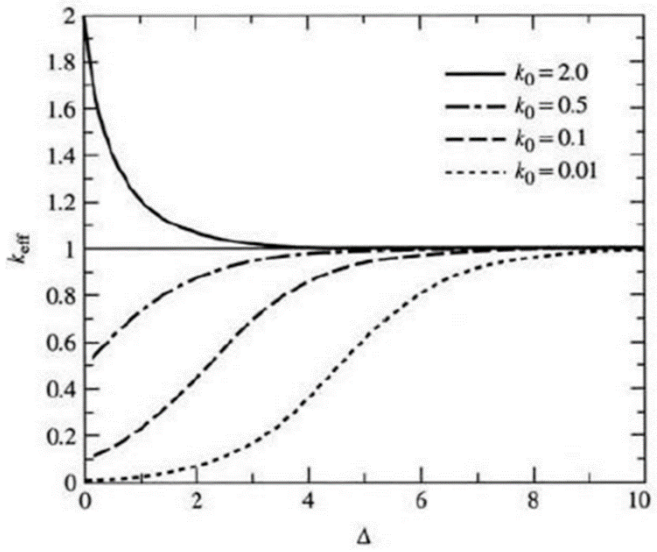

Figure 2-28. The effective distribution coefficient as a function of the exponent $\Delta = V\delta/D$ from the Burton-Prim-Slichter Equation 2-9 [2.122]

The value of δ in the previous equation, relies on the diffusivity of the solute, the liquid viscosity, and the conditions of fluid flow ahead of the crystallization interface and can vary from 10^{-3} m for very low stirring to 10^{-5} m for vigorous stirring [2.120, 2.121].

Hence, using an effective partition coefficient in a numerical solidification model that includes the effects of solidification velocity, back diffusion, and degree of stirring, could be used to provide the processing parameters that yield the highest efficiency in a fractional crystallization process. Additionally, using an accurate thermodynamic database such as that provided by the thermodynamic software FactSage, the solidification model could be extended to a

multicomponent system to be able to evaluate the theoretical refining performance of fractional crystallization applied to aircraft Al scrap.

2.7: References

[2.1] Resource Recovery and Recycling from Metallurgical Wastes. Vol. Volume 7. 1-12, Elsevier, 2006.

[2.2] U.S. Geological Survey, Mineral commodity summaries 2012: U.S. Geological Survey. 198, Reston, Virgina, 2012.

[2.3] W.D. Menzie, J.J.B., D.I. Bleiwas, E.L. Bray, T.G. Goonan, M. Grecia The Global Flow of Aluminum From 2006 Through 2025: U.S. Geological Survey Open-File Report 2010–1256, 73 p., available at http://pubs.usgs.gov/of/2010/1256/. 2010.

[2.4] Gendron, R.S., M. Ingulstad, and E. Storli, Aluminum Ore: The Political Economy of the Global Bauxite Industry. University of British Columbia Press, 2013.

[2.5] Bayer, K.J., Patent US515895 A. Process of making alumina. 1894.

[2.6] Grjotheim, K. and H. Kvande, Introduction to Aluminium Electrolysis. Beuth, Berlin, 2011.

[2.7] W.T. Choate and J.A.S. Green, U.S. Energy Requirements for Aluminum Production, Historical Perspective, Theoretical Limits and New Opportunities. For U.S. DOE (EERE). 2007, BCS, Inc. p. 1-150.

[2.8] Green, J.A.S., Aluminum Recycling and Processing for Energy Conservation and Sustainability. 1-271, ASM International, 2007.

[2.9] Itzkowitch, Z. 1ere PIateforme europeenne de demantelement aeronautique, Dossier de presse Bartin AERO Recycling. 2008.

[2.10] Schlesinger, M.E., Ilegbusi, O.J., Iguchi, M., Wahnsiedler, W., Aluminum Recycling. CRC PressINC, United States, 2007.

[2.11] Green, J.A.S., Aluminum Recycling and Processing for Energy Conservation and Sustainability. ASM International. p. 155.

[2.12] Nancy, M., Energy and Environmental Profile of the U.S. Aluminum Industry, Prepared for the U.S. Department of Energy Office of Industrial Technologies. Energetics, INC., Columbia, Maryland, 1997.

[2.13] Das, S.K., J. G., Light metals., 2007: p. 1161-1166.

[2.14] Mascle, C., et al., Procedia CIRP, 2015. Vol. 26: p. 299-304.

[2.15] The Aluminum Association. International Alloy Designations and Chemical Compositions for Wrought Aluminum and Wrought Aluminum Alloys. 2009, The Aluminum Association: Arlington, VA.

[2.16] Montagna, D., Makar, H.V., U.S. Patent No. 4,330,090. Method for wrought and cast aluminum separation. 1982.

[2.17] Ambrose, F., et al., Conservation & Recycling, 1983. Vol. 6(1–2): p. 63-69.

[2.18] Wotruba, H. and H. Harbeck, Sensor-Based Sorting, in Ullmann's Encyclopedia of Industrial Chemistry. 2000, Wiley-VCH Verlag GmbH & Co. KGaA.

[2.19] Gaustad, G., E. Olivetti, and R. Kirchain, Resources, Conservation and Recycling, 2012. Vol. 58: p. 79-87.

[2.20.] Sommer, E.J., Parrish, R.H., Spencer, D.B., Roos, C.E., U.S. Patent No. 8,553,838,B2. High speed materials sorting using x-ray fluorescence. 2003.

[2.21] Kevorkjjan, V., JOM, 2010. Vol. 62(8): p. 37-42.

[2.22] Hussain, L.B. and W.E. Soon, Mater. Manuf. Processes, 2001. Vol. 16(3): p. 375-386.

[2.23] Hussain, L.B. and I.A.A. Hakim, Mater. Manuf. Processes, 2007. Vol. 22(7-8): p. 916-921.

[2.24] Das, S.K., J. Green, and J.G. Kaufman, JOM, 2007. Vol. 59(11): p. 47-51.

[2.25] McAvoy, B., McNeish, J., Stevens, W., The Alcan decoater process for UBC decoating, in 2nd International Symposium on Recycling of Metals Engineered Materials, J.H.L. Van Linden, Stweart, D. L., Sahai, Y., Editor. 1990, TMS-AIME: Warrendale, PA. p. 203.

[2.26] Chattopadhyay, A.K., Zentner, M.R., 1990.

[2.27] Lytle, F.W., Greegor, R. B., Bibbins, G. L., Blohowiak, K. Y., Smith, R. E., Tuss, G. D., Corros. Sci., 1995. Vol. 37(3): p. 349-369.

[2.28] Yu, Z., Ni, H., Zhang, G., Wang, Y., Dong, S., Zhao, G., Appl. Surf. Sci., 1992. Vol. 62(4): p. 217-221.

[2.29] Sinko, J., Prog. Org. Coat., 2001. Vol. 42(3–4): p. 267-282.

[2.30] Bierwagen, G.P. and D.E. Tallman, Prog. Org. Coat., 2001. Vol. 41(4): p. 201-216.

[2.31] Carlton, G.N., Aiha Journal, 2003. Vol. 64(5): p. 668-672.

[2.32] Arndt, S. and R. Canum, Metal Finishing, 2007. Vol. 105(5): p. 49-50.

[2.33] Tangestanian, P., M. Papini, and J.K. Spelt, Wear, 2001. Vol. 248(1–2): p. 128-139.

[2.34] Hart, W.G.J., Report NLR-TP-2003-357: Paint stripping techniques for composite aircraft components. 2003, Structures and Materials Department, National Aerospace Laboratory NLR: Netherlands.

[2.35] Olevitch, A., Cryogenic mechanical means of paint removal. US Patent 5044129 A, Sept 3, 1991. 1991.

[2.36] WMRC, TN98-046: Paint removal options - Paint Factsheet No. 6, in Waste Management and Research Center. 1998: Champaign, IL.

[2.37] Barletta, M., A. Gisario, and V. Tagliaferri, J. Mater. Process. Technol., 2006. Vol. 173(2): p. 232-239.

[2.38] Ranalli, R.J., U.S. Patent No. 5,662,762 A. Laser-based system and method for stripping coatings from substrates. 1997.

[2.39] Kozol, J., JOM, 2001. Vol. 53(3): p. 20-21.

[2.40] Kvithyld, A., Meskers, C. E. M., Gaal, S., Reuter, M., Engh, T., JOM, 2008. Vol. 60(8): p. 47-51.

[2.41] Stoye, D. and W. Freitag, Paints, coatings, and solvents. Wiley-VCH, Weinheim; New York, 1998.

[2.42] Malloy, J.C., PITTURE E VERNICI-EUROPE-, 2002. Vol. 78: p. 7-18.

[2.43] Malloy, J.C., Metal Finishing, 2010. Vol. 108(11–12): p. 343-347.

[2.44] Evans, R. and G. Guest., The Aluminium Decoating Handbook. Wolverhampton, U. K., 2000.

[2.45] Miller, R.E., Patent No. 4,147,531. Method and apparatus for removing surface contaminants from metallic scrap. 1979.

[2.46] Evans, M. and D.H. Miller, US Patent No. 4,200,262. Method and apparatus for removing combustible material from metal scrap. 1980.

[2.47] Perry, O.H. and G. Riley, US Patent No. 5,451,033. Heat processing apparatus. 1995.

[2.48] Robak, C.B., D.C. Evans, and E.M. Ramsey, US Patent No. 4,784,603. Process for removing volatiles from metal. 1988.

[2.49] Fitzpatrick, N.P. and R.E.G. Lee, US Patent No. 4,654,088. Decoating of aluminum scrap. 1987.

[2.50] Schwing, E., P. Sommer, and H. Uhrner, US Patent No. 4,599,067. Apparatus for the thermal removal of lacquer from metallic and ceramic articles. 1986.

[2.51] Tremblay, F., et al., US Patent No. 5,364,443. Process for combined decoating and melting of aluminum scrap contaminated with organics. 1994.

[2.52] Dube, G. and F. Tremblay, US Patent No. 5,405,428. Decontamination and/or surface treatment of metals. 1995.

[2.53] Michael, J., The future of aircraft paint removal methods. 1989, Air Force Institute of Technology: Wright-Paiterson Air Force Base, Ohio.

[2.54] Foster, F.P., Patent CA 23047. Detacheur de peinture/Paint remover, in Canadian Intellectual Property Office. 1885, Myers & Son: Canada.

[2.55] Ellis, B. and E.J. Carleton, U.S. Patent No. 2,327,701 A. Paint and varnish remover composition. 1943.

[2.56] Kuentzel, L.E., U.S. Patent No. 2507985. Paint remover composition. 1950.

[2.57] Wollbrinck, T., Journal of the American Institute for Conservation Journal of the American Institute for Conservation, 1993. Vol. 32(1): p. 43-57.

[2.58] Operowsky, R.M., Metal Finishing, 1999. Vol. 97(5): p. 466-467.

[2.59] Luey, K., D. Coleman, and G. Ternet, Replacement of Methylene Chloride in NVR and Paint Removal Applications. 2000, DTIC Document.

[2.60] Pauli, R., Products Finishing, 1997. Vol. 61(9): p. 84-89.

[2.61] Del Nero, V., Siat, C., Marti, M. J., Aubry, J. M., Lallier, J. P., Dupuy, N., Huvenne, J. P., AIP Conference Proceedings, 1996. Vol. 354(1): p. 469-476.

[2.62] Young, C.N., Clayton, C. R., Yesinowski, J. P., Wynne, J. H., Watson, K. E., Prog. Org. Coat., 2014. Vol. 77(1): p. 232-241.

[2.63] Young, C.N., Clayton, C. R., Wynne, J. H.,Yesinowski, Daniels, G. C., Prog. Org. Coat., 2015. Vol. 88: p. 212-219.

[2.64] Vieth, W.R., Diffusion in and through polymers : principles and applications. Hanser Publishers ; Distributed in the U.S.A. and in Canada by Oxford University Press, Munich; New York; New York, 1991.

[2.65] Hansen, C.M., Hansen solubility parameters : a user's handbook. CRC Press, Boca Raton, 2007.

[2.66] Hansen, C.M., The three dimensional solubility parameter and solvent diffusion coefficient. 1967, Technical University of Denmark: Danish technical press, Copenhagen.

[2.67] Hansen, C.M., Product R&D, 1969. Vol. 8(1): p. 2-11.

[2.68] Hare, C.H., Journal of Protective Coatings & Linings, 1997. Vol. 14(5): p. 69-81.

[2.69] O'Donoghue, M., Garrett, R., Graham, R., Datta, V J., Vitomir, S., White, D., Peer, L., Journal of Protective Coatings & Linings, 2000. Vol. 17(5): p. 74-93.

[2.70] Croll, S.G., J Coat Technol Res, 2010. Vol. 7(1): p. 49-55.

[2.71] Ebenezer N.; Graham, J.L., Determination of the relative activity of selected paint stripping components with epoxy and polyurethane aerospace coatings. Published Master Degree Thesis. 2011, University of Dayton.

[2.72] Taylor, M., Aluminium-Dusseldorf, 2003. Vol. 79(1-2): p. 44-51.

[2.73] Majidi, O., S.G. Shabestari, and M.R. Aboutalebi, J. Mater. Process. Technol., 2007. Vol. 182(1–3): p. 450-455.

[2.74] Utigard, T.A., et al., Jom-Journal of the Minerals Metals & Materials Society, 1998. Vol. 50(11): p. 38-43.

[2.75] Utigard, T.A., R.R. Roy, and K. Friesen, Can. Metall. Q., 2001. Vol. 40(3): p. 327-334.

[2.76] Nakajima, K., et al., Environmental Science & Technology, 2010. Vol. 44(14): p. 5594-5600.

[2.77] Boeree, C.R., AES/GT/11-19 Zinc Removal from Aircraft aluminum-alloy scrap. 2011, Delft University of Technology.

[2.78] Wei, Q., et al., Zinc Removing from Aluminum alloy by Vacuum Distillation, in Advances in Metallurgical and Mining Engineering, H.X. Zhu and L.J. Wang, Editors. 2012. p. 303-306.

[2.79] Engh, T.A., C.J. Simensen, and O. Wijk, Principles of metal refining. Oxford University Press, Oxford; New York, 1992.

[2.80] Engh, T.A. and T. Pedersen, Removal of Hydrogen from Molten Aluminium by Gas Purging, in Essential Readings in Light Metals. 2013, John Wiley & Sons, Inc. p. 218-225.

[2.81] Conti, C. and P. Netter, Separations Technology, 1992. Vol. 2(1): p. 46-56.

[2.82] Ali, S., D. Apelian, and R. Mutharasan, Can. Metall. Q., 1985. Vol. 24(4): p. 311-318.

[2.83] Damoah, L.N.W. and L. Zhang, Metallurgical and Materials Transactions B-Process Metallurgy and Materials Processing Science, 2010. Vol. 41(4): p. 886-907.

[2.84] Apelian, D. and K. Choi, Metal Refining by Filtration, in Foundry Processes, S. Katz and C. Landefeld, Editors. 1988, Springer US. p. 467-493.

[2.85] Olson , R.A. and L.C.B. Martins, Adv. Eng. Mater., 2005. Vol. 7(4): p. 187-192.

[2.86] Hendrickx, P. and M. Brochu, 'Recycling of Al scrap by comminution and spark plasma sintering: Part Unpublished material, 2016.

[2.87] Davis, J.R. and J.R. Davis, Aluminum and aluminum alloys. ASM international, 1993.

[2.88] Dawless, R.K. and S.C. Jacobs, U.S. Patent No. 4,239,606 A.Production of extreme purity aluminum. 1980.

[2.89] Wolstenholme, G.A., Aluminum Extraction, in Molten Salt Technology. 1982, Springer. p. 13-55.

[2.90] Dewan, M., et al. Control and removal of impurities from Al melts: A review. in Mater. Sci. Forum. 2011. Trans Tech Publ.

[2.91] Zhang, L., Gao, J., Damoah, L.N.W. Robertson, D.G., Miner. Process. Extr. Metall. Rev., 2012. Vol. 33(2): p. 99-157.

[2.92] Mondolfo, L.F., Al–Fe Aluminum–Iron system, in Aluminum Alloys. 1976, Butterworth-Heinemann. p. 282-289.

[2.93] Mondolfo, L.F., Al–Fe–Si Aluminum–Iron–Silicon system, in Aluminum Alloys. 1976, Butterworth-Heinemann. p. 534-537.

[2.94] Cao, X. and J. Campbell, Int. J. Cast Met. Res., 2004. Vol. 17(1): p. 1-11.

[2.95] Zhenming, X., L. Tianxiao, and Z. Yaohe, Journal of materials science, 2003. Vol. 38(22): p. 4557-4565.

[2.96] Matsubara, H., N. Izawa, and M. Nakanishi, Journal of Japan Institute of Light Metals, 1998. Vol. 48(2): p. 93-97.

[2.97] de Moraes, H.L., et al., Materials Transactions, 2006. Vol. 47(7): p. 1731-1736.

[2.98] Flores-V, A., et al., Intermetallics, 1998. Vol. 6(3): p. 217-227.

[2.99] Shabestari, S. and J. Gruzleski, Metall and Mat Trans A, 1995. Vol. 26(4): p. 999-1006.

[2.100] Zhao, L., et al., Metallurgical and Materials Transactions B, 2010. Vol. 41(3): p. 505-508.

[2.101] Le Brun, P., et al., Removal of intermetallic particles for the purification of aluminum alloys, in Light Metals 2007, M. Sorlie, Editor. 2007. p. 657-664.

[2.102] Li, T.-x., et al., TRANSACTIONS-NONFERROUS METALS SOCIETY OF CHINA-ENGLISH EDITION-, 2003. Vol. 13(1): p. 121-125.

[2.103] Kim, J.-H. and E.-P. Yoon, J. Mater. Sci. Lett., 2000. Vol. 19(3): p. 253-255.

[2.104] Van der Donk, H., G. Nijhof, and C. Castelijns, The removal of iron from molten aluminium. 1995, Minerals, Metals and Materials Society, Warrendale, PA (United States).

[2.105] Sloan, G.J., and McGhie, A.R., Techniques of melt crystallization. Wiley, New York, 1988.

[2.106] Ulrich, J. and T. Stelzer, Melt Crystallization, in Crystallization. 2013, Wiley-VCH Verlag GmbH & Co. KGaA. p. 289-304.

[2.107] Chemtech, S. Fractional crystallization. Fractional crystallization (brochure). Sulzer Chemtech, Switzerland 2016 [cited 2016.

[2.108] Regner, A., Method of separating constituents of alloys by fractional crystallization. U.S. Patent 2,471,899. 1949, United Chemical and Metallurgical Works National Corporation, Prague, Czechoslovakia.

[2.109] Qiu, K., Duan, W., Chen Q. Basic principles of control of continuous crystallizer in metal refining. Mineral Processing and Extractive Metallurgy, 2001. 110, 161-164 DOI: doi:10.1179/mpm.2001.110.3.161.

[2.110] Kurz, W. and D.J. Fisher, Fundamentals of solidification. Trans Tech Publications, Switzerland; Rockport, MA, 1986.

[2.111] Dawless, R.K. and R.E. Graziano, U.S. Patent No. 4,221,590 A. Fractional crystallization process. 1981.

[2.112] Shingu, H., Arai, K., Sakaguchi, M., Nishide, T., Watanabe, O., Tashiro, Y., Otsuka, R., Tsukamoto, K., U.S. Patent No. 4,469,512 A. Process for producing high-purity aluminum. 1984.

[2.113] Hong, T. and I. Nurgul, U.S. Patent No. 20,140,202,653 A1. Method for purifying high-purity aluminium by directional solidification and smelting furnace therefor. 2011.

[2.114] Kahveci, A.I., Unal, A., Recycling of Metals and Engineered Materials, 2000: p. 979-991.

[2.115] De Vries, P.A., and Wouters, H. A., Method for fractional crystallisation of a molten metal. U.S. Patent 7,419,530 B2. 2008, Aleris Switzerland GmbH c/o K+P Treuhangesellschaft, Schaffhausen, CH.

[2.116] Wouters, H.A., Beunder, E.M., Boender, W., Hogenboom, M.A., Kieft, R., Storm, J.C., Crystallisation method for the purification of a molten metal, in particular recycled aluminium. U.S. Patent 7,892,318 B2. 2011, Aleris Switzerland GmbH c/o K+P Treuhandgesellchaft, CH.

[2.117] Verdier, J.F., Butruille, J.R., Leroy, M., Valax, D., Process for recycling aluminum alloy scrap coming from the aeronautical industry. U.S. Patent 8,202,347 B2,. 2012, Constellium France.

[2.118] Sillekens, W.H., Verdoes, D., Van, W., Schade, J.F.M. Refining aluminium scrap by means of fractional crystallisation: technical feasibility. in Proceeding of the Fourth ASM International Conference and Exhibition on the Recycling of Metals, ASM Europe. 1999.

[2.119] Boender, W., Waringa, C.J., Krielaart, G.P., Folkertsma, A., Verdoes, D. Refining aluminium scrap with fractional crystallisation: Assessing its feasibility with thermodynamics. in Light Metals: Proceedings of Sessions, TMS Annual Meeting. 2002. Warrendale, Pennsylvania.

[2.120] Pfann, W.G., Normal Freezing and the Distribution Coefficient, in Zone Melting. 1958, John Wiley & Sons New York. p. 8-27.

[2.121] Burton, J.A., R.C. Prim, and W.P. Slichter, The Journal of Chemical Physics, 1953. Vol. 21(11): p. 1987-1991.

[2.122] Scheel, H.J. and T. Fukuda, Crystal growth technology. Wiley Online Library, 2003.

3: Objectives

In the scope of the CRIAQ-ENV412 research program, this thesis focuses on the study of the recycling process of Al components from a Bombardier CRJ-100ER aircraft by a liquid state route. This study will allow the determination of the recycling strategies of aircraft Al scrap to achieve the production of high-value added alloys while avoiding the downgrading of the scrap. In order to accomplish this goal, particular attention is given to study the removal of impurities associated with the aircraft corrosion protection coating, the alloying elements, and the potential pick-up of Fe and Si during handling the scrap. Thus, three particular objectives have been set as follows:

1. Study the removal of the aircraft corrosion protection coating by two methods: thermal decoating and chemical stripping.

2. Predict the chemical composition that could be obtained from different sections of the aircraft fuselage under study.

3. Study the theoretical refining of Al by a fractional crystallization process emphasising the reduction of Fe and Si and the Al yield at different processing conditions.

4: Thermal Decoating of Aerospace Aluminum Alloys for Aircraft Recycling[3]

J.A. Muñiz-Lerma†, I.-H. Jung†, and M. Brochu*†

† Department of Mining and Materials Engineering, McGill University, 3610 University Street, Wong Building, Montreal, QC, H3A 0C5, Canada

4.1: Preface

During the aircraft recycling process, the presence of a corrosion protection coating in aircraft Al alloys is an important source of impurities that must be removed prior to the scrap melting process. To the best of the author's knowledge, the following chapter explores for the first time the removal of such coatings using a thermal processing route. Certain processing parameters such as decoating temperature and residence time, as well as the determination of the energy barrier required for thermal decoating and the characterization of the residues, which are potential airborne contaminants of the process, were investigated and discussed in the results section of the chapter.

4.2: Abstract

Recycling of aircraft Al alloys can be complex due to the presence of their corrosion protection coating that includes inorganic compounds containing Cr(VI). In this study, the characterization and thermal degradation behavior of the coating on Al substrates coming from an aircraft destined for recycling are presented. Elements such as Sr, Cr, Si, Ba, Ti, S, C, and O were found in three different layers by EDS elemental mapping corresponding to $SrCrO_4$, Rutile-TiO_2, SiO_2, and $BaSO_4$ with an overall particle size D_{50}= 1.96 μm. The thermal degradation profile analyzed by

---

3 Published: **Muñiz Lerma, J.A.,** Jung, I. H., Brochu, M., *Thermal Decoating of Aerospace Aluminum Alloys for Aircraft Recycling.* Met. Trans. B, 2016. p. 1-10.

DOI: 10.1007/s11663-016-0629-6

TGA showed four different stages. The temperature of complete degradation at the fourth stage occurred at 753.15 K (480 °C) at lower heating rates. At higher heating rates and holding an isotherm at the same temperature, the residence time to fully decompose the aircraft coating has been estimated as 4.0 ± 0.2 min. The activation energy calculated by the Flynn–Wall–Ozawa and the modified Coats-Redfern methods for multiple fraction of decomposition showed a non-constant behavior indicating the complexity of the reaction. Finally, the concentration of Cr(VI) released to the environment during thermal decoating was obtained by UV–Vis spectroscopy. It was found that 2.6 ± 0.1 μg of Cr(VI)/mm^2 of Al substrate could be released unless adequate particle controls are used.

4.3: Introduction

Aluminum is one of the most widely used metals in the world after steel [4.1]. The high demand of Al is due to the unique combination of its physical properties such as relatively high strength combined with low weight for exceptional strength/density ratios, very high corrosion resistance, and toughness. Furthermore, its ability to be readily recycled without the loss of product integrity and minimal material loss through oxidation is known to be its most significant property [4.2]. Recycling, which is defined as the use of waste as feedstock to produce products with applications distinct from disposal, is highly relevant in the Al industry because of the energy savings that it represents. Recycling Al requires only ~2.8 kWh of energy per kg and emits just ~0.6 kg of CO_2/kg of Al compared to the extraction of Al from bauxite which consumes around ~45 kWh/kg of Al and emits around ~12kg of CO_2/kg of Al [4.3]. Thus, recycling Al has the potential to save 95 % of the energy cost and environmental emissions related to the production of primary Al, helping to increase the sustainability of the Al industry.

Generally, the Al recycling process involves two fundamental steps: scrap pre-treatment and refining, where the main aim of the process is to decrease the amount of impurities during recycling [4.4]. One of the main impurities found in Al scrap is the organic or organic/inorganic coating which provides the Al substrates with corrosion protection and esthetics [4.5]. However, this coating is responsible for increasing the amount of metal lost by oxidation, gaseous emissions, and salt flux disposal once Al is recycled. Through scrap pre-treatment, a thermal process called

decoating is carried out. This process consists of the thermal degradation and/or oxidation of the coating compounds from the Al substrates, minimizing the above-mentioned problems during re-melting of recycled Al [4.6].

In order to understand and optimize the decoating process, kinetic and thermal studies have been carried out on polyester-coated Al substrates, as well as on used beverage cans, and painted Mg alloys in automotive objects [4.7-4.11]. However, no studies have been found in the literature corresponding to the thermal decoating of aircraft Al alloys during recycling, which is currently a topic of interest for the aerospace industry. Up to now, aerospace recycling practices include aircraft dismantling and the reuse of high tech equipment, while the remaining metallic components of the aircraft, which contain between 65 and 75 % of coated Al alloys, are disposed of in graveyards where they will need treatment before being recycled [4.12, 4.13].

In general aviation (GA), a three-layered coating system is used as corrosion protection for aircraft Al alloys [4.14]. This coating system is mainly made up of a surface treatment, an epoxy-polyamide primer, and a polyurethane topcoat. The surface treatment consists of an amorphous layer primarily composed of mixed hydrated Cr(III)/Cr(VI) oxide with a ratio close to 3:1 [4.15, 4.16]. The epoxy-polyamide primer consists of an epoxy-polyamide matrix containing chromate pigments such as barium chromate ($BaCrO_4$) or strontium chromate ($SrCrO_4$) and fillers [4.17]. Finally, the topcoat is made up of a polyurethane layer that contains inorganic pigments, which protects against environmental erosion and mechanical abrasion of the Al alloys [4.18].

Similar to the recycling of used beverage cans and automotive Al scrap, the recycling process of GA aircraft Al alloys requires a decoating process to remove the layered coating system used for corrosion protection. Thus, it is important to understand the kinetics and thermal degradation behavior of this layered coating attached to aircraft Al components. In addition, it is worth mentioning that Cr(VI), which is present in the epoxy-polyamide primer as $BaCrO_4$ or $SrCrO_4$ [4.19], is responsible for promoting cancer in the respiratory system even at low concentration. As a result, the maximum permissible exposure limit (PEL) for Cr(VI) established by the Occupational Safety and Health Agency (OSHA) is considered to be 0.005 mg/m^3 of air as an 8 h time-weighted average (TWA) [4.20]. Taking this exposure limit into consideration, it is

imperative to quantify the content of Cr(VI) contained in the epoxy-polyamide primer on the aircraft prior to recycling.

This paper presents a fundamental characterization of the layered coating attached to aircraft Al substrates and the degradation behavior of said coatings under specific thermal conditions. The characterization is mainly focused on the identification of inorganic phases present in the coating to identify changes in phase composition after thermal treatment, specifically the inorganic phases containing Cr(VI). The thermal degradation behavior will be defined using the determination of the energy barrier as well as the required time to promote complete decoating of the layers on aircraft Al substrates. Thermogravimetric analysis (TGA), field Emission scanning electron microscopy (FE-SEM), X-Ray diffraction (XRD), Raman spectroscopy (RS), and ultraviolet-visible spectroscopy (UV-Vis) were used to characterize the samples.

4.4: Experimental Procedure

An Al substrate (AA 7075) coated with a GA-layered corrosion protection coating, was obtained from the bottom skin of the horizontal stabilizer section of a CRJ-100ER regional aircraft subjected to recycling. The coating characterization was carried out by field emission scanning electron microscopy (FE-SEM) using a Hitachi SEM SU3500 coupled with energy dispersive X-Ray spectroscopy (EDS). The sample preparation for SEM analysis was performed following the procedure proposed by Farrier et al. [4.21]. In order to identify the phases present in the primer coating, X-Ray diffraction analysis (XRD) and Raman spectroscopy were carried out. XRD analysis was achieved by using a Phillips PW1070 diffractometer (Cu Kα λ=1.54056 Å) with a step size of 0.02 ° and a dwell time of 0.2 s/step. On the other hand, Raman spectroscopy was performed by using a Renishaw inVia Raman microscope equipped with a low-power (25 mW) argon-ion laser (514.5 nm). The Raman analysis was carried out using 10 % of the laser power (2.5 mW) and an exposure time of 10 s.

Thermogravimetric analysis (TGA) was used to study the decoating process. For this purpose, the thermal degradation behavior and the corresponding activation energy of the coated Al substrates were achieved with a TGA-Q500 instrument. The size of the samples was determined based on

the limitations of the equipment. Thus, small coupons of 40 ± 5 mg were cut from the previously mentioned Al substrate. The coupons were heated up to 823 K (550 °C) using four different heating rates: 5, 10, 15, and 20 K/min and an air flow rate of 60 mL/min. Then, the samples were isothermally held at the selected temperature for 20 minutes.

In order to determine the residence time required to thermally decompose the aircraft coating, three experiments were conducted for each condition presented in Table 4-1. The isotherm section had a duration of 30 minutes; and the residence time was estimated from the beginning of the isotherm until the end point of the last reaction using the TA instruments Universal Analysis 2000 version 4.2E software.

To determine and quantify the amount of Cr(VI) present in the coated substrates, a bottom external doubler part from the horizontal stabilizer made of AA 2024 was used. It is worth to mention that this part was selected because it only contains a chromate conversion coating and a layer of a fluid-resistant primer which facilitates the analysis of Cr(VI) without the effect of the topcoat. To estimate the mass of primer contained per surface area of Al, three coated substrates of approximately 20 x 18 mm were weighted. Then, the substrates were immersed into a commercial stripping solution Greensolv 274WL at 80 °C until the coating was totally removed and the primer mass was estimated by mass difference between the coated and un-coated substrates. To quantify the amount of Cr(VI), the primer from the aircraft component was scratched with the aim to obtain pure primer flakes. The scratched primer flakes were then dry milled at ambient temperature and digested in an alkaline solution following the procedure EPA 3060A. Three samples of 25 ± 1.5 mg of the milled primer were placed into separate beakers. Then, 50 mL of a digestion solution, which was prepared previously by the dissolution of 20 mg of NaOH and 30 mg of Na_2CO_3 in reagent water in one-liter volumetric flask, was added followed by the addition of 400 mg of $MgCl_2$. Subsequently, the samples were heated up to around 363 K (90 °C) and 368 K (95 °C) with continuous magnetic stirring. After heating, the samples were gradually cooled without removing the magnetic stirring until room temperature was reached. Once cooled down, the samples were filtered through a 0.45 µm filter paper, and their pH was adjusted to 7.5 ± 0.5 with the addition of 5 M HNO_3 solution. Then the determination of Cr(VI) present in the primer was performed by a Perkin Elmer Lambda 20 UV-Vis Spectrometer following the colorimetric EPA method 7196A. Standard solutions containing 0.5, 1, and 3 ppm of $K_2Cr_2O_7$ were prepared, and a

calibration curve was created. As a means to develop the color of the samples and standards, 95 mL of the digested solutions and standards were transferred to a 100 mL volumetric flask. Subsequently, 2 mL of a diphenylcarbazide solution (250 mg of 1,5-diphenylcarbazide in 50 mL of acetone) was added to the transferred solutions and standards, followed by the addition of 10 % H_2SO_4 solution with the aim to reduce the pH to 2 ± 0.5. Finally, an appropriate quantity of the solutions and standards were transferred to a 1 cm absorption cell where their absorbance was measured at 540 nm.

Table 4-1. Experimental conditions to determine the decoating residence time

Condition	Heating rate K/min	Isotherm K (°C)
1	50	723.15 (450)
2	75	
3	100	
4	50	743.15 (470)
5	75	
6	100	
7	50	753.15 (480)
8	75	
9	100	
10	50	773.15 (500)
11	75	
12	100	

4.5: Results and Discussions

4.5.1: Aircraft Coating Characterization

Figure 4-1, shows the EDS compositional map corresponding to the cross section of the coated Al substrate. It can be clearly seen that the coating is made up of three different layers. These layers correspond to a primer, a sanding surfacer, and topcoat [4.22] with thicknesses of approximately 12 ± 2 µm, 20 ± 2 µm, and 73 ± 2 µm respectively. The first and second layers (from bottom to top) are heterogeneous materials containing inorganic compounds embedded into an organic

matrix, while the third layer contains essentially an organic matrix. In the EDS compositional map, the signals of Ti kα and Ba Lα overlaps each other. However, the presence of S signal in the sanding surfacer section suggests the presence of the extender $BaSO_4$ instead of the TiO_2 pigment in this section. Nevertheless, Ti in the form of TiO_2 might be present in the primer coating since the EDS map of this element shows and intense band in the bottom part that is not present in the Ba and S maps. Thus, elements such as Sr, Cr, Si, Mg, Ti, C, and O are mainly present in the primer, while Ba, S, C, and O are present in the sanding surfacer.

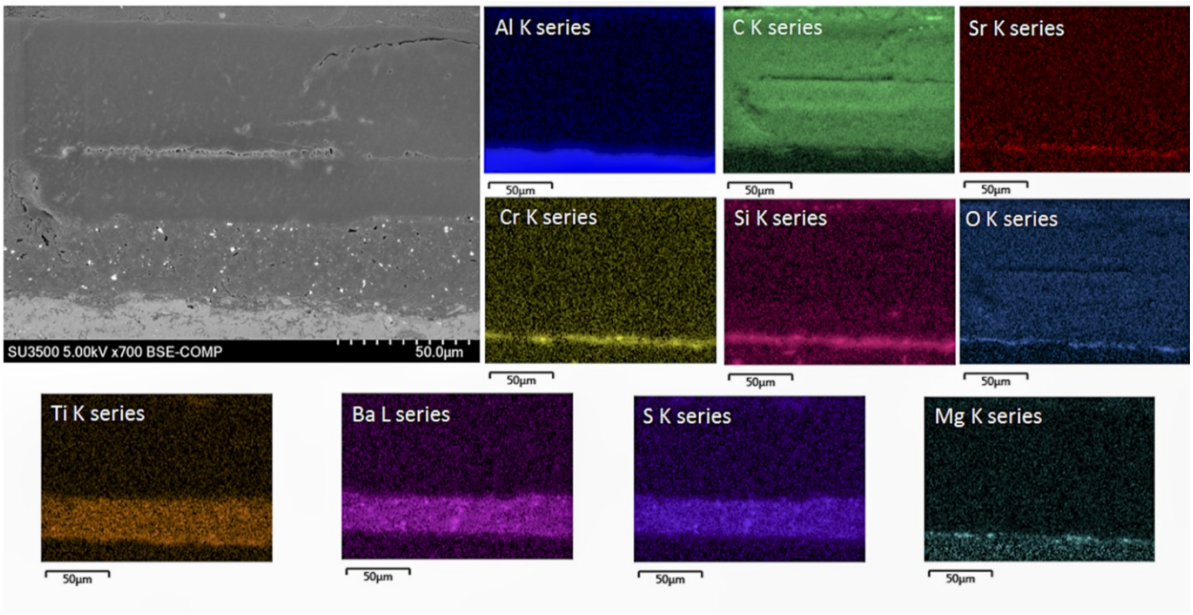

Figure 4-1. Backscattered electron micrograph corresponding to the cross section of a coated Al substrate and its elemental mapping.

In order to identify the inorganic phases of the primer, XRD analysis was carried out in this section. The analysis shown in Figure 4-2, provides evidence for a number of crystalline phases[4], including aluminum (Al), titanium dioxide (Rutile-TiO_2), strontium chromate ($SrCrO_4$), and silicon dioxide

[4] The crystalline phases were identified using the JCPDS cards 00-004-0787, 00-021-1276, 00-035-0743, and 01- 085-0457 from the PANanalytical X'pert high-score plus ICDD PDF 2003 database.

(quartz-SiO_2). The Al peaks correspond to the Al substrate while the $SrCrO_4$, TiO_2, and the SiO_2 peaks represent the corrosion inhibitor, pigment, and extender, respectively [4.23]. Based on the XRD analysis, most of the elements found by elemental mapping in the primer section were indexed by an inorganic phase; nevertheless, Mg could not be accounted for by indexing. However, it is well known that magnesium silicate, typically Talc-$Mg_3Si_4O_{10}(OH)_2$, is used as extender pigment in paint systems [4.23]; thereby, this phase could be overlapped in the XRD analysis with the $SrCrO_4$ peaks at 2θ angles of 25.7, 27.3, 28.5, 35.9, 53.02, and 54.04.

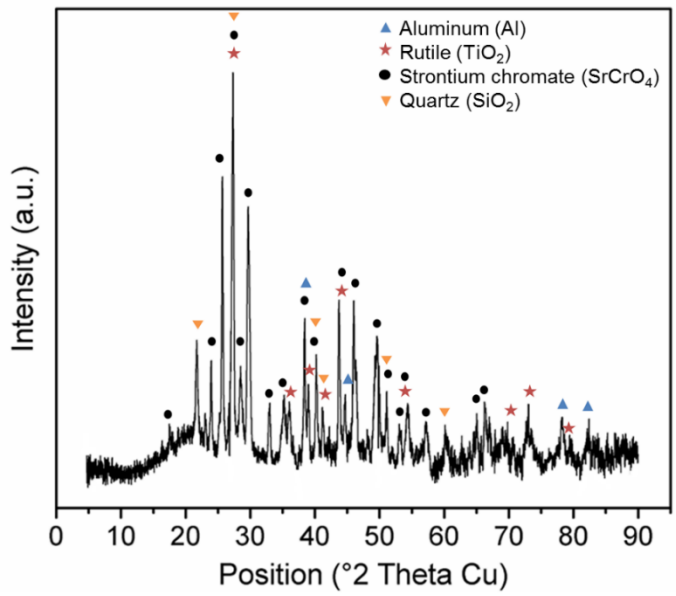

Figure 4-2. X-ray diffraction analysis of the primer layer.

According to Figure 4-3, the phases are present in different morphologies such as spherical, irregular, and plate-like particles. These particles vary in size from submicron up to 12 µm with a cumulative particle size distribution as shown in Figure 4-4. The median, D_{50}, corresponds to 1.96 µm, D_{10} to 0.91 µm, and D_{90} to 3.21 µm. Broad size distributions of inorganic particles in chromate-inhibited primers have been previously reported by Scholes et al. [4.24], with sizes ranging from submicron up to 10 µm, and by Lapuma et al. [4.19] from submicron up to ~ 35 µm with a distribution D_{50} of 5.5 µm.

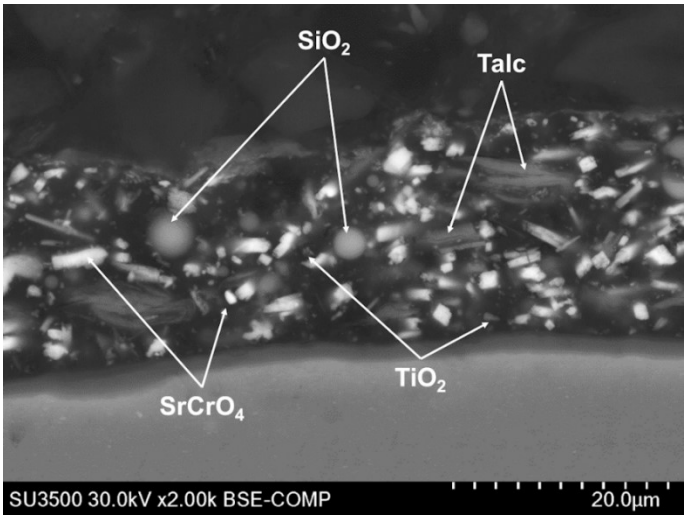

Figure 4-3. Detailed BSE micrograph of the inorganic compounds contained in the primer.

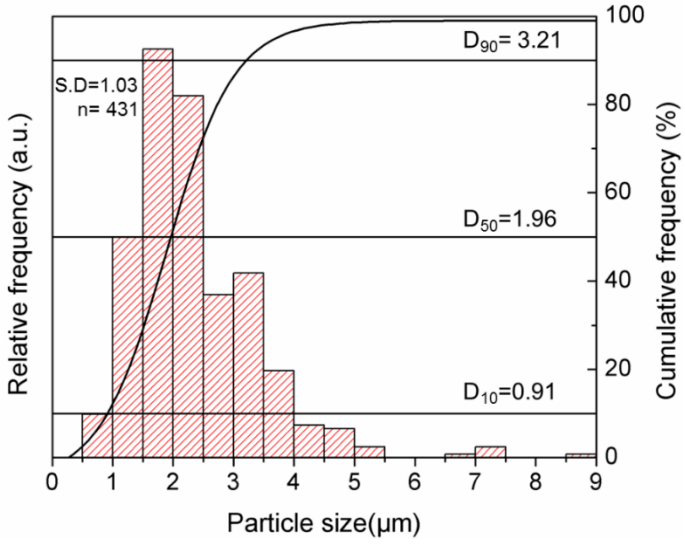

Figure 4-4. Particle size distribution of the inorganic compounds contained in the primer.

4.5.2: Thermal Analysis

Representative aircraft Al substrates before and after thermal decoating are shown, respectively, in Figure 4-5 (a) and (b). Before thermal decoating, the paint had a smooth and shiny surface. After decoating, the organic compounds present in the polymer matrix were fully degraded. However, a rough layer of gray and green colored residue, corresponding to the inorganic pigments and fillers of the paint, remained attached to the substrate indicating partial decoating. Therefore, a mechanical force applied by rubbing was necessary to completely decoat the Al substrates. This observation was also made by Meskers et al. [4.7] in their studies of decoating Mg substrates.

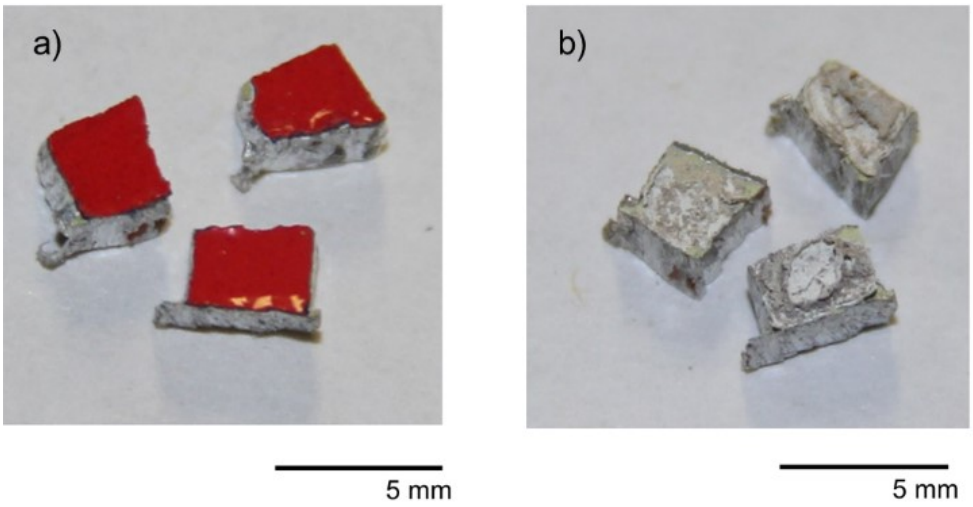

Figure 4-5. Aircraft Al substrates before and after decoating

The thermogravimetric traces presented in Figure 4-6, show the thermogravimetry (TG), the derivative thermogravimetry (DTG), and the deconvoluted DTG curves obtained by the decomposition of the coated Al substrates at heating rates of 5, 10, 15, and 20 K/min and 60 ml/l of air flow. By TG analysis, the overall weight loss at the end of the decoating process was evaluated using twelve samples (three samples per heating rate). The results showed an average weight loss of 5.0 ± 0.2 %, which corresponds to the organic matrix of the coating used in the aircraft Al substrates. The obtained thermal degradation profiles are similar to the ones from

polyurethane polymers [4.25-4.27], which are commonly used as fluid-resistant coatings in aerospace applications [4.14].

As in the case of polyurethane polymers, the DTG curves of the aircraft-coated Al substrates indicate that the thermal degradation of the coating occurs in four main different stages. This is indicated in the thermogravimetric traces with the numeric notation from 1 to 4. The first degradation stage of these polymers is characterized by the breaking of the polymer chains. The second and third stages correspond to the decomposition of compounds with high molecular weight leaving char on the substrate. Finally, in the last stage of the process, the remaining char is degraded forming a thin film of inorganic particles on the substrate. However, according to a deconvolution and fitting treatment of the obtained DTG curves carried out using a Lorentzian multi-peak curve, the first part of the degradation process is split into two peaks giving the first and second degradation stage. Additionally, two deconvoluted peaks are necessary to fit the third degradation stage. This observation suggests that a complex degradation process may be taking place [4.26], a detailed explanation will be given at the end of this section.

During decoating processing, the temperature of the kiln and residence time of the scrap are among the most important parameters to control in order to avoid melting and oxidation of the Al substrates [4.5]. In TGA, the temperature of the reaction peak maxima (T_p) is defined as the temperature where the maximum rate of mass loss occurs in every stage of decomposition. Hence, the minimum kiln temperature will correspond to the lowest temperature that permits the completion of the four degradation stages. In this context, the T_p of each degradation stage at different heating rates are observed in Table 4-2. It is evident that T_p temperatures were displaced to higher temperatures as the heating rate was increased. This peak shifting has been attributed by various authors to the effect of heat transfer, which promotes thermal lag resulting in a delayed decomposition temperature [4.9, 4.11, 4.28, 4.29].

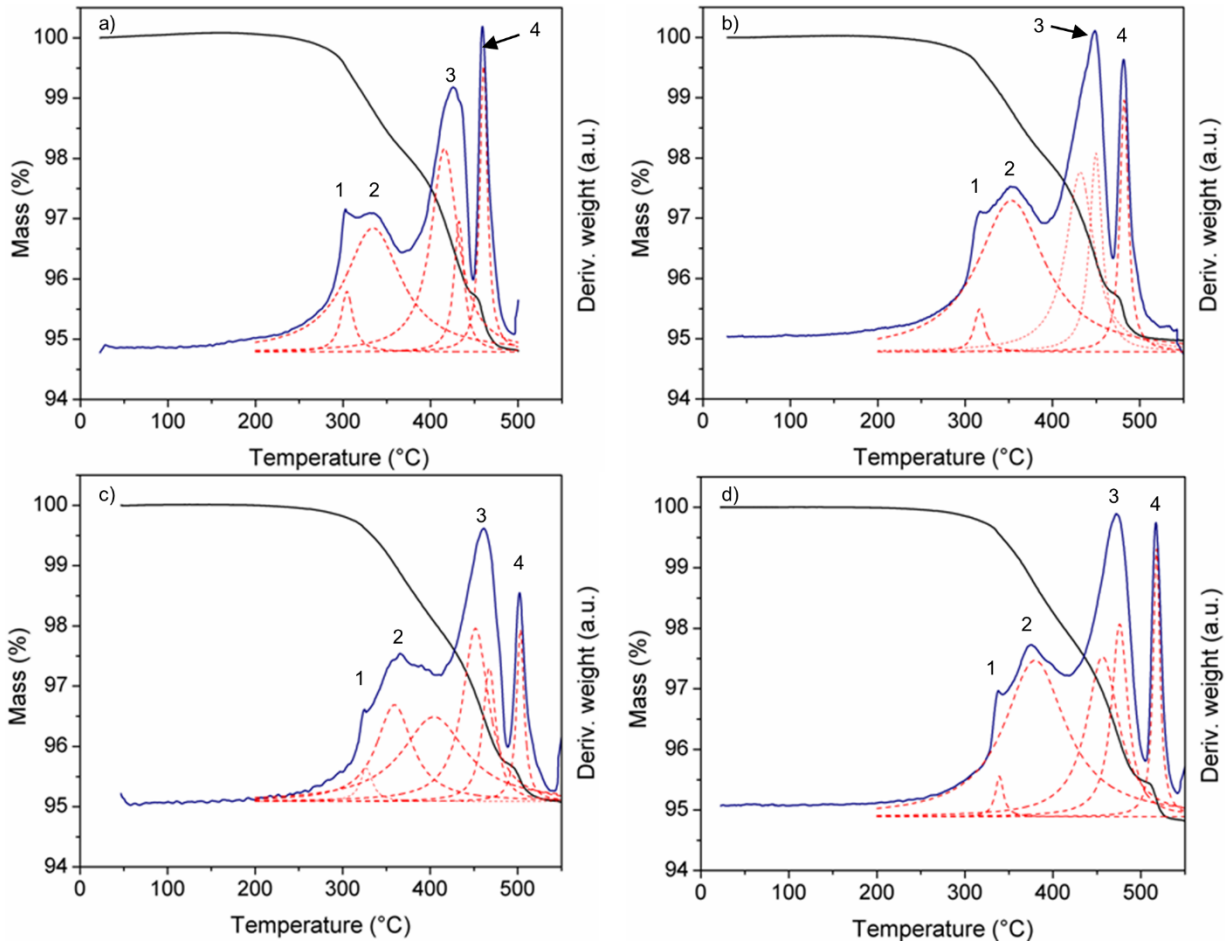

Figure 4-6. Decomposition thermograms of coated Al substrates showing the TG, DTG, and the deconvoluted DTG curves5 at (a) 5 K/min, (b) 10 K/min, (c) 15 K/min, and (d) 20 K/min.

Based on the obtained T_p at the last degradation stage shown in Table 4-2, the coating of the Al substrates used in this study can be decoated by non-isothermal processes at lower heating rates, i.e., lower than 10 K/min. At this heating rate, the minimum kiln temperature to promote complete coating decomposition corresponds to 753 ± 1.7 K (480 ± 1.7 °C). This temperature is not above the solidus temperatures of the typical alloys used in aircraft applications such as AA2024 and AA7075. Thus, thermal decoating is possible without melting the substrates. However, long decoating times of approximately 48 minutes are expected at this heating condition.

[5] The COD R^2 values are 0.97 (5 K/min), 0.98 (10 K/min), 0.97 (15 K/min), and 0.98 (20 K/min).

Table 4-2. Reaction peak maximum temperatures at every stage of decomposition and different heating rates.

Heating rate (K/min)	Temperature peak maxima, T_p K (°C)			
	Stage 1	**Stage 2**	**Stage 3**	**Stage 4**
5	576 ± 0.4 (303)	597 ± 3.2 (324)	697 ± 3.5 (424)	727 ± 7.6 (454)
10	588 ± 0.2 (315)	621 ± 4.4 (348)	716 ± 3 (443)	753 ± 1.7 (480)
15	596 ± 2.7 (323)	636 ± 2.3 (363)	731 ± 2.9 (457)	773 ± 1.7 (500)
20	608 ± 9.3 (335)	645 ± 3.7 (372)	743 ± 2.4 (470)	789 ± 2 (516)

With the aim to reduce the decoating time, the effect of the isotherm temperature and the heating rate on the residence time was studied. Four isotherms were selected and three different heating rates were employed to reach each isotherm. Then, the residence time was estimated as the required time to completely decompose the coating after the selected isotherms were reached. The dependence of the isothermal temperature and the heating rate on the residence time is observed in Figure 4-7. As the isothermal temperature is decreased from 773 K (500°C) to 723 K (450 °C), the residence time increases exponentially for each heating rate. Furthermore, as the heating rate is increased from 50 to 100 K/min to reach the isotherm section, the residence time is decreased. These effects are attributed to the thermal decomposition kinetics which is parameterized in terms of temperature and conversion rate [4.30]. Thus, based on the previous results and considering the solidus temperatures of aircraft Al alloys, the optimum decoating temperature for an isothermal process is 753 K (480 °C). This temperature yields a residence time of 4.0 ± 0.2 minutes for the three different heating rates. It is nevertheless important to mention that the residence time was estimated based on laboratory scale. Therefore, further research has to be done to determine the industrial processing parameters such as feeding rate, scrap size, and chamber temperature in order to achieve the recommended heating conditions.

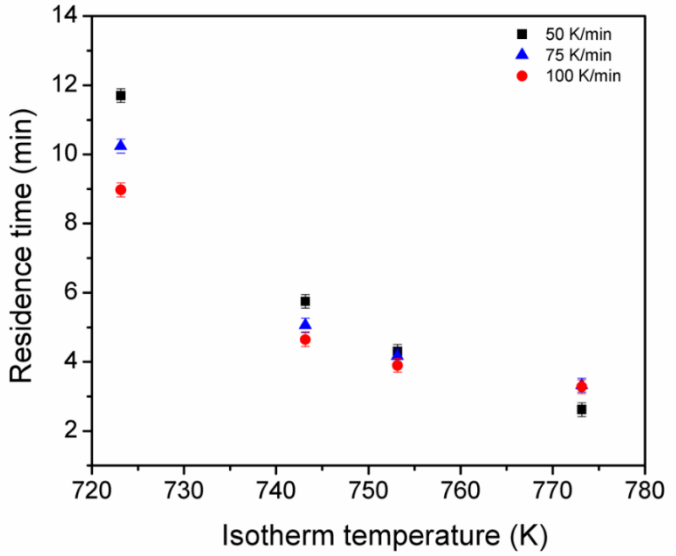

Figure 4-7. Dependence of isotherm temperature and heating rate on the decoating residence time.

In order to determine the energy barrier required to promote decoating, the kinetic of degradation was determined in terms of activation energy E_a following the recommendations of the ICTAC Kinetics committee [4.30]. Two different methods were used in this study to obtain E_a at every fraction of decomposition α. The first method corresponds to the isoconversional Flynn-Wall-Ozawa, which is represented by the Equation 4-1 [4.31, 4.32]:

$$\log \beta = \log \left[A \frac{f(\alpha)}{d(\alpha)/dT} \right] - \frac{E_a}{RT} \qquad \text{Equation 4-1}$$

where β is the employed heating rate, A and E_a the kinetic parameters, the exponential factor and the activation energy respectively, R represents the universal gas constant, $f_{(\alpha)}$ corresponds to the reaction model, and T is the temperature at constant fraction of decomposition α. This method calculates E_a/R from the slope m of the line obtained by plotting $log\ \beta$ against $1/T$ at every α. Then, activation energy E_a is obtained and refined by means of the Doyle approximation implemented in the ASTM E1641 using the Equation 4-2 where b corresponds to a numerical integration constant, until a change of less than 1% in E_a was observed.

$$E_a = -\frac{R}{b}[m] \qquad \text{Equation 4-2}$$

On the other hand, the second isoconversional method employed in this work was the multi-heating rate application of the Coats-Redfern equation modified by Burnham and Braun which is represented in the Equation 4-3 [4.33].

$$\ln\left[\frac{\beta}{T^2\left(1-\frac{2RT}{E_a}\right)}\right] = -\frac{E_a}{RT} + \ln\left(-\frac{AR}{E_a \ln(1-\alpha)}\right) \qquad \text{Equation 4-3}$$

By means of this method, E_a is calculated by plotting the left side of the Equation 4-3 against *1/T* for each heating rate at fixed α assuming that $(1-2RT/E_a)$ is constant [4.34]. This plot will provide a straight line with slope $m = (-E_a/R)$ for every α. Then E_a is obtained by simple isolation for every α.

The plots of log β vs *1/T* (Flynn-Wall-Ozawa method) and $-\ln(\beta/T^2)$ vs *1/T* (Coats-Redfern modified method) are shown in Figure 4-8 (a) and (b), respectively. The regression analysis of the data points provided slopes, which were used to determine the activation energies, E_a for every 0.1 variation of α as shown in Table 4-3. The highest activation energy required to fully decompose the aircraft coating was obtained at the last degradation step being ~170 kJ/mol. This energy is within the highest energy required to thermally decompose automotive scrap (161-170 kJ/mol) and polyester-coated Al substrates (162 ± 9 kJ/mol), which were also obtained at the last degradation step [4.7,4. 9]. Thus, this energy barrier might be related to the combustion of char as it has been proposed by Kvithyld *et al.* [4.9].

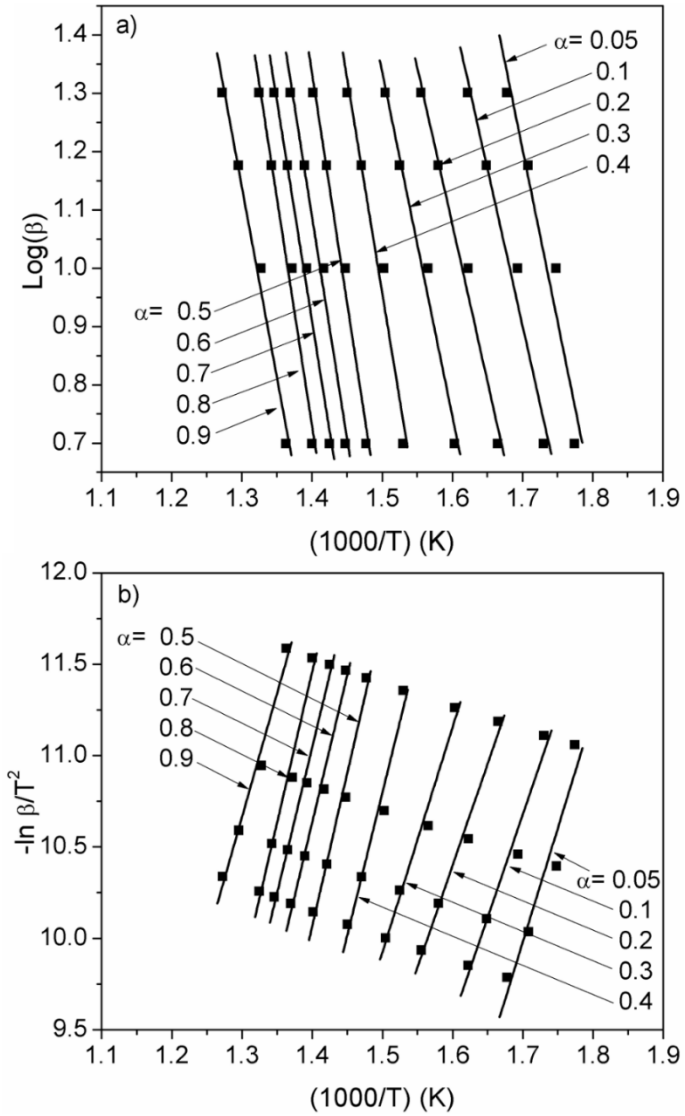

Figure 4-8. Dependence of (a) log β vs 1/T and (b) ln (β/T^2) vs 1/T used to obtain the activation energy by the Flynn-Wall-Ozawa and the modified Coats-Redfern methods, respectively.

Table 4-3. Activation energy Ea at each decomposition fraction α calculated by the Flynn-Wall-Ozawa and the modified Coats-Redfern methods

α	Flynn-Wall-Ozawa		Coats-Redfern (modified)		Segmented polyurethane[26]
	E_a (kJ/mol)	R^2	E_a (kJ/mol)	R^2	E_a (kJ/mol)
0.1	93 ± 3	0.97	93 ± 12	0.96	108
0.2	93 ± 2	0.98	93 ± 9	0.98	114
0.3	103 ± 2	0.98	102 ± 9	0.97	124
0.4	130 ± 3	0.97	130 ± 16	0.96	132
0.5	138 ± 3	0.98	139 ± 13	0.98	146
0.6	134 ± 2	0.98	134 ± 12	0.98	132
0.7	133 ± 2	0.99	132 ± 9	0.98	132
0.8	137 ± 3	0.98	137 ± 14	0.97	162
0.85	170 ± 3	0.98	170 ± 16	0.98	-
0.9	112 ± 2	0.98	113 ± 10	098	-
Maximum E_a	170 ± 3	-	170 ± 16	-	162

Further analysis of the activation energy behavior during decoating of the aircraft components is shown in Figure 4-9. It can be observed that the activation energy over the entire decomposition fraction α is not constant. This variation indicates the complexity of the decomposition process of the coating which can be dominated by multiple reactions [4.34]. At lower α values (α=0.05 to 0.15), the activation energy decreases from 103 kJ/mol to 89.9 kJ/mol. Then, activation energy increases up to 130 kJ/mol from α=0.15 to 0.4. This range of α values (from 0.05 to 0.4), corresponds to the first and second stage of thermal degradation reported in Table 4-2 that might be associated with the removal of volatile components, trapped gas, and low molecular weight materials present in the system [4.7, 4.9-4.11]. On the other hand, at medium α values (α=0.4 to 0.8) which correspond to the third stage of degradation, the variation of the activation energy at each fraction of decomposition becomes much smaller. This variation creates a slight decline followed by an increase giving rise to a small dip that could be associated with the statistical error. However, the presence of two deconvoluted peaks at this stage of decomposition indicates that more than one reaction with similar activation energy is taking place [4.30, 4.34]. The activation energy obtained at medium α values, might correspond to the energy necessary to promote bond

scission and further evaporation of higher molecular weight materials in the coating [4.7, 4.9-4.11]. Finally, at higher α (α=0.8 to 0.95), the activation energy suddenly increased up to 170 kJ/mol at α= 0.85 to subsequently decrease to 91.57 kJ/mol at α=0.95. From the graph in Figure 4-9, it can be observed that the higher value of activation energy matches the abrupt change in the curve of α vs temperature at α= 0.85. Based on this observation, we can conclude that the values observed at α=0.8 to 0.95 correspond to the last degradation stage of the coated Al substrates used in these experiments. This last degradation stage is related to the combustion of carbon to yield CO_2, leaving the inorganic compounds of the coating on the Al substrate [4.10].

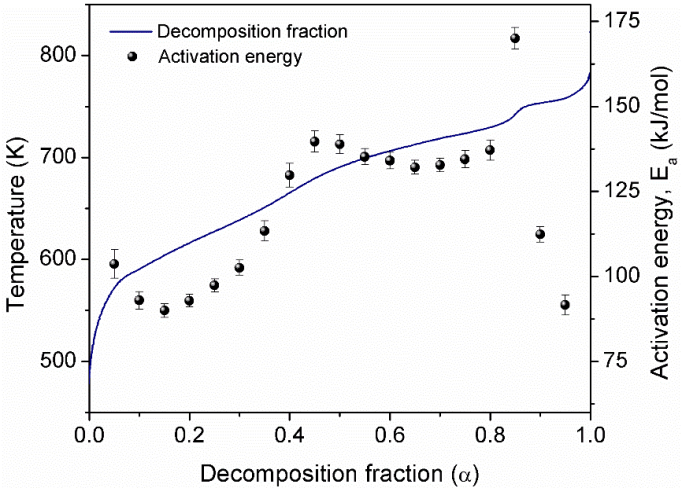

Figure 4-9. Decomposition fraction under non-isothermal conditions obtained at 10 K/min, and the relationship between Ea and α estimated by the Flynn-Wall-Ozawa method.

4.5.3: Cr(VI) Determination and Decoating Residues Characterization

The average concentration of Cr(VI) obtained per mg of scratched primer corresponds to 36.566 ± 0.002 µg/mg of primer. This value might be lower than the concentration of Cr(VI) obtained by fresh primers, which has been determined by other authors to be around 67 µg/mg of dry primer [4.19]. However, during the service life of an aircraft, the fuselage is usually exposed to different environmental conditions such as low humidity, high humidity, and corrosive environments. Due to this exposition, the chromate contained in the primer can be released decreasing its initial

concentration [24, 35, 36]. In order to quantify the amount of Cr(VI) per surface area, a measurement of the primer mass contained per mm^2 of Al substrate was carried out. It was found that approximately 72 ± 8 µg of primer was present in 1 mm^2 of substrate. Therefore, the amount of Cr(VI) per surface area was estimated as 2.6 ± 0.1 µg of Cr(VI) per mm^2 of Al substrate.

After thermal decoating processing, the XRD pattern of the residues did not present a significant difference compared with the XRD pattern in Figure 4-2. Additionally, the Raman spectrum shown in Figure 4-10, displays bands corresponding to $SrCrO_4$ in the frequencies 339, 348, 374, 859, 866, 893, 915, and 929 cm^{-1}, which agrees with the data base published by Burgio *et al*. [4.37] and a report on cured epoxy-polyamide primers by Scholes *et al*. [4.24]. In addition to these bands, peaks at frequencies 447 and 612 cm^{-1} were also found which correspond to Rutile-TiO_2 [4.38]. However, the strong band of Quartz-SiO_2 located at 466 cm^{-1} [4.37] was not observed. We attribute the failure to observe this band to the low signal intensity and to the overlapping of this peak with the wide band of TiO_2 centered at 447 cm^{-1}.

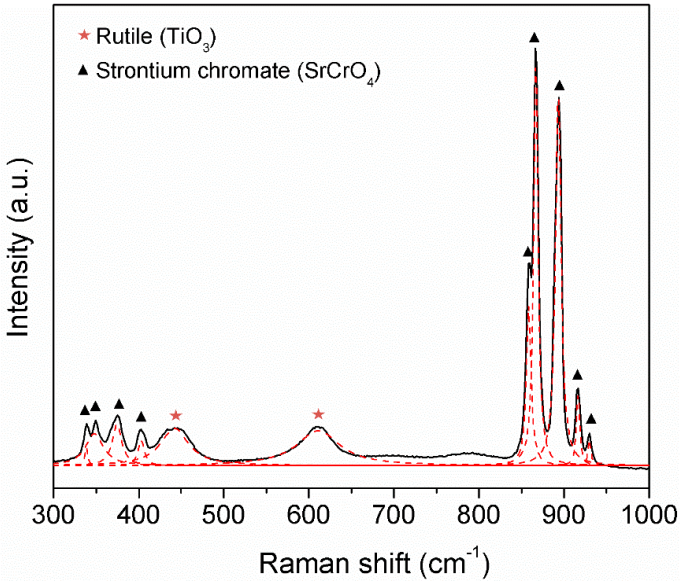

Figure 4-10. Raman spectra of the decoated residues.

According to these results, the inorganic compounds present in the primer did not suffer any change in phase composition after thermal treatment due to their high thermal stability as reported

by other authors [4.39-4.42]. Thus, the Cr(VI) compound and the rest of the residues, can be considered as airborne pollutants with particle size D_{50}= 1.96 μm that can be deposited in the human trachea and bronchioles [4.19]. Furthermore, the concentration of $SrCrO_4$ contained in the aircraft Al substrates after decoating processing, could exceed the maximum permissible values reported by OSHA in the absence of adequate particle matter controls such as those recommended by the 29 CFR 1910.1026 [4.20].

4.6: Conclusions

The characterization of the coating system of the aircraft Al substrates employed in this work was carried out. An organic/inorganic coating system consisting of three different layers was observed. These layers contained a mixture of inorganic phases identified as $SrCrO_4$, Rutile-TiO_2, SiO_2, and $BaSO_4$, and Talc-$Mg_3Si_4O_{10}(OH)_2$ which are not modified after thermal treatment. The thermal degradation profiles of the coated Al substrates showed four stages of decomposition and a total mass loss of 5 ± 0.2%. The first and second stages are associated with the removal of volatile components, trapped gas, and low molecular weight materials. The third stage might be related to the bond scission and further evaporation of higher molecular weight materials of the coating while the fourth stage corresponds to the combustion of char. The optimum required temperature to promote thermal decoating of the aircraft Al coatings was found to be at an isotherm of 753.15 K (480 °C). The residence time for thermal decoating at this temperature was estimated as 4.0 ± 0.2 min. On the other hand, the energy barrier that has to be overcome for thermal decoating was determined as 170 kJ/mol by the Flynn-Wall-Ozawa and the modified Coats-Redfern methods. Finally, the estimated concentration of Cr(VI) contained in the corrosion inhibitor ($SrCrO_4$) per surface area was 2.6 ± 0.1 μg of Cr(VI)/mm^2 of Al substrate. After thermal decoating, the Cr(VI) may be present as an inorganic residue of strontium chromate.

4.7: Acknowledgments

The authors would like to thank the Consortium de Recherche et d'Innovation en Aérospatiale au Québec (CRIAQ), Bombardier, Bell Helicopter, Sotrem-Maltech, BFI, Nano Quebec, and Aluminerie Alouette for funding this project, as well as the Secretary of Public Education of México for the complementary scholarship awarded to one of the authors.

4.8: References

[4.1] U.S. Geological Survey, Mineral Commodity Summaries 2012: U.S. Geological Survey. 198, Reston, Virgina, 2012.

[4.2] Das, S.K. and W. Yin, JOM, 2007. Vol. 59(11): p. 57-63.

[4.3] Green, J.A.S., Aluminum Recycling and Processing for Energy Conservation and Sustainability. 1-271, ASM International, 2007.

[4.4] Nancy, M., Energy and Environmental Profile of the U.S. Aluminum Industry, Prepared for the U.S. Department of Energy Office of Industrial Technologies. Energetics, INC., Columbia, Maryland, 1997.

[4.5] Kvithyld, A., Meskers, C. E. M., Gaal, S., Reuter, M., Engh, T., JOM, 2008. Vol. 60(8): p. 47-51.

[4.6] Schlesinger, M.E., Ilegbusi, O.J., Iguchi, M., Wahnsiedler, W., Aluminum Recycling. CRC PressINC, United States, 2007.

[4.7] Meskers, C.E.M., Reuter, M. A., Boin, U., Kvithyld, A., Metall. Mater. Trans. B, 2008. Vol. 39(3): p. 500-517.

[4.8] Kvithyld, A., Gaal, S., Kowalewski, P., Engh, T. A., TMS Annual Meeting & Exhibition. 1091-1095, 2003.

[4.9] Kvithyld, A., T.A. Engh, and R. Illes, TMS Annual Meeting & Exhibition. 1055-1060, 2002.

[4.10] Kvithyld, A., J. Kaczorowski, and T.A. Engh, TMS Annual Meeting & Exhibition. 151-156, 2004.

[4.11] Zuo, X. and L. Zhang, TMS Annual Meting & Exhibition. 1107-1112, 2008.

[4.12] Itzkowitch, Z. 1ere PIateforme europeenne de demantelement aeronautique, Dossier de presse Bartin AERO Recycling. 2008.

[4.13] Asmatulu, E., M. Overcash, and J. Twomey, J. Ind. Eng., 2013. Vol. 2013: p. 1-8.

[4.14] Chattopadhyay, A.K. and M.R. Zentner, Aerospace and aircraft coatings. Federation of Societies for Coatings Technology, Philadelphia, PA, 1990.

[4.15] Lytle, F.W., Greegor, R. B., Bibbins, G. L., Blohowiak, K. Y., Smith, R. E., Tuss, G. D., Corros. Sci., 1995. Vol. 37(3): p. 349-369.

[4.16] Yu, Z., Ni, H., Zhang, G., Wang, Y., Dong, S., Zhao, G., Appl. Surf. Sci., 1992. Vol. 62(4): p. 217-221.

[4.17] Sinko, J., Prog. Org. Coat., 2001. Vol. 42(3–4): p. 267-282.

[4.18] Bierwagen, G.P. and D.E. Tallman, Prog. Org. Coat., 2001. Vol. 41(4): p. 201-216.

[4.19] LaPuma, P.T., Fox, J. M., Kimmel, E. C., Regul. Toxicol. Pharm., 2001. Vol. 33(3): p. 343-349.

[4.20] Occupational Safety and health administration (OSHA), Standard - 29 CFR number 1910.1026, Cr(VI).

[4.21] Farrier, L.M. and S.L. Szaruga, Mater. Charact., 2005. Vol. 55(3): p. 179-189.

[4.22] Bauer, J.P. and E.N. Ruddy, Metal finishing, 1996. Vol. 94(4): p. 28-39.

[4.23] Köhler, K., Simmendinger, P., Roelle, W., Scholz, W., Valet, A., Slongo, M., Paints and Coatings, 4. Pigments, Extenders, and Additives. Wiley-VCH Verlag GmbH & Co. KGaA, 2000.

[4.24] Scholes, F.H., Furman, S. A., Hughes, A. E., Nikpour, T., Wright, N., Curtis, P. R., Macrae, C. M., Intem, S., Hill, A. J., Prog. Org. Coat., 2006. Vol. 56(1): p. 23-32.

[4.25] Pashaei, S., Siddaramaiah, and A.A. Syed, J. Macromol. Sci., Part A: Pure Appl.Chem., 2010. Vol. 47(8): p. 777-783.

[4.26] Petrović, Z.S., Zavargo, Z., Flyn, J.H., Macknight, W. J., J. Appl. Polym. Sci., 1994. Vol. 51(6): p. 1087-1095.

[4.27] Zhang, Y., Xia, Z., Huang, H., Chen, H., J. Anal. Appl. Pyrolysis, 2009. Vol. 84(1): p. 89-94.

[4.28] Di Nola, G., W. de Jong, and H. Spliethoff, Fuel Process. Technol., 2010. Vol. 91(1): p. 103-115.

[4.29] Vamvuka, D., Kakaras, E., Kastanaki, E., Grammelis, P., Fuel, 2003. Vol. 82(15–17): p. 1949-1960.

[4.30] Vyazovkin, S., Burnham, A. K., Criado, J. M., Pérez-Maqueda, L. A., Popescu, C., Sbirrazzuoli, N., Thermochim. Acta, 2011. Vol. 520(1–2): p. 1-19.

[4.31] Flynn, J.H. and L.A. Wall, J Res Nat Bur Stand, 1966. Vol. 70(6): p. 487-523.

[4.32] Ozawa, T., Bull. Chem. Soc. Jpn., 1965. Vol. 38(11): p. 1881-1886.

[4.33] Burnham, A.K. and R.L. Braun, Energy & Fuels, 1998. Vol. 13(1): p. 1-22.

[4.34] Brown, M.E., et al., Thermochim. Acta, 2000. Vol. 355(1–2): p. 125-143.

[4.35] Prosek, T. and D. Thierry, Prog. Org. Coat., 2004. Vol. 49(3): p. 209-217.

[4.36] Furman, S.A., Scholes, F.H., Hughes, A.E. Jamieson, D.N., Macrae, C.M., Glenn, A.M., Corros. Sci., 2006. Vol. 48(7): p. 1827-1847.

[4.37] Burgio, L. and R.J.H. Clark, Spectrochim. Acta, Part A, 2001. Vol. 57(7): p. 1491-1521.

[4.38] Mammone, J.F., Sharma, S. K., Nicol, M., Solid State Commun., 1980. Vol. 34(10): p. 799-802.

[4.39] L'vov, B.V. and V.L. Ugolkov, Thermochim. Acta, 2004. Vol. 411(1): p. 73-79.

[4.40] Stacey J.S., S.R., Liu S., Li G., Navrotsky A., Boerio G.J., Woodfield Brian F., Am. Mineral., 2009. Vol. 94(2-3): p. 236-243.

[4.41] Kotsis, I. and A. Balogh, Ceram. Int., 1989. Vol. 15(2): p. 79-85.

[4.42] Athavale, V.T., Jatkar, S. K. K., J. Indian Inst. Sci., 1938. Vol. 21.

5: Paint and primer decoating of an aged aircraft aluminum component by chemical stripping[6]

Jose A. Muñiz-Lerma†, Milan Marić‡, In-Ho Jung†, and Mathieu Brochu*†

† Department of Mining and Materials Engineering, McGill University, 3610 University Street, Montréal, QC, H3A 0C5, Canada.

‡ Department of Chemical Engineering, McGill University, 3610 University Street, Montréal, Québec, Canada H3A 0C5, Canada.

5.1: Preface

In the previous chapter, it was reported that the inorganic compounds contained in the aircraft protection coating remained as particulate matter residues resulting from thermal decoating. Within these residues, particles containing hexavalent chromium, which were used as corrosion inhibitor agents in aircraft primers, were detected. The following chapter explores chemical stripping as an alternative method to remove the protection coating from aircraft components while simultaneously containing particulate hazardous materials in a damp state, thus eliminating the risk of becoming airborne pollutants. The study described below reports the stripping efficiency of non-dimethyl chloride based-solutions applied to aircraft substrates, as well as its correlation to the thermodynamic Hansen Solubility Parameters (HSP) by means of the Flory-Huggins/HSP, the relative energy number (RED), and the Flory-Rehner models.

5.2: Abstract

The removal of pigmented organic coatings from aircraft aluminum components is of paramount importance during the aircraft recycling process. In this study, the surface characterization and

[6] Submitted: Progress in Organic Coatings. Manuscript under revision, November, 2015

chemical stripping efficiency of the interior and exterior aircraft coating systems from aluminum substrates were analyzed. Surface analysis carried out by X-Ray photoelectron spectroscopy (XPS) has confirmed that the aircraft primer and topcoat consisted of an epoxy-polyamide and a polyurethane matrix, respectively. The chemical stripping efficiency of the exterior and interior coatings was evaluated by four commercial aircraft stripping solutions. The most effective solution was able to remove both the exterior and interior aircraft coating systems. This effectiveness was attributed to the molar volume of the active solvent and the alkaline environment present in the solution. The stripping efficiency of the commercial solutions was correlated to the Flory-Huggins/Hansen solubility parameters, the relative energy number (RED), and the Flory-Rehner models.

5.3: Introduction

Nowdays, aerospace companies are facing an increasing amount of waste generation coming from aircraft at their end-of-life (EOL). It has been estimated that approximately 12,000 aircraft will be at their EOL over the next twenty years, reaching a peak of 1000 aircraft disposed annually by 2023 [5.1, 5.2]. In order to solve this growing problem, aerospace companies, such as Airbus, Boeing, and Bombardier, express interests in reducing the environmental impact of commercial aviation through the management of EOL aircraft [5.1, 5.3, 5.4]. According to the Airbus *Process for Advanced Management of End-of-Life of Aircraft (PAMELA)* project, around 85 wt% of the aircraft can be either reused (15 wt%) or recycled (70 wt%), within which aluminum (Al) parts account for the highest recycling rate [5.3]. Recycling aluminum from aircraft at their EOL is highly relevant to the Al and aerospace industries. This relevance relies on the reduction of ~ 95% of the embodied energy and greenhouse gas emissions associated with primary Al production [5.5, 5.6].

A typical commercial aircraft contains around 65 wt% to 75 wt% of engineered aluminum alloys (AA) from the 2XXX, 6XXX, and 7XXX series. These alloys are usually mostly accompanied by a three-layer corrosion protection coating [5.7, 5.8]. The first layer is a conversion coating which acts as a corrosion protection and improves the adhesion between the Al substrate and the second layer of coating. The conversion coating is typically produced chemically (chromate conversion

coating) [5.9] or anodically in chromic and phosphoric acid, or boric/sulphuric acid baths [5.10]. The second layer consists of an epoxy polyamide matrix, containing chromate pigments such as barium chromate ($BaCrO_4$) or strontium chromate ($SrCrO_4$) and fillers [5.11]. The primary function of this pigmented organic layer is to inhibit corrosion of the Al components. It is worth to mention that alternative surface treatments and primers free of chromate compounds are becoming standard products in new commercial aircraft [5.12, 5.13]. Nevertheless, the typical conversion coatings and primers containing chromates are found in old aircraft waiting for final disposal. Lastly, the third layer is an inorganic pigmented topcoat, typically made of flexible two-component polyurethane. This layer protects the aircraft fuselage against environmental erosion and mechanical abrasion [5.14].

During aircraft aluminum recycling, the primer and the topcoat are the primary source of impurities. Such impurities are generally exogenous inclusions from the pigments [5.15], which reduce the quality of the recycled products, and thus prevent direct recycling into primary-grade Al alloys. Additionally, it has been proven that the presence of organic coatings during aluminum recycling increases the metal loss due to oxidation, gaseous emissions, and salt flux disposal during the re-melting of aluminum scrap [5.16]. Therefore, it is imperative to remove the pigmented organic coatings from aircraft aluminum scrap that is subjected to recycling.

For maintenance purposes, different techniques such as blasting, dry ice stripping, laser and xenon flash lamp stripping, have been used in the aircraft industry to remove the corrosion protection coating [5.17-5.23]. However, at least three common disadvantages can be found in these techniques. To begin with, the release of airborne carcinogenic dust containing Cr (VI) from the aircraft coating is a major problem. Secondly, the paint removal operation must be carried out at the dismantling facilities since the aircraft must be decoated prior to primary grinding. Finally, some sections of the aircraft might not be feasible for stripping using these techniques due to their geometries. Another traditional paint removal technique with potential for application in the aircraft recycling process is chemical stripping. It is a geometry-independent paint removal method that has the processing advantage of keeping hazardous materials such as Cr (VI) in a damp state [5.16, 5.24, 5.25]. Methylene chloride has been the most effective solvent used in paint stripping formulations to remove aircraft paint systems [5.26]. Nevertheless, due to its high toxicity, its usage in stripping formulations is restricted [5.26, 5.27]. Research efforts oriented

towards discovering new solvent alternatives have identified N-methyl-2-pyrrolidone (NMP) and dimethyl sulfoxide (DMSO) as sufficient replacements [5.26, 5.28].

Typically, the cross-link density of polyester-urethane and epoxy-polyamide increases over time affecting the ability of the solvent to penetrate the coating [5.29]. Over a typical 30 to 40 year lifespan of an aircraft, the external fuselage is repainted several times [5.30, 5.31]. However, there is ambiguous information related to the maintenance of the interior corrosion coating. To the best of our knowledge, little attention has been paid to the removal of the aged coatings from aircraft fuselages prior to the recycling of high-value aluminum alloys. Therefore, it is important to know if the chosen solvents will efficiently remove the organic coatings present on aircraft aluminum components at their EOL.

The present study explored the chemical removal route of the pigmented coatings contained on aged aircraft components subjected to recycling. The stripping efficiency of the employed solutions was correlated to the physicochemical Hansen solubility parameters (HSP) by the application of the thermodynamic Flory-Huggins/HSP, the relative energy number (RED), and the Flory-Rehner models.

5.4: Experimental Section

The aluminum (AA2024) cover skin shown in Figure 5-1 obtained from the vertical stabilizer of a Bombardier CRJ100 regional aircraft subjected to recycling, was used in this study. The cover skin was received coated with a corrosion protection coating system in the external and the internal section of the fuselage. The external protection coating was constituted by a conversion coating, a layer of fluid-resistance epoxy-polyamide primer with thickness of 12 ± 2 µm, a polyurethane sanding surfacer layer of approximately 20 ± 2 µm thick, and a fluid-resistant polyurethane topcoat with a thickness of 73 ± 2 µm. On the other hand, the internal protection coating of the cover skin consisted of a conversion coating, and a layer of fluid-resistance epoxy-polyamide primer with a thickness of approximately 16 ± 2 µm without topcoat. It is important to note that the specific base component and hardener, as well as the base component and activator used to produce the epoxy-polyamide primers and polyurethane sanding surfacer, and topcoat applied to the aircraft

component under study are unknown. Detailed description of the inorganic phases present in the corrosion protection coating of the external and internal sections of the aircraft fuselage skin can be found in a previous publication [5.32].

The surface of the external and internal section of the cover skin was analyzed by X-Ray photoelectron spectroscopy (XPS) by a Thermo Scientific Kα X-Ray photoelectron spectrometer equipped with an Al Kα X-Ray source (1486.6 eV, 0.843 nm). The high-resolution spectra were collected using 50 eV pass energy and an X-Ray spot diameter of 400 µm. To prevent charging of the polymeric coatings, samples were hit with a flood gun, shooting medium during all measurements. For both surface specimens, the binding energies of the component peaks in each spectrum were determined after charge correction by referencing to the carbon - carbon bond at 284.8 eV. Data processing was carried out with the Thermo Avantage v5.956.

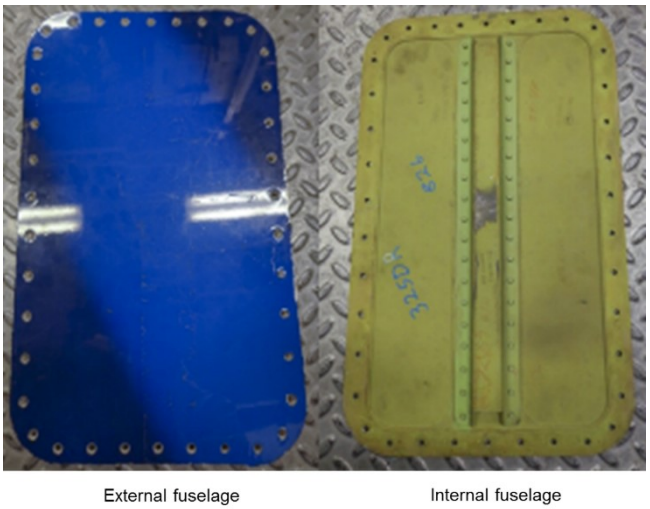

Figure 5-1. Fuselage cover skin coming from the Bombardier CRJ100 regional aircraft showing the external and internal sections.

Cross sections of the interface between the aluminum substrate and the corrosion protection coating in the external and internal sections of the cover skin were characterized using a field emission scanning electron microscopy (FE-SEM, Hitachi SU3500). The sample preparation was performed following the procedure proposed by Farrier et al [5.33].

Chemical stripping of the pigmented organic coatings was carried out using four different commercial stripping solutions provided by Greensolv (Table 5-1). The decoating procedure started by bringing the stripping solution from room temperature to 80°C keeping this temperature constant over all the experiments. Following the preheating, one test coupon of around 20 cm^2 was placed inside each solution until the coating was fully removed or after a period of 8 h to determine the workability of the stripping solutions. Simple marks of "Yes" or "No" were used to qualitatively evaluate the stripping power of each solution for complete or a lack of stripping respectively. The solution showing the best performance was selected to further study the stripping efficiency.

For the study of the stripping efficiency coupons of approximately 250 cm^2 from the same fuselage cover skin were immersed in the selected solution, preheated and kept at 80 °C. As soon as the solution reached 80 °C, the first coupon was immersed in the solution, and removed until the organic coatings were completely striped. Six more coupons were then evaluated in the same solution following the aforementioned immersion and removal procedure. Accordingly, the time required to remove the paint from each substrate was recorded. Then, the stripping ratio, defined as the time required to remove the coatings from the substrate per surface area, was estimated and plotted as a function of the stripping solution lifetime (cumulative paint removal time).

Table 5-1Active solvent and alkaline activator of the commercial stripping solutions.

ID	Active solvent*	Alkaline activator
A	NMP	NaOH
B	NMP	-
C	DMSO	NaOH
D	DMSO	-

*, NMP refers to N-methyl pyrrolidone and DMSO to Dimethyl sulfoxide.

-, Stripping solution without alkaline activator.

5.5: Results and Discussions

5.5.1: External and Internal Aircraft Coatings Surface Characterization

As received external and internal coatings of the aged aircraft fuselage cover skin was analyzed by XPS. Obtained spectra from the external coating were presented in Figure 5-2. From the C_{1s} spectra (Figure 5-2a), four peaks were identified, C – C/C – H, C – O, C – N, and C = O bonds, with binding energies of approximately 284.8, 286, 286.8, and 289 eV respectively [5.34, 5.35]. The high resolution O_{1s} peak is consistent with the C_{1s} profile, and it has been resolved into two main components related to O = C and O – C – O bonds with binding energies of ~ 531.8 eV and ~ 533.4 eV, respectively [5.34]. Finally, one peak was observed in the N_{1s} spectra which corresponds to C–NH bonds with binding energy of ~ 400 eV [5.36]. Generally speaking, polyurethane resins are commonly found in the aircraft topcoat, as a result of polymerization reaction between isocyanate groups (from cycloaliphatic and/or aliphatic isocyanates) and hydrogen atom (e.g. as – OH, – NH_2, –COOH functional groups) as shown in Scheme 1 [5.35, 5.37, 5.38]. Consequently, amine (C– NH) and carbonyl (O = C) groups were expected to present in the surface of the external coating. Polyether has been widely used in synthesized polyurethane coating for improved hydrolysis resistance as seen in fluid resistant topcoats [5.38, 5.39]. This gives rise to the ether bonds (C – O – C) in the O_{1s} spectra. The peak centered at ~ 289 eV is attributed by a carbon oxygen double bond, corresponding N – C = O signals from urethane or urea [5.35, 5.40].

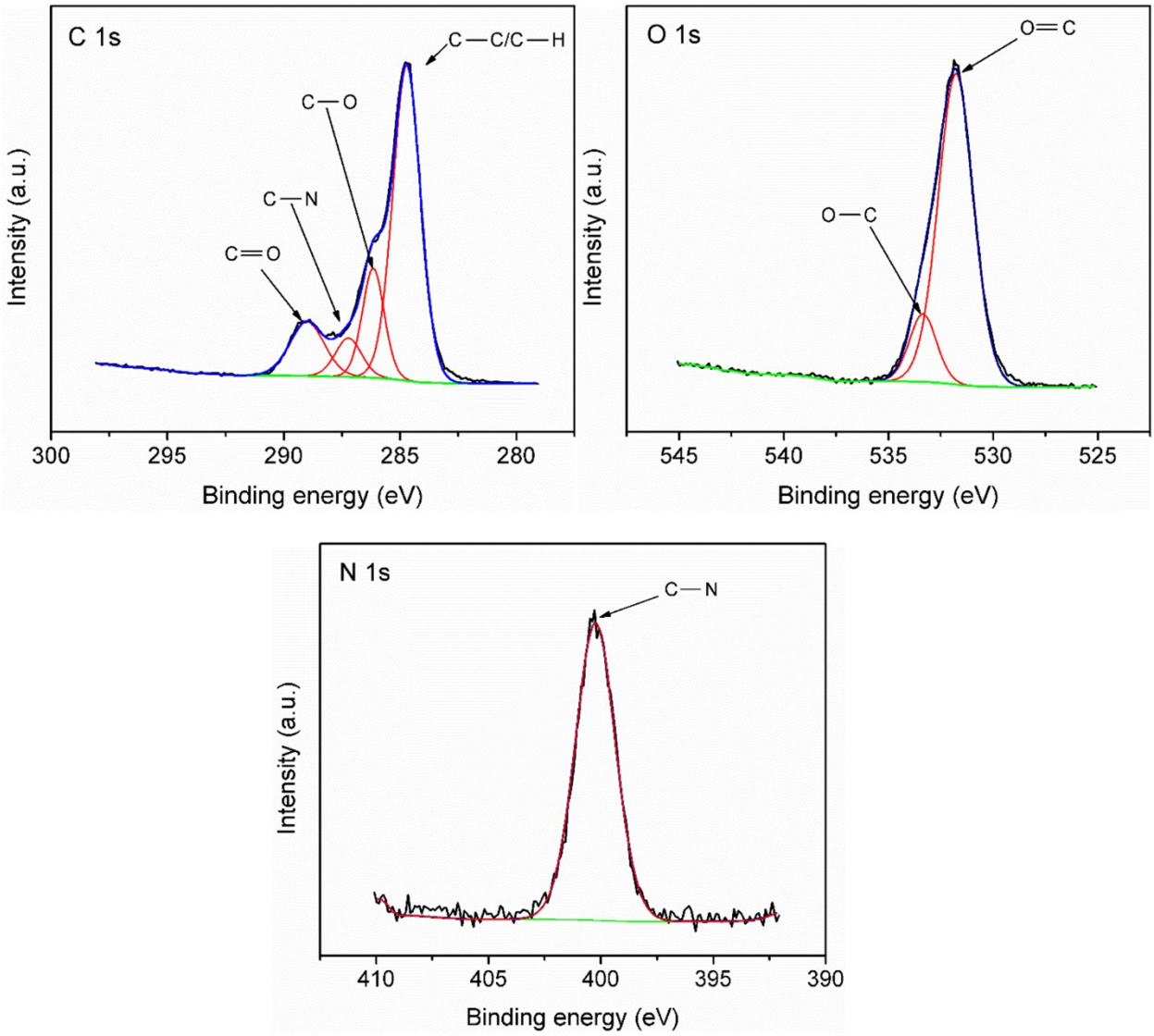

Figure 5-2. XPS high resolution spectra of the aircraft topcoat measured for C1s, O1s, and N1s. Experimental data are shown in black, background in green, deconvoluted peaks in red, and overall fit in blue.

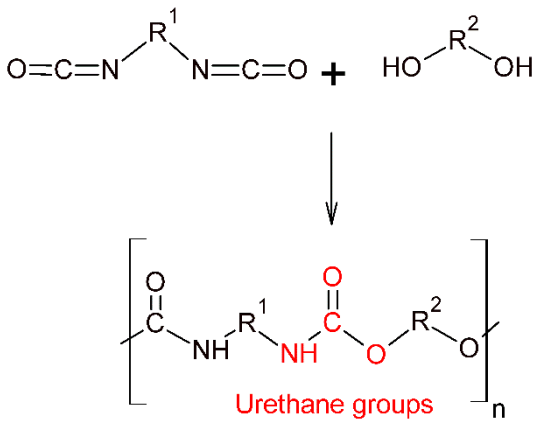

Scheme 1.General reaction to form polyurethane resin from diols and isocyanates [5.38].

Figure 5-3 shows the high resolution XPS spectra for (a) C_{1s}, (b) O_{1s}, (c) N_{1s}, and (d) P_{2p} from the internal section of the fuselage. Four main peaks were observed in the C_{1s} spectrum. The first peak was located at around ~ 284.8 eV, and might be assigned to the contributions of C – C/C – H bonds from the aliphatic and aromatic species in the material. The second peak was found approximately at 286.2 eV, suggesting C – N/C – O bonds. The third peak was localized at ~ 287.2 eV that could be due to the existence of C = O as in amide functional groups. Finally, a fourth peak was deconvoluted at ~289, which was assigned to a C = O bond from carboxylic acid [5.41, 5.42].

The obtained high resolution O_{1s} spectra from Figure 5-3, has been separated into four characteristic peaks. The peak at ~ 530.7 eV is related to a metal to oxygen single bond, M – O, that could correspond to the O_{2-} anions of the pigments such as TiO_2 [5.43]. The peak centered at ~ 531.7 eV can be assigned to a double binding = O in the carbonyl of an amide functional group, N – C = O and phosphate groups. The third band is centered at ~ 533 eV. This peak can be assigned to C – O and/or C – O – C, C – O – P, and P – O – P bonds. Finally, a fourth peak located at ~ 533.6 might be assigned to C = O as in carboxylic acid [5.41, 5.42]

The N_{1s} spectra shows only one characteristic C – N peak, centered at ~ 399.8 eV [5.36]. Finally, the P_{2p} spectra was fit by two different peaks corresponding to its core-line doublets $P_{2p1/2}$ and $P_{2p3/2}$ with the characteristic spin-orbit splitting of 0.84 eV and ratio of $P_{2p1/2}$:$P_{2p3/2}$ of 0.5 [5.44].

Thus, the peaks observed between ~132 and ~ 134 eV could correspond to P – O – C bonds and/or PO_3^- groups in phosphate species [5.42, 5.45].

The existence of amide functional groups (CH_2 – CO – NH), elucidated in the C_{1s} and further confirmed by the presence of = O and C – N bonds in the O_{1s}, and N_{1s} spectra lines, confirms the use of a polymer containing polyamides in the primer coating of the internal section of the fuselage. These results were expected since it is well known that the polymeric coating used in the internal section of the fuselage, contains a primer made of an epoxy resin hardened by curing agents such as polyamides like the one shown in Scheme 2 [5.46, 5.47]. These curing agents contain amine terminated groups that are able to react with epoxide groups from the epoxy resin by nucleophilic reactions in the electron-deficient carbon, while the electron-rich oxygen can react with electrophiles as it is shown in Scheme 3 [5.48, 5.49]. The detection of phosphorus in the epoxy polyamide primer, could be explained by the presence of inorganic pigments containing phosphates [5.50]. However, inorganic compounds containing phosphates were not detected in the coating by the characterization techniques employed in our previous study [5.32], such as XRD, Raman, and EDS. Thus, the presence of phosphorous might be related to the presence of a flame retardant coating containing phosphorous species. [5.51, 5.52]

The aircraft cover skin under study have been exposed to natural environmental conditions, such as humidity, temperature, and sunlight, for an undetermined time during the aircraft service. Thus, it is expected to have a degraded coating characterized by its surface composition. Yang et al., [5.35] observed that after weathering tests of polyurethane coatings, the peak intensity at ~ 289 eV increased in the C1s spectra. The intensity increment was attributed to the coating photodegradation process, leading to an increase of the urea groups at the surface of the polyurethane coatings. In the case of the epoxy-polyamide coatings, Horner and Boerio [5.41] reported that after coating exposure to hydroxyl ions (OH), a decrease in the concentration of amide functional groups and an increase of carboxylic acid were observed. Such observation was attributed to the hydrolysis of amide groups in the coating which produces carboxylates and amines. Nevertheless, due to the lack of information regarding to the fresh coatings applied in the aircraft skin under study, the change of intensity in the XPS spectra between the freshly applied and the natural aged coating cannot be compared in the present study. Nevertheless, at the surface

of the studied aircraft coatings, the photodegradation and hydrolysis products might be present on the polyurethane and epoxy-polyamide coatings as previously reported [5.35, 5.41].

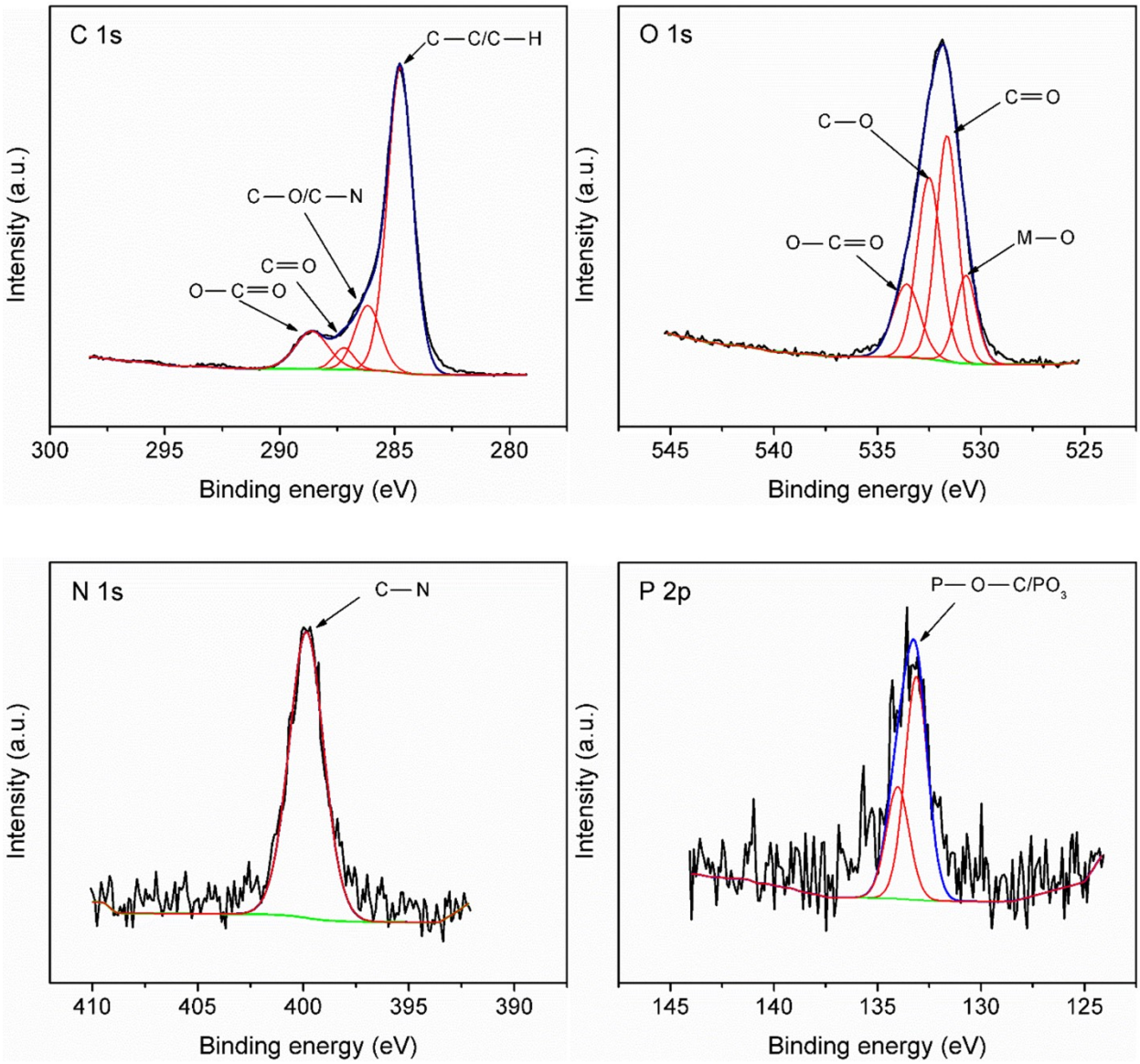

Figure 5-3. XPS high resolution spectra of the aircraft primer measured for C1s, O1s, N1s and P2p. High resolution peaks are shown in black, background in green, peak fit in red, and overall fit in blue.

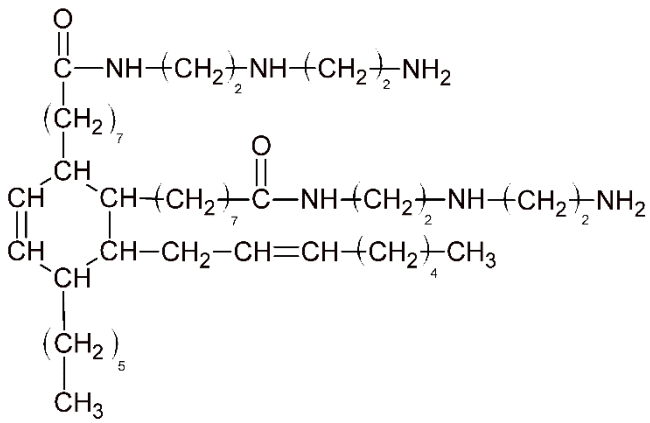

Scheme 2. Structure of a typical polyamide curing agent obtained from the condensation products of dimer acids and alkylene polyamines such as ethylene diamine [5.47].

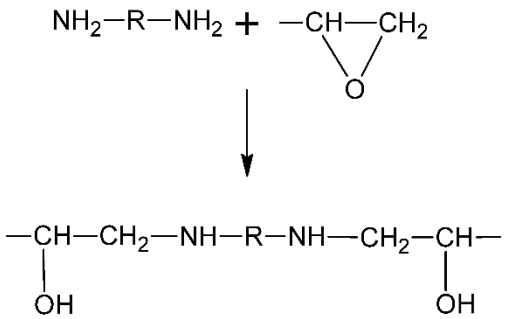

Scheme 3. Typical reaction of amine terminated groups with epoxide groups showing a ring opening by nucleophilic attack, resulting in a poly(urea) [5.49].

5.5.2: Chemical decoating

Four different types of chemical stripping solutions identified as A, B, C, and D were used for stripping tests on aircraft fuselage samples. The main differences between the chemical removers were their active ingredients and the presence or absence of an alkaline activator. Table 5-2 shows the chemical removal results of the aircraft fuselage samples after immersing one small coupon for a period of 8 h in each solution heated at 80°C. The stripping solutions A, B, and D showed similar results. After 3.75 h, the organic coating system present on the external section of the

fuselage skin was fully stripped. Nevertheless, the organic coating in the internal section was not removed. The stripping solution C was proven to be more effective by removing the organic coatings from both surfaces of the fuselage skin after 2.10 h.

Table 5-2. Chemical stripping results of the Bombardier CRJ-100 aircraft fuselage coupons by using commercial stripping solutions.

Substrate section	Commercial stripping solutions			
	A	B	C	D
External fuselage	Yes	Yes	Yes	Yes
Internal fuselage	No	No	Yes	No
Stripping time (h)	After 3.75	After 3.75	After 2.10	After 3.75

To further study the stripping solution lifetime, the solution C was selected and tested on 7 aircraft coupons, each one of approximately 250 cm^2. Figure 5-4 illustrates the ratio of the stripping time to the stripped surface as a function of the stripping solution lifetime. The stripping ratio of the first immersed sample was 5.5 x 10^3 h/cm^2, while the ratio of the second sample increased up to 7.0 x 10^3 h/cm^2. A constant stripping efficiency was observed between 6.2 and 13.7 h of the stripping solution lifetime showing ratios of around 7.5 x 10^3 h/cm^2. Then, after 13.72 h of keeping the stripping solution working at 80 °C, the ratio suddenly increased to 8.0 x 10^3 h/cm^2 and 1.0 x 10^2 h/cm^2 for the last two tested samples, respectively. Based on these results, it is evident that the removal rate of the commercial stripping solution C decreased as the solution life increased. This observation is in agreement with the study carried out by Ebenzer et al. [5.53], on the determination of the relative activity of selected paint stripping components with epoxy and polyurethane aerospace coatings. In their study, they found that the active solvent in the stripping solutions was not the only important factor for the aircraft paint removal. In fact, they observed that the presence of co-solvents such as alcohols and phenols, and activators such as water, which are usually present in the formulation of commercial stripping solutions, drastically increased the removal rate. In

particular, the authors reported that water, in combination with a mixture of phenol and alcohol, was more efficient to strip aircraft coatings emphasizing that the addition of water improves the removal rate. Thus, the efficiency reduction of the C solution might be related to the water evaporation during the hot stripping process of aircraft panels.

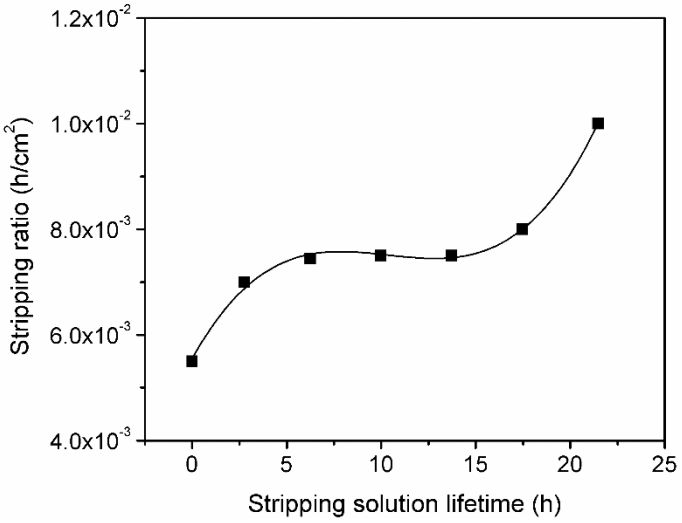

Figure 5-4. Stripping ratio behavior of the CRJ-100 aircraft fuselage panel as a function of the stripping solution life.

5.5.3: Chemical decoating selectivity

A sketch illustrating the mechanism of cross-linked polymers proposed by Nero et al. [5.28] is presented in Figure 5-5. In broad terms, the stripping solutions wet, diffuse, and penetrate the coatings causing the polymer to swell. After swelling, compressive stresses are built up within the swollen coating, decreasing its strength and giving rise to delamination. Moreover, once the stripping solution has penetrated the coating and reached the substrate, the adhesive bonds (hydrogen or dipolar bonds) between the coating and the substrate are broken. Finally, formation of blisters and lifting of the coating is produced by vapor pressure of the solvent or by the reaction between a selective ingredient in the solution and the substrate [5.28, 5.54-5.56]. Thus, the

stripping selectivity of the solutions is mainly affected by the swelling feasibility and the adhesive strength between the aluminum substrate and the polymer.

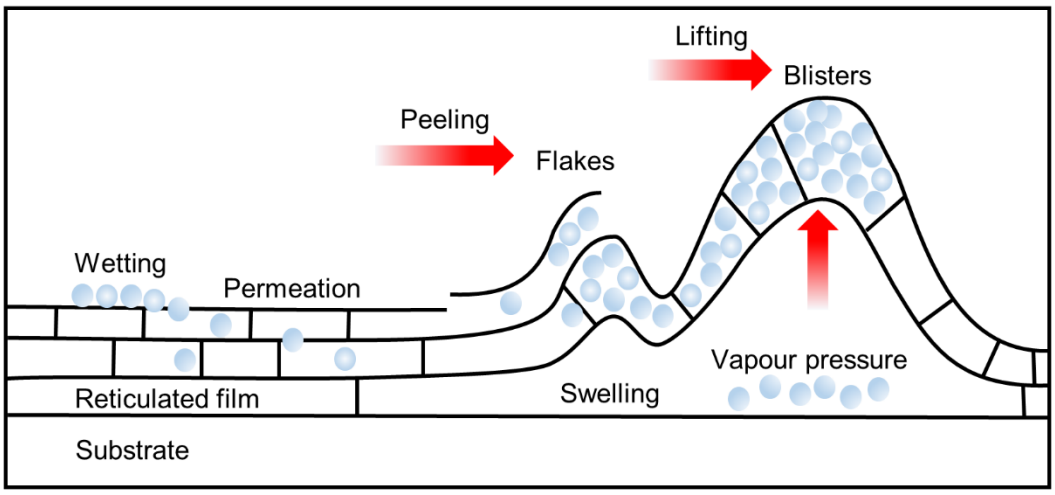

Figure 5-5. Chemical stripping mechanism of a cross-link polymer. Reprinted with permission from Del Nero V., Siat C., Marti M. J., et al. Copyright AIP Conference Proceedings, 1996, AIP Publishing LLC. [5.28]

Figure 5-6 a and b, depicts the back-scattered electron micrographs from cross sections of the external and internal sections of the fuselage skin before chemical stripping, respectively. It is evident that a layer of aluminum oxide, with a thickness of ~ 1.2 µm resulting from an anodizing treatment [5.10], is visible in the internal section but not in the external section under study. During the aircraft service life, the aluminum fuselage is usually abraded or chemically deoxidized after removing the aircraft paint for maintenance or aesthetics purposes. As a result, the original conversion coating in the exterior skin is removed. Before the application of a new protection coating in the aircraft fuselage, the abraded or chemically deoxidized aluminum surface is treated by a chemical conversion coating [5.57]. In old aircraft alodine solutions were commonly employed to chemically produce the conversion coating layer [5.58] Anodizing provides a higher adhesive strength by means of mechanical interlocking over chemical conversion coatings, such

as alodine [5.59]. Hence, in a first instance, the lack of the anodic coating in the external section of the cover skin might facilitate the chemical stripping of aluminum components.

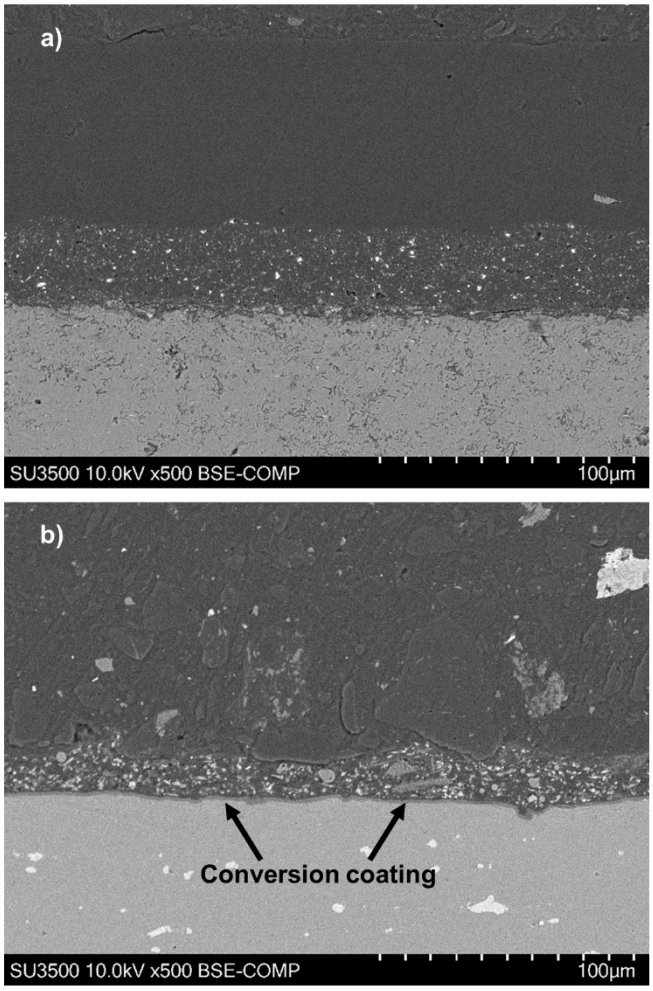

Figure 5-6. Cross section of the (a) external and (b) internal section of the fuselage skin before chemical decoating

Swelling of polymer networks by stripping solutions relies on the intermolecular bond strength between the polymer-polymer, solvent-solvent, and polymer-solvent. If the interaction of these bonds is similar, the stripping solution will easily interact with the polymer network. Hence, by diffusion, the stripping solution will swell the polymer [5.60]. We have tried to correlate the

stripping power of the commercial stripping solutions to the physicochemical Hansen solubility parameters (HSP), i.e., the non-polar dispersion forces (δ_d), the polar forces (δ_p), and the hydrogen-bonding forces (δ_h) by the application of the thermodynamic Flory-Huggins/HSP, the relative energy number (RED) and the Flory-Rehner model [5.29, 5.61, 5.62]

The Flory-Huggins/HSP model, shown in Equation 4, gives a measure of the interaction between the polymer chains (1) and the solvent molecules (2) by means of the enthalpic interaction parameter, $\chi_{1,2}$, where υ corresponds to the molar volume of the solvent, R is the molar gas constant, T is the absolute temperature, and the HSP δ_d, δ_p, and δ_{hb}, represent the contribution of non-polar dispersion forces, polar forces, and hydrogen-bonding effects, respectively [5.61, 5.62].

Equation 4

$$\chi_{1,2}=0.6\frac{\upsilon_1}{RT}\left[\left(\delta_{1,d}-\delta_{2,d}\right)^2+0.25\left(\delta_{1,p}-\delta_{2,p}\right)^2+0.25\left(\delta_{1,hb}-\delta_{2,hb}\right)^2\right]$$

In addition to the Flory-Huggins/HSP model, the RED number is also a key parameter to evaluate the solvent quality. This number is given by Equation 5 where R_a corresponds to the ratio between the solubility distance of two materials, and R_o corresponds to the interaction ratio of the polymer [5.62]

Equation 5

$$RED=\frac{R_a}{R_o}$$

$$R_a=\sqrt{4(\delta_{d2}-\delta_{d1})^2+\left(\delta_{p2}-\delta_{p1}\right)^2+(\delta_{hb2}-\delta_{hb1})^2}$$

Finally, the Flory-Rehner model shown in Equation 6, was used to calculate the swelling ratio of the aircraft coatings, S = 1/ ϕ. Where ϕ = volume fraction of the polymer in the swollen system, υ

=crosslink density (mole/volume), V = molar volume of the solvent, and $\chi_{1,2}$ = Flory-Huggins interaction parameter.

Equation 6

$$\ln(1-\phi)+\phi+\chi_{1,2}\phi^2+\upsilon V\left(\phi^{1/3}-\frac{\phi}{2}\right)=0$$

Previous studies [5.35, 5.40] have reported that degradation products of polyurethane and epoxy-polyamide coatings due to weathering, are only evident at the surface of the coatings while the bulk of the polymer remains chemically unmodified. Assuming that the surfactants commonly found on commercial stripping solutions overcome the effect of the surface degradation [5.63], the present study considered the physical and thermodynamic data from the bulk of the coatings. Thus, the HSP, the molar volumes, and the interaction radius shown in Table 5-3 were used.

Table 5-3. Hansen solubility parameters, molar volumes, and interaction radius data used for calculations taken from the literature [5.62].

Solvent/coating	HSP ($Mpa^{1/2}$)			υ (cm^3/mol)	R_o ($Mpa^{1/2}$)
	δ_d	δ_p	δ_{hb}		
DMSO	18.4	16.4	10.2	71.3	-
NMP	18	12.3	7.2	96.5	-
Epoxy-Polyamide	16.6	14	2.8	-	14.9
Polyester-urethane	17.9	13.3	10.7	-	17.1

-, No data

At lower values of $\chi_{1,2}$ and RED, a higher affinity of solvent/polymer is expected [5.62] In Figure 5-7, the $\chi_{1,2}$ and the RED corresponding to the systems NMP/Polyester-urethane, NMP/Epoxy-polyamide, DMSO/Polyester urethane, and DMSO/Epoxy-polyamide are presented. It demonstrated that the polyesther-urethane coating showed higher affinity to the solvents NMP and DMSO than to the epoxy-polyamide coating. Furthermore, it can also be noticed that in the epoxy-polyamide coating, the solvent NMP showed a higher affinity than DMSO did. Taking these results into account, it is expected that the solvent NMP would be more efficient than DMSO to remove the organic coating systems present in the fuselage skin under study. Experimentally, the exclusive use of the HSP parameters and the molar volume of the solvent by the $\chi_{1,2}$ and RED number accurately predicted the removal of the external coating system, where approximately 70% of the coating is made of polyester-urethane [5.32]. Nevertheless, such models failed to predict the removal of the organic coating system present in the internal section of the fuselage, where an epoxy-polyamide polymer constitutes 100% of the organic coating system.

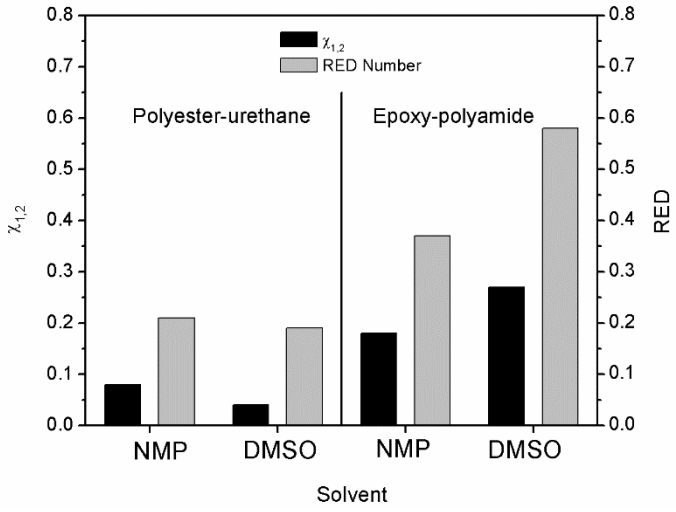

Figure 5-7. Interaction parameters $\chi_{1,2}$ and RED corresponding to the solvents NMP and DMSO in polyester-urethane and epoxy-polyamide polymers.

Considering that swelling has an important influence on chemical stripping, the crosslink density of the polymer and the molar volume of the solvent, have to be taken into account [5.60]. Thus, in

order to consider such physical parameters, the Flory-Rehner model was employed in this study [5.54]. This model was solved numerically by a bisection method of finding its root and was used to predict the swelling ratio for polyester-urethane and epoxy-polyamide aircraft coatings. Due to the lack of literature regarding to the crosslink density of weathered aircraft organic coatings, the values obtained by Croll, S.G. et al. [5.64] for model polyester-urethane and epoxy-polyamide clear aircraft coatings were used in the present study. The calculated swelling ratio for the polyester-urethane and epoxy-polyamide coatings as a function of the crosslink density is shown in Figure 5-8 and Figure 5-9, respectively. The swelling ratio of the coatings increases as the crosslink density decreases. According to the free-volume theory of transport for crosslinked polymers developed by Vrentas and Vrentas [5.65], decreasing the crosslink density of the polymers increases the solvent-self diffusion coefficient in a polymer-penetrant mixture. Thus, the surface degradation of the external coating system as a consequence of exposure to UV radiation and rain, will cause the solvent to permeate the coatings easily.

The molar volume of the solvent molecules is also important in polymer swelling. Smaller molecules are not only expected to be more thermodynamically aggressive, but also lead to higher diffusion coefficients [5.62, 5.66]. The solvent with smaller molar volume, i.e., DMSO, will present a higher activity than NMP does, resulting in a higher diffusion coefficient. Consequently, a higher swelling ratio can be expected for the solvent DMSO than that for NMP.

From the Flory-Rehner model, it can be predicted that the use of stripping solutions containing DMSO as an active solvent, allow higher stripping power than the solutions containing NMP allow. DMSO is highly polar and aprotic with a low molar volume and a high boiling point [5.67]. These characteristics enable the solvent to act only as a hydrogen-bond acceptor, to penetrate the coating, and to have a low evaporation rate. However, this solvent has a high cohesion energy, which allows the formation of solvent clusters [5.28]. Under this circumstance, the penetration rate of the solvent through the polymer film is reduced. Addition of proprietary amounts of sodium hydroxide, co-solvents, and activators such as water to the stripping solution containing DMSO (solution C) could promote weakening of the intermolecular forces of DMSO as proposed by Del Nero et al [5.28]. This effect increases the free molecular DMSO, enhancing the solvent molecule mobility and the ability to swell. Furthermore, once the alkaline-DMSO solution diffuses through the coating and reaches the aluminum substrate, the sodium hydroxide will react with the substrate

to generate H^+. Such a reaction increases the vapor pressure between the coating and the substrate, generating blisters and lifting of the epoxy coating. Thus, the combination of DMSO, NaOH, water, and proprietary additives results in the efficient stripping power observed in the caustic solution C. The molecular interaction between co-solvents and activators with DMSO and the epoxy-polyamide coatings is not the objective of this study and further research in this field is needed to completely understand the stripping mechanism of an aged epoxy-polyamide primer from aircraft substrates.

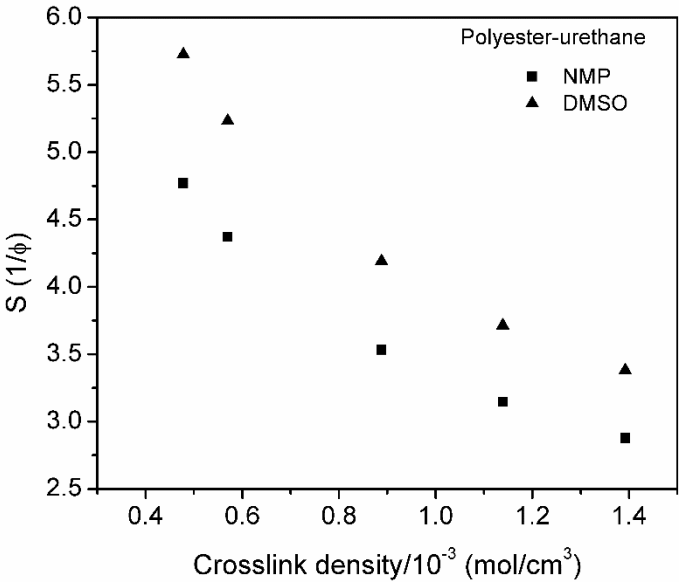

Figure 5-8. Swelling ratio of a polyester-urethane coating promoted by the solvents NMP and DMSO as a function of crosslink density.

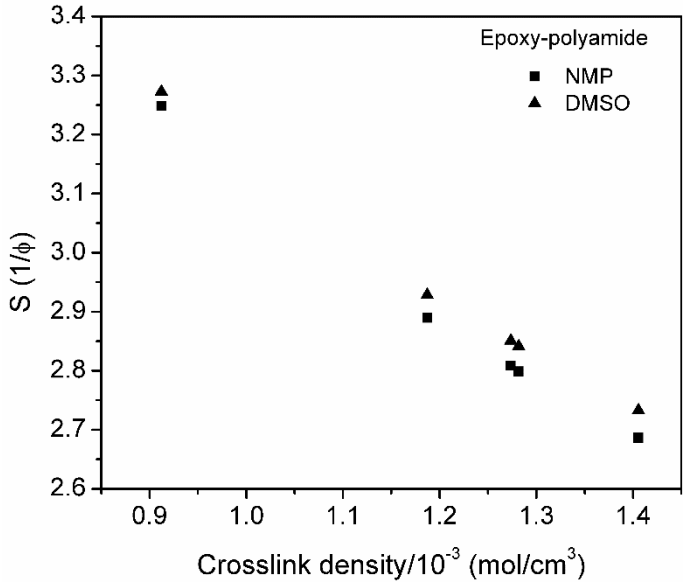

Figure 5-9. Swelling ratio of an epoxy-polyamide coating promoted by the solvents NMP and DMSO as a function of crosslink density.

5.6: Conclusion

The chemical structure of the coatings corresponded to a polyurethane topcoat and an epoxy-polyamide primer. The chemical stripping of the coatings was tested by four different commercial stripping solutions, where the main difference between the products was their active ingredient and the presence or absence of an alkaline activator. The stripping solutions containing NMP in the presence and absence of NaOH, and the solution containing DMSO free of NaOH demonstrated similar stripping performance being able to remove only the coating system applied in the external section of the fuselage. On the other hand, the solution containing DMSO and NaOH effectively removed the coating systems applied to the internal and external sections of the fuselage. The presence of an anodic film in the internal section of the fuselage might difficult the stripping of the coatings due to the strong adhesion between the anodized conversion coating and the polymer compared with the conversion coating formed by an Alodine treatment.

In an attempt to correlate the stripping power of the commercial solutions to the HSP, the Flory-Huggins/HSP, RED number and the Flory-Rehner models were employed. The Flory-Rehner

model led to more realistic predictions, showing that the solvent DMSO had a better interaction with the aircraft coatings compared to the solvent NMP. Nevertheless, the high cohesion energy of the DMSO solvent can lead to the formation of clusters that can decrease the penetration rate. However, by the presence of alkaline activators, the penetration rate was apparently increased giving rise to the effective stripping of the coating system applied in the aircraft fuselage substrates.

5.7: Acknowledgments

The authors would like to thank the Consortium de Recherche et d'Innovation en Aérospatiale au Québec (CRIAQ), Bombardier, Bell Helicopter, Sotrem-Maltech, BFI, Nano Quebec, and Aluminerie Alouette for funding this project under the CRIAQ ENV-412 grant. Furthermore, the authors are grateful to Mr. Martin Pageau for providing the stripping solutions utilized in this work. Muñiz-Lerma acknowledges the complementary scholarship provided by the Secretary of Public Education of México.

5.8: References

[5.1] AFRA. Aircraft Fleet Recycling Association. 2014; Available from: http://www.afraassociation.org/.

]5.2] AFRA. Aircraft Fleet Recycling Association.: Aircraft Retirement Tsunami. A 1000 Aircraft a Year to leave Service by 2023. 2014; Available from: http://www.afraassociation.org/news.cfm?newsid=162.

[5.3] Airbus, S.A.S. Eco-efficiency and Sustainability -G9- Issue 1. Process for Advanced Management of End of Life of Aircraft Available from: http://ec.europa.eu/environment/life/project/Projects/index.cfm?fuseaction=home.showFile&rep=file&fil=ACADEMY_PAMELA.pdf.

[5.4] CRIAQ-ENV412. Process for advanced management and technologies of aircraftend-of-life. 2015; Available from: http://www.polymtl.ca/env412/index.php.

[5.5] Das, S.K., J. G., Light metals., 2007: p. 1161-1166.

[5.6] Green, J.A.S., Aluminum Recycling and Processing for Energy Conservation and Sustainability. 1-271, ASM International, 2007.

[5.7] Itzkowitch, Z. 1ere PIateforme europeenne de demantelement aeronautique, Dossier de presse Bartin AERO Recycling. 2008.

[5.8] Chattopadhyay, A.K. and M.R. Zentner, Aerospace and aircraft coatings. Federation of Societies for Coatings Technology, Philadelphia, PA, 1990.

[5.9] MIL-DTL-5541F: Chemical conversion coatings on aluminum and aluminum alloys. 2006.

[5.10] MIL-A-8625: Anodic coatings for aluminum and aluminum alloys. 2003.

[5.11] Sinko, J., Prog. Org. Coat., 2001. Vol. 42(3–4): p. 267-282.

[5.12] Osborne, J., Nonchromate conversion coatings in use at Boeing. 2006, ASETSDefense: Layton, Utah.

[5.13] Osborne, J., Chromate-free Exterior Painting for Boeing Commercial Aircraft. 2009, ASETSDefense: Westminster, Co.

[5.14] Bierwagen, G.P. and D.E. Tallman, Prog. Org. Coat., 2001. Vol. 41(4): p. 201-216.

[5.15] Kvithyld, A., Meskers, C. E. M., Gaal, S., Reuter, M., Engh, T., JOM, 2008. Vol. 60(8): p. 47-51.

[5.16] Schlesinger, M.E., Ilegbusi, O.J., Iguchi, M., Wahnsiedler, W., Aluminum Recycling. CRC PressINC, United States, 2007.

[5.17] Tangestanian, P., M. Papini, and J.K. Spelt, Wear, 2001. Vol. 248(1–2): p. 128-139.

[5.18] Hart, W.G.J., Report NLR-TP-2003-357: Paint stripping techniques for composite aircraft components. 2003, Structures and Materials Department, National Aerospace Laboratory NLR: Netherlands.

[5.19] Olevitch, A., Cryogenic mechanical means of paint removal. US Patent 5044129 A, Sept 3, 1991. 1991.

[5.20] WMRC, TN98-046: Paint removal options - Paint Factsheet No. 6, in Waste Management and Research Center. 1998: Champaign, IL.

[5.21] Barletta, M., A. Gisario, and V. Tagliaferri, J. Mater. Process. Technol., 2006. Vol. 173(2): p. 232-239.

[5.22] Ranalli, R.J., U.S. Patent No. 5,662,762 A. Laser-based system and method for stripping coatings from substrates. 1997.

[5.23] Kozol, J., JOM, 2001. Vol. 53(3): p. 20-21.

[5.24] Arndt, S. and R. Canum, Metal Finishing, 2007. Vol. 105(5): p. 49-50.

[5.25] Stoye, D. and W. Freitag, Paints, coatings, and solvents. Wiley-VCH, Weinheim; New York, 1998.

[5.26] Luey, K., D. Coleman, and G. Ternet, Replacement of Methylene Chloride in NVR and Paint Removal Applications. 2000, DTIC Document.

[5.27] Pauli, R., Products Finishing, 1997. Vol. 61(9): p. 84-89.

[5.28] Del Nero, V., Siat, C., Marti, M. J., Aubry, J. M., Lallier, J. P., Dupuy, N., Huvenne, J. P., AIP Conference Proceedings, 1996. Vol. 354(1): p. 469-476.

[5.29] Flory, P.J. and J. Rehner, The Journal of Chemical Physics, 1943. Vol. 11(11): p. 521-526.

[5.30] Agarwala, V.S. and K. Rajeshwar. Paint and coating removal technologies: past, present and future. in CORROSION 2001. 2001. NACE International.

[5.31] Ribeiro, J.S. and J.d.O. Gomes, Procedia CIRP, 2015. Vol. 26: p. 311-316.

[5.32] Muñiz Lerma, J.A., I.-H. Jung, and M. Brochu, Metallurgical and Materials Transactions B, 2016. Vol. 47(3): p. 1976-1985.

[5.33] Farrier, L.M. and S.L. Szaruga, Mater. Charact., 2005. Vol. 55(3): p. 179-189.

[5.34] Mishra, A.K., Chattopadhyay, D. K., Sreedhar, B., Raju, K. V. S. N., Prog. Org. Coat., 2006. Vol. 55(3): p. 231-243.

[5.35] Yang, X.F., Vang, C., Tallman, D. E., Bierwagen, G. P., Croll, S. G., Rohlik, S., Polym. Degrad. Stab., 2001. Vol. 74(2): p. 341-351.

[5.36] Beamson, G., Briggs, D., High resolution XPS of organic polymers : the Scienta ESCA300 database. Wiley, Chichester [England]; New York, 1992.

[5.37] Parsons, P., Surface Coatings Volume 1 Raw Materials and Their Usage. 1994, Springer Netherlands: Dordrecht.

[5.38] Oil and C.C.A. Australia, Polyurethane Resins, in Surface Coatings Vol I-Raw Materials and Their Usage. 1983, Springer Netherlands: Dordrecht. p. 105-119.

[5.39] Rahman, M.M., Hasneen, A., Chung, I., Kim, H., Lee, W., Chun, J. H., Compos. Interfaces, 2013. Vol. 20(1): p. 15-26.

[5.40] Kim, H. and M.W. Urban, Langmuir, 2000. Vol. 16(12): p. 5382-5390.

[5.41] Horner, M.R., Boerio, F. J., The Journal of Adhesion, 1990. Vol. 32(2-3): p. 141-156.

[5.42] Wang, J.S., Wang, D. Y., Liu, Y., Ge, X. G, Wang, Y. Z., J. Appl. Polym. Sci., 2008. Vol. 108(4): p. 2644-2653.

[5.43] McCafferty, E., Wightman, J. P., Surf. Interface Anal., 1998. Vol. 26(8): p. 549-564.

[5.44] Bomben K.D., M.J.F., Sobol P.E., Stickle W.F. , Handbook of X-ray photoelectron spectroscopy : a reference book of standard spectra for identification and interpretation of XPS data. Physical Electronics, Eden Prairie, Minn., 1995.

[5.45] Bourbigot, S., Le Bras, M., Gengembre, L., Delobel, R., Appl. Surf. Sci., 1994. Vol. 81(3): p. 299-307.

[5.46] Chattopadhyay, A.K., Zentner, M.R., 1990.

[5.47] Ellis, B., Chemistry and technology of epoxy resins. Blackie Academic & Professional, London; New York, 1993.

[5.48] Parker, R.E., Isaacs, N. S., Chem. Rev., 1959. Vol. 59(4): p. 737-799.

[5.49] Shechter, L., Wynstra, J., Kurkjy, R. P., Industrial & Engineering Chemistry, 1956. Vol. 48(1): p. 94-97.

[5.50] Bethencourt, M., Botana, F. J., Marcos, M., Osuna, R. M., Sánchez-Amaya, J. M., Prog. Org. Coat., 2003. Vol. 46(4): p. 280-287.

[5.51] Lasch, H.W., Jukkola, E. E., Fire-Retardant Coatings for Aircraft Use, in Fire retardants paints. 1954, American Chemical Society. p. 67-81.

[5.52] Wang, J.-S., et al., Polym. Degrad. Stab., 2009. Vol. 94(4): p. 625-631.

[5.53] Ebenezer N.; Graham, J.L., Determination of the relative activity of selected paint stripping components with epoxy and polyurethane aerospace coatings. Published Master Degree Thesis. 2011, University of Dayton.

[5.54] Croll, S.G., J Coat Technol Res, 2010. Vol. 7(1): p. 49-55.

[5.55] O'Donoghue, M., Garrett, R., Graham, R., Datta, V J., Vitomir, S., White, D., Peer, L., Journal of Protective Coatings & Linings, 2000. Vol. 17(5): p. 74-93.

[5.56] Hare, C.H., Journal of Protective Coatings & Linings, 1997. Vol. 14(5): p. 69-81.

[5.57] AC 43.13-1B - Acceptable methods, techniques, and practices - Aircraft inspection and repair. 1988, FAA: United states.

[5.58] Osborne, J.H., Prog. Org. Coat., 2001. Vol. 41(4): p. 280-286.

[5.59] Petrie, E.M., Metal Finishing, 2007. Vol. 105(9): p. 49-56.

[5.60] Wypych, G., Handbook of solvents. ChemTec ; William Andrew Pub., Toronto, Ont.; Norwich, N.Y., 2001.

[5.61] Lindvig, T., Michelsen, M. L., Kontogeorgis, G. M., Fluid Phase Equilib., 2002. Vol. 203(1–2): p. 247-260.

[5.62] Hansen, C.M., Hansen solubility parameters : a user's handbook. CRC Press, Boca Raton, 2007.

[5.63] Wollbrinck, T., Journal of the American Institute for Conservation Journal of the American Institute for Conservation, 1993. Vol. 32(1): p. 43-57.

[5.64] Croll, S.G., X. Shi, and B.M.D. Fernando, Prog. Org. Coat., 2008. Vol. 61(2–4): p. 136-144.

[5.65] Vrentas, J. and C. Vrentas, J. Appl. Polym. Sci., 1991. Vol. 42(7): p. 1931-1937.

[5.66] Saleem, M., et al., J. Appl. Polym. Sci., 1989. Vol. 37(3): p. 617-625.

[5.67] Dimethyl Sulfoxide (DMSO) a Dipolar, Aprotic Reaction Solvent, L.L.C. Gaylord Chemical Company, Editor. 2007.

6: Fractional Crystallization Model of Multicomponent Aluminum Alloys: A Case Study of Aircraft Recycling [7]

Jose A. Muñiz-Lerma†, Manas Paliwal†, In-Ho Jung†, and Mathieu Brochu*†

† Department of Mining and Materials Engineering, McGill University, 3610 University Street, Montréal, QC, H3A 0C5, Canada.

6.1: Preface

After the EOL aircraft is dismantled, sorted, and decoated, the next step in the aircraft recycling process is refining. In this process, excess alloying elements and detrimental impurities such as Fe and Si must be reduced to levels deemed acceptable to be classified as high-value products. This chapter explores the technical viability of refining aircraft aluminum scrap by means of fractional crystallization. The prediction of the refining and recovery efficiencies of aluminum by this method was assessed using a one-dimension solidification model which included, in addition to solid back diffusion, two of the most important processing parameters: stirring and solidification velocity. These two parameters were explored and the corresponding solidification velocities and stirring levels able to provide the highest efficiencies are reported in this chapter.

6.2: Abstract

A one-dimension numerical solidification model has been used to predict the recovery and refining efficiency of fractional crystallization applied to a blend of aircraft Al scrap with variations of Fe and Si. The variation of these impurities has been carried out to account for the pick-up of impurities during handling the scrap. The model incorporates the effect of melt stirring by using an effective partition coefficient. Moreover, the kinetic factors that affect the formation of primary

[7] To be submitted to the journal of Metallurgical and Materials Transactions B.

Al FCC during fractional crystallization such as solidification velocity, thermal gradient, cooling rate and solute back diffusion are accounted in the solidification model. The results suggest that the optimum solidification velocities able to yield the highest refining and recovery efficiencies, range between 1.0 x 10^{-6} m/s and 1.0 x 10^{-5} m/s when medium to high stirring levels are applied. If solidification occurs faster than the predicted velocities, refining of Al might not occur. The recovery of refined Al has been estimated as 31 wt.% of the initial liquid when the process is carried out at 1 x 10^{-6} m/s and the Fe and Si concentrations are 1 % and 2 % respectively. If any of these impurities increase, the Al recovery is reduced.

6.3: Introduction

Aerospace industry is facing an increasing waste generation coming from decommissioned aircraft [6.1].It has been estimated that over the next twenty years approximately 12,000 aircraft will be at their end of life (EOL), reaching a peak of annual 1000 aircraft disposal by 2023 [6.2, 6.3]. In order to reduce the environmental footprint generated by the growing decommissioned aircraft, research initiatives aiming to improve the management of aircraft at their end of service life have been carried out [6.2, 6.4, 6.5]. The Airbus project "*Process for Advanced Management of End-of-Life of Aircraft (PAMELA)"*, reported that around 85% (in weight) of the aircraft under study can be either reused (15%) or recycled (70%); where Al components from the 2XXX and 7XXX series account for the highest recycling volume [6.4]. Recycling these Al components, would correspond to the saving of around 95% of the embodied energy and greenhouse gas emissions associated with the primary Al production for the same volume [6.6, 6.7].

One of the main problems for the recycling of aerospace Al alloys, in addition to the high amount of alloying elements, is the pickup of detrimental impurities such as Fe and Si during handling the EOL aircraft fuselage [6.6]. If remaining in the recycled products, the presence of these impurities negatively impact the fracture toughness of the alloys [6.8]. Up to now, conventional refining methods were not found successful for the removal of Fe and Si during the production of secondary alloys. Thus, developing processing approach to produce high value-added alloys from aircraft scrap in a closed-loop recycling process, remains to be achieved. Unfortunately, this situation promotes the scrap dilution with primary Al to produce cast products, downgrading the alloy value.

According to Zhang et al. [6.9], substantial research efforts have been made to reduce the concentration of Fe and Si from the Al matrix. Generally, elements such as Mn, Cr, Co, and Sr, have been used as additives to neutralize the Fe and Si-containing precipitates. Then, these precipitates are further removed from the matrix by techniques such as filtration or gravitational, electromagnetic, and centrifuge separation. Despite the advances, the high-energy intensive three-layer electrolysis process remains the most effective process to remove Fe and Si from Al. Nevertheless, a promising technology that can be envisaged as a refining method for aircraft Al scrap, is fractional crystallization [6.10-6.15]. In this technique, the impure material is processed between the solidus and liquidus temperature, where solid and liquid phases co-exist. A controlled cooling in this region allows the material to slowly solidify with the impurities segregating at the solid-liquid interface. As the solidification proceeds, a pure solid phase forms along one end of the ingot whereas a high impurity concentration section moves to the outer end which can be discarded. Essentially, the fractional crystallization process is governed by solidification kinetics such as partitioning of impurities between solid and liquid phase, back diffusion of solutes, solidification velocity and degree of melt stirring [6.16, 6.17]. Only few studies have been reported in the literature focusing on the effect of these important variables on the fractional crystallization process applied to Al recycling. Sillekens et al. [6.18], estimated the theoretical purification efficiency for a number of alloying elements considering the lever rule principle in their respective binary system. Boender et al. [6.19], studied the thermodynamic capabilities of fractional crystallization for the binary system Al-Si, and the ternary systems Al-Si-Fe, Al-Si-Mn, and Al-Cu-Mg under non-equilibrium conditions. The refining predictions were obtained using Scheil-type simulations considering an equilibrium partition coefficient. Even though these studies elucidate the theoretical refining of Al alloys based on equilibrium thermodynamics, only binary and ternary systems were considered. In order to optimize the fractional crystallization process, it is important to understand the partitioning of solutes at the micro scale. Thus, the effect of solidification velocity, back diffusion of solute elements, and degree of stirring, have to be considered to predict the refining efficiency of Al scrap.

The purpose of the present study is to explore the refining efficiency at a microstructure level of aircraft Al scrap by fractional crystallization. The refining feasibility was assessed by using a one-dimension multicomponent solidification model that takes into account an effective partition

coefficient, solute back diffusion in the primary Al FCC phase, solidification velocity, and degree of melt stirring. Accurate thermodynamic data were obtained from the FTlite database incorporated to the Factsage thermodynamic software [6.20].

6.4: Solidification Model

The fractional crystallization process is a macro scale phenomena where ingots of several meters in length are directionally solidified to produce a pure solid (Al FCC) phase. The impure material is held in a mushy zone and solidified under controlled cooling rate. Stirring conditions are naturally induced in the melt due to induction or resistance heating. The solidified ingot will typically consist of columnar or equiaxed dendrites along with different secondary phases formed at the dendritic boundary. The growth direction of the dendrites and the advance of solidification front is governed by thermal conditions during the process. The temperature profile and the area fraction of the solid and liquid phases can be captured with the macro scale fluid dynamics model. However, the critical information regarding the solute distributions (microsegregation) is difficult to ascertain from these models. Theoretically, the recovery of any solute at the end of fractional crystallization is dependent on its average concentration in the solid phase. Moreover, the segregation occurring at the dendritic boundary also affects the final recovery efficiency. Therefore, in the present work the refining efficiencies of different solutes are predicted from a microstructural solidification model with the length scale of the secondary arm spacing. The schematics of various length scales is shown in Figure 6-1. The present solidification model is based in the previous work of Paliwal et al. [6.21-6.23] and it captures the effect of the processing parameters such as solidification velocity , thermal gradient, cooling rate, back diffusion of solutes and coarsening on the microstructural development. The effect of melt stirring during fractional solidification is incorporated to the model by the so-called effective partition coefficient of solute at liquid and solid interface given by Burton et al. [6.24] The input variables considered are, therefore, alloy composition, solidification velocity *(V)*, thermal gradient *(G)*, and cooling rate *(CR)*, which is obtained by the product of G and V, and stirring conditions.

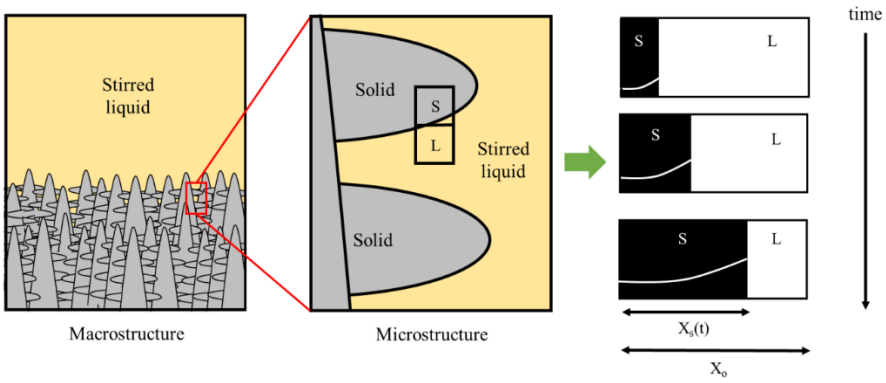

Figure 6-1. Scale length of the present fractional crystallization model.

The calculation procedure is shown in Figure 6-2 (a) and (b). Once the input variables are established, the secondary dendrite arm spacing (SDAS) in the solidified microstructure is estimated. The SDAS is calculated using the Kattamis and Flemings's model shown in Eqn 1 [6.25] in its extension to a multicomponent system as proposed by Rappaz and Boettinger in Eqn 2 [6.26].

$$\lambda_2 = 5.5\left(Mt_f\right)^{1/3} \qquad [1]$$

$$M = \frac{-\Gamma}{\sum_{i=1}^{n} m^i\left(1-k_o^i\right)\left(C_{Lu}^i - C_o^i\right)/D_l^i} ln\left[\frac{\sum_{i=1}^{n} m^i\left(1-k_o^i\right)C_{Lu}^i/D_l^i}{\sum_{i=1}^{n} m^i\left(1-k_o^i\right)C_o^i/D_l^i}\right] \qquad [2]$$

were λ_2, is the SDAS, Γ is the Gibbs-Thompson coefficient, D_l is the diffusivity of the solute in the liquid phase, C_{Lu} is the univariant liquid composition where the solidification process in fractional crystallization is terminated, C_o is the initial solute composition, m is the liquidus slope, k_o is the equilibrium partition coefficient, and t_f is the solidification time.

The first step during the microsegregation prediction loop is the computation of the distribution coefficient of solutes, which expresses the ability of the impurities to segregate and thus the refining efficiency during fractional crystallization. During solidification, an enriched layer of solute, known as the diffusion boundary layer, δ, builds up ahead of the solid-liquid interface in

the liquid domain. The thickness of this layer effectively sets the diffusion distance in the liquid phase and beyond this layer the concentration in the liquid phase equals the overall solute. The solute concentration in this zone determines the effective solute segregation (k_{eff}) at non-equilibrium conditions [6.27].

Burton et al. [6.24] proposed a steady-state equation to describe the effective distribution of solute in crystals grown from a melt considering the building up of impurities in δ. The authors assumed that beyond this layer, the fluid flow keeps the concentration uniformly equal to C_l. However, within δ, the growth velocity and diffusion contribute to transporting the excess solute away from the growing crystal. Their mathematical analysis led them to derive the well-known effective distribution coefficient equation, depicted in Eqn. 3:

$$k_{eff}^{i} = \frac{k_o^i}{k_o^i + \left(1 - k_o^i\right) e^{-\frac{V \cdot \delta}{D_l^i}}} \qquad [3]$$

where V is the solidification velocity, δ the thickness of the diffusion boundary layer ahead the solidification front, and D_l corresponds to the diffusivity of the solute in the liquid [6.24]. In contrast to the k_o which mainly depends on the equilibrium phase diagram, the k_{eff} varies with D_l, V, and δ. The value of δ relies on the diffusivity of the solute in the liquid phase, the viscosity and especially in the conditions of fluid flow ahead of the solid-liquid interface. It has been reported that typically, in fractional crystallization processes, the value of δ can be in the order of 10^{-3} m for very low stirring to 10^{-5} m for vigorous stirring at the macroscale level [6.27-6.29]. Nevertheless, at the microstructure level the δ values reported before are not reasonable to be considered due to the model length scale. The present model considers the half of the secondary dendrite arm spacing (SDAS) as the control volume for microsegregation. We have assumed that the δ is reasonably smaller than the previously reported values. Hence, we have considered 0.1, 1, and 10 % of the SDAS to account for slow, medium, and high stirring conditions.

The k_{eff} and therefore the refining efficiency, can be manipulated by controlling the solidification velocity and the fluid flow ahead of the solid-liquid interface. The model proposed by Burton et al. [6.24], known as the BPS model, has been widely used to predict the k_{eff} for the purification of metals [6.28-6.33]. Thus, in the present work, the effect of melt stirring and

solidification velocity are incorporated in the microsegregation model replacing the k_o previously used by Paliwal et al. [6.21-6.23] by the k_{eff} proposed by Burton et al. [6.24]. The k_o of each solute used to estimate k_{eff} was obtained from FactSage using the FTlite database [6.20], and the D_l values are given in Table 6-1.

The next step in the microsegregation model is the determination of the time dependent solid diffusion domain in the primary phase, i.e., FCC-Al phase. In this step, the effective distribution coefficient of solutes in Eqn. 3 at the solid-liquid interface and homogeneous temperature ahead of the interface are assumed. Additionally, complete mixing in the liquid phase ahead of the diffusion boundary layer is also assumed. It should be noted that the effect of diffusion boundary is taken into account by the effective distribution coefficient. Taking these into consideration, the solute balance in the secondary dendrite arm spacing at a specific time step is given as:

$$\int_0^{x_s^i} C_s^i \, dx + \int_{x_s^i}^{x_o} C_l^i \, dx = x_o C_o^i \qquad [4]$$

where $x_s^i(t)$ is the domain of solid diffusion in FCC-Al phase, x_o is the half of the SDAS, C_l^i, is the concentration of solute in the solid phase, and C_o^i is the initial solute concentration in the alloy. With the assumption of complete mixing in the liquid phase, the liquid composition C_l^i remains homogeneous at all time. Then, differentiating Eqn. [4] with respect to time we obtain:

$$\int_0^{x_s^i} \frac{\partial C_s^i}{\partial t} dx + \left(k_{eff}^i - 1\right) C_l^i \frac{dx_s^i}{dt} + \left(x_o - x_s^i\right) \frac{dC_l^i}{dt} = 0 \qquad [5]$$

The solute back diffusion in the solid FCC Al domain $0 \leq x \leq x_s^i$ is governed by the Fick's second law:

$$\frac{\partial C_s^i}{\partial t} = D_s^i \frac{\partial^2 C_s^i}{\partial x^2} \qquad [6]$$

where D_s^i is the solute diffusivity in solid FCC Al. Substituting Eqn. [6] into Eqn. [5] gives:

$$\int_0^{x_s^i} D_s^i \frac{\partial^2 C_s^i}{\partial x^2} dx + \left(k_{eff}^i - 1\right) C_l^i \frac{dx_s^i}{dt} + \left(x_o - x_s^i\right) \frac{dC_l^i}{dt} = 0 \qquad [7]$$

Assuming no mass flow of solute from the end of the secondary dendrite arm spacing, $\left| D_s^i \frac{\partial C_s^i}{\partial x} \right|_{x=x_s^i} = 0$, a constant D_s for each solute per time step, and replacing the derivative of the third term by $\frac{dC_l^i}{dt} = \frac{CR}{m^i}$, equation [7] becomes the governing equation for the solute balance written as:

$$\left| D_s^i \frac{\partial C_s^i}{\partial x} \right|_{x=x_s} + \left(k_{eff}^i - 1\right) C_l^i \frac{dx_s^i}{dt} + \left(x_o - x_s^i\right) \frac{CR}{m^i} = 0 \qquad [8]$$

where the first term corresponds to the back-diffusion of solute into the solid phase considering the D_s^i presented in Table 6-1 and the following two terms represent the redistribution of solute due to the movement of the solid-liquid front. Discretizing equation [8] using Euler forward treatment [6.34] gives:

$$x_s^{new^i} = x_s^{old^i} + \Delta t \left[\frac{\left| D_s^i \frac{\partial C_s^i}{\partial x} \right|_{x=x_s}^{old} + \left(x_o - x_s^i\right) \frac{CR}{m^i}}{\left(1 - k_{eff}^i\right) C_l^i} \right] \qquad [9]$$

$$x_s = \left(\sum_{i=0}^{n} x_s^{new^i} \right) / n \qquad [10]$$

where Δt is the calculation time step, and $\left| D_s^i \frac{\partial C_s^i}{\partial x} \right|_{x=x_s}^{old}$ provides the back diffusion term evaluated at the previous time step by numerically solving Eqn. [6]. This term requires the computation of

the solute profiles controlled by diffusion in the solid domain of the half dendrite arm spacing, $0 \leq x \leq x_s(t)$.

Table 6-1. Diffusion parameters of solute elements i, in liquid (D_l^i) and FCC Al (D_s^i) [6.35].

$D_l^{Cu} = 1.06x10^{-7}exp^{-2886/T}$	$D_s^{Cu} = 4.44x10^{-5}exp^{-16469/T}$
$D_l^{Mg} = 9.90x10^{-5}exp^{-8611/T}$	$D_s^{Mg} = 1.49x10^{-5}exp^{-14821/T}$
$D_l^{Zn} = 5.12x10^{-8}exp^{-2670/T}$	$D_s^{Zn} = 1.19x10^{-5}exp^{-14280/T}$
$D_l^{Fe} = 2.34x10^{-7}exp^{-4209/T}$	$D_s^{Fe} = 3.62x10^{-1}exp^{-26322/T}$
$D_l^{Si} = 1.34x10^{-7}exp^{-3608/T}$	$D_s^{Si} = 1.38x10^{-5}exp^{-14464/T}$

In order to solve Eqn. [6], a one-dimension Finite Difference Control Volume Formulation is employed in the present study. For this approach, the computational domain is divided into a series of overlapping control volumes such as there is one control volume surrounding each grid node. The differential equation is then integrated over each control volume. A fully implicit scheme is used to solve Eqn. [6] and a tridiagonal matrix algorithm is employed to calculate the solute distribution in the FCC-Al phase and the back diffusion term.

Fractional crystallization is only carried out in the region where the liquid and the primary Al FCC phase coexists. Thus, the microsegregation calculations are terminated once the solidification reaches the univariant line. If the solidification process is not terminated at the univariant composition, the formation of second phases rich in solute decreases the efficiency of fractional crystallization. After the microsegregation calculation is terminated, the total fraction of solid f_s, is determined as x_s/x_o.

Once the segregation profiles have been obtained for each solute, the average solute concentration (C_f^i) in the Al FCC phase is automatically obtained by calculating the area under the curve of the solute profiles in the solid Al FCC phase. Then, the refining ratio which is the ratio of solute in the solid Al phase to the initial solute composition C_f^i/C_o^i is determined to further calculate the refining efficiency η, by Eqn 11:

$$\eta = \frac{\left(C_o^i - C_f^i\right)}{C_o^i} * 100 \qquad [11]$$

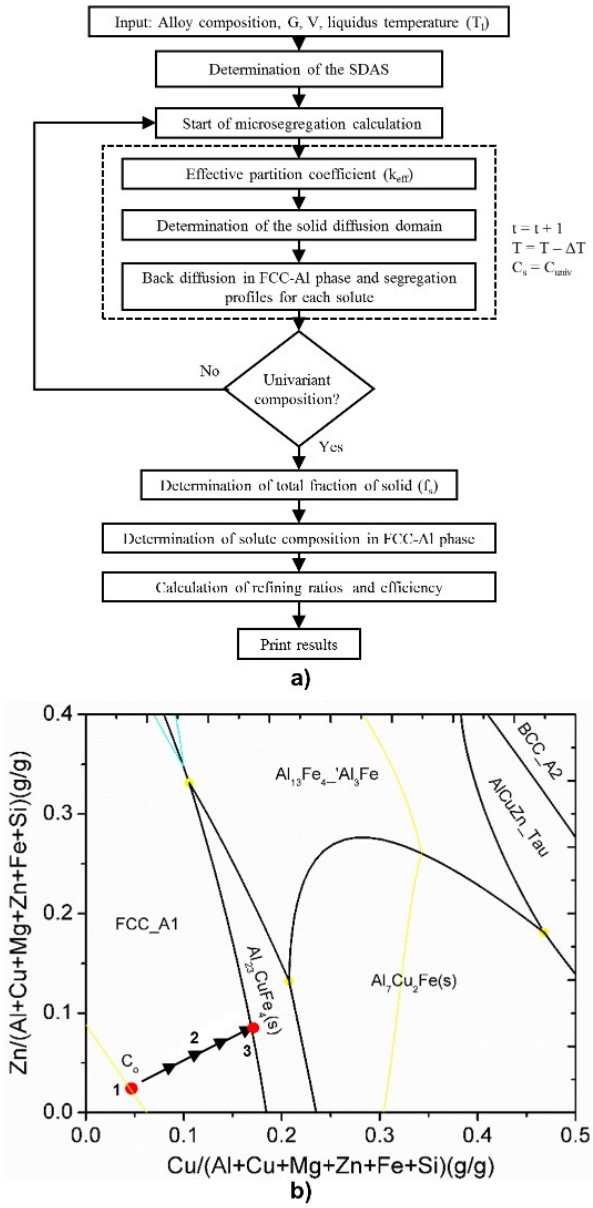

Figure 6-2. Schematic of the calculation procedure for the solidification model. (a) Flow chart, and (b) representation in liquidus projection for Al-Cu-Zn-2.13Mg-0.5Fe-0.5Si alloy (wt.%), where 1 is the initial composition, Co, 2 is the course of fractional solidification, and 3 is the univariant composition corresponding to the termination of solidification.

6.4.1: Modeling Cases

A test case scenario has been used to establish the generality of the model. The hypothetical alloy composition selected for this purpose is of Al-0.5Cu-0.5Mg-0.5Zn-0.5Fe-0.5Si (wt, %). The solidification model was carried out over a range of solidification velocities (V) varying from 10^{-6} to 10^{-3} m/s considering three different values of the diffusion boundary layer (δ) such as 0.1, 1, and 10 % of the SDAS obtained for each velocity at a constant thermal gradient of 5000 K/m.

A real case scenario of recycling has been used in the present work. For this purpose, an Al scrap composition resulting from the blend of Al components coming from a Bombardier CRJ-100ER aircraft has been considered. The studied alloy corresponds to Al-2.43Cu-2.13Mg-4.67Zn (wt. %). Additions of Fe and Si have been considered to account for the pick-up of unwanted impurities during the dismantling and handling of the scrap. Before the application of the solidification model, a thermodynamic analysis using the thermodynamic software FactSage, has been carried out to determine the concentration limit of Fe and Si that can be treated by fractional crystallization considering the chemical compositions depicted in Table 6-2. Subsequently, the solidification model is applied to a selected alloy in order to predict the refining efficiency at the microstructure scale.

Table 6-2. Aircraft scrap base alloy composition Al-2.43Cu-2.13Mg-4.67Zn with additions of (x)Fe and (y)Si (wt. %) used to estimate the thermodynamic Al yield in fractional crystallization.

Alloy	(y)Si
System A [1Fe-(y)Si]	1, 1.1, 1.2, 1.3, 1.6, 2, 2.5, 3, 4, 5
System B [1.2Fe-(y)Si]	
System C [1.3Fe-(y)Si]	

6.5: Results and Discussions

6.5.1: Test Case Scenario

The SDAS calculated using the Rappaz and Boettinger model [6.26] for the test alloy Al-0.5Cu-0.5Mg-0.5Zn-0.5Fe-0.5Si (wt, %), is depicted in Fig. 3. The estimated SDAS for this alloy ranges between 2.0 x 10^{-4} and 2.0 x 10^{-5} m depending on the cooling rate. Thus, it is expected that the diffusion boundary layer thickness, δ, taken as 0.1, 1, and 10% of the SDAS becomes smaller as the cooling rate is increased.

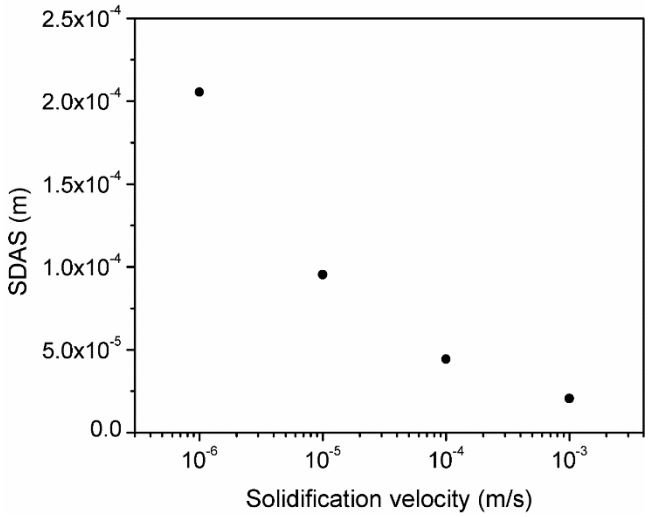

Figure 6-3. Variation of the SDAS of the test alloy Al-0.5Cu-0.5Mg-0.5Zn-0.5Fe-0.5Si (wt, %) as a function of solidification velocity.

The k_{eff}, variation of the test alloy composition as a function of solidification velocity and the thickness of the diffusion boundary layer is shown in Figure 6-4. It can be observed that both, the solidification velocity and the stirring conditions have an important effect on the partition coefficient of solutes. As the solidification velocity tends towards zero, the effective partition coefficient approaches to the equilibrium value. On the other hand, as the solidification velocity is increased, the partition coefficient departs from the equilibrium and tends towards the unity when the fluid flow, controlled by stirring, is decreased. Generally, it can be observed that if the process

is carried out at solidification velocities in the range of 1.0 x 10^{-6} and 1.0 x 10^{-5}, the diffusion boundary layer thickness does not play a significant role. Under these conditions, the combined effect of a slow solidification velocity and stirring maintains the k_{eff} close to the equilibrium.

The stirring level plays an important role when the solidification is achieved at higher velocities, i.e., higher than 1 x 10^{-5} m/s. At these velocities, a high stirring energy is required to maintain the partition coefficient close to the equilibrium conditions. Additionally, the deviation from the equilibrium at fast solidification velocities varies from solute to solute and directly depends on the liquid diffusivity and the equilibrium partition of the species [6.24].

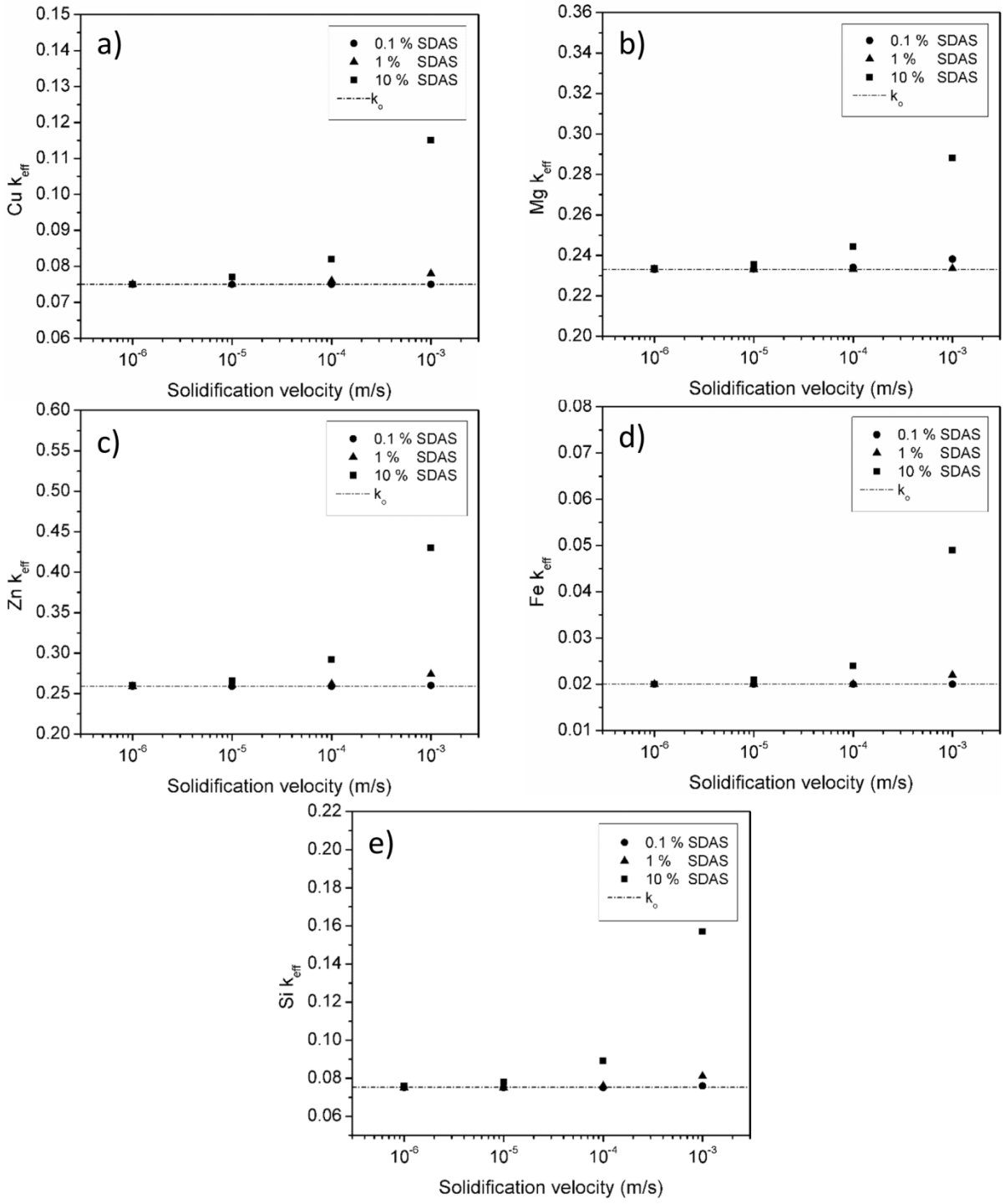

Figure 6-4. Variation of the effective partition coefficient of (a) Cu, (b) Mg, (c) Zn, (d) Fe, and (e) Si, in the alloy Al-0.5Cu-0.5Mg-0.5Zn-0.5Fe-0.5Si (wt, %) as a function of solidification velocity and stirring conditions.

To elucidate the effect of stirring on the impurity segregation, the simulated segregation profile of Zn generated at a solidification velocity of 1 x 10^{-4} m/s and δ values of 0.1, 1, and 10% of the SDAS is presented in Figure 6-5. In addition to the effect of back diffusion, the variation of the k_{eff}, as a consequence of stirring, clearly modifies the segregation profile of Zn due to the boundary conditions of the solidification model. The first solid to form during the solidification process will have the composition resulting from the product of k_{eff}, times the initial composition of the solute, C_o. Thus, at higher k_{eff} values, a higher solute concentration in the primary Al FCC phase will be obtained.

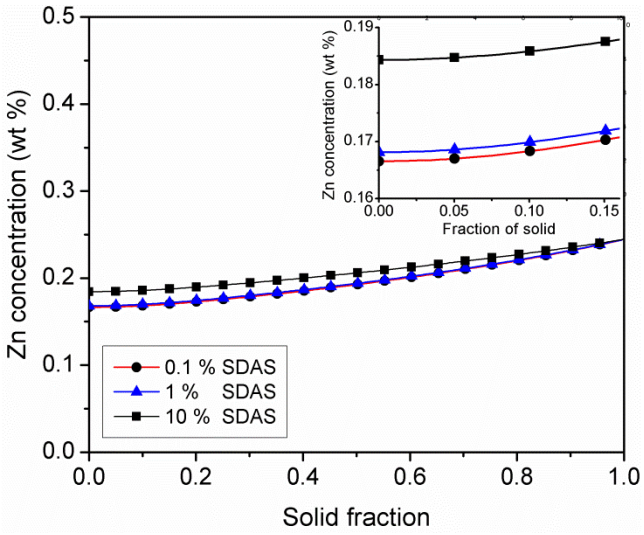

Figure 6-5. Segregation profile of Zn in the alloy Al-0.5Cu-0.5Mg-0.5Zn-0.5Fe-0.5Si (wt, %) solidified at 1.0 x 10-4 m/s at δ values of 0.1, 1, and 10% of the SDAS.

In fractional crystallization, the maximum thermodynamic removal limit that any impurity can achieve is limited by the equilibrium partition coefficient. Figure 6-6, presents the refining efficiencies of the alloying elements of the test alloy as a function of the solidification conditions. Such efficiencies are compared with the efficiencies simulated under Scheil cooling conditions. At a low solidification velocity, i.e., 1.0 x 10^{-6} m/s, no difference on the refining efficiency is observed even when a δ of 10 % of the SDAS is employed. The efficiency obtained at this solidification condition is mainly affected by back diffusion. In fact, as the solidification velocity

is increased, the back diffusion effect is not the dominant factor affecting the refining efficiency. This effect can be clearly seen in Figure 6-6 (c) corresponding to the efficiency of Zn. From this figure, the transition between the effect of back diffusion and the k_{eff}, effect is present at around 1.0 x 10^{-4} m/s and a δ value of 0.1 and 1 %. At this point, the efficiency reaches almost the equilibrium to subsequently decrease due to the increment of k_{eff}. The lowest refining efficiency is obtained when the fluid flow ahead of the solidification interface is not sufficiently strong to decrease the δ to a value of 0.1 % of the SDAS. It is important to note that the refining efficiency of the solutes is close to equilibrium when the solidification velocities range between 1.0 x 10^{-4} and 1.0 x 10^{-3} m/s. Nonetheless, such equilibrium can only be achieved when sufficiently strong stirring is applied. A small increment in the δ due to a deficient stirring, causes the refining efficiency to decrease steeply.

In general, at strong stirring conditions the solute pile-up at solid-liquid interface is minimized and the effective partition coefficient is close to equilibrium. However, the solute build up at the solid-liquid interface occurs at weak stirring conditions even at low solidification velocities in the order of magnitude of 10^{-5} m/s. As the solidification velocity is increased, the stirring effect is unable to push the accumulated solute into the far field of the liquid phase resulting in the increase of the partitioning coefficient. The overall effect of this phenomena is the partition of more solute in the solid phase resulting in a decrease of overall efficiency. It is noted that the combined effect of stirring and solidification velocity on solute distribution is captured in the present solidification model. In the following section, the present model is applied to a real case scenario of refining Al scrap from the aerospace industry.

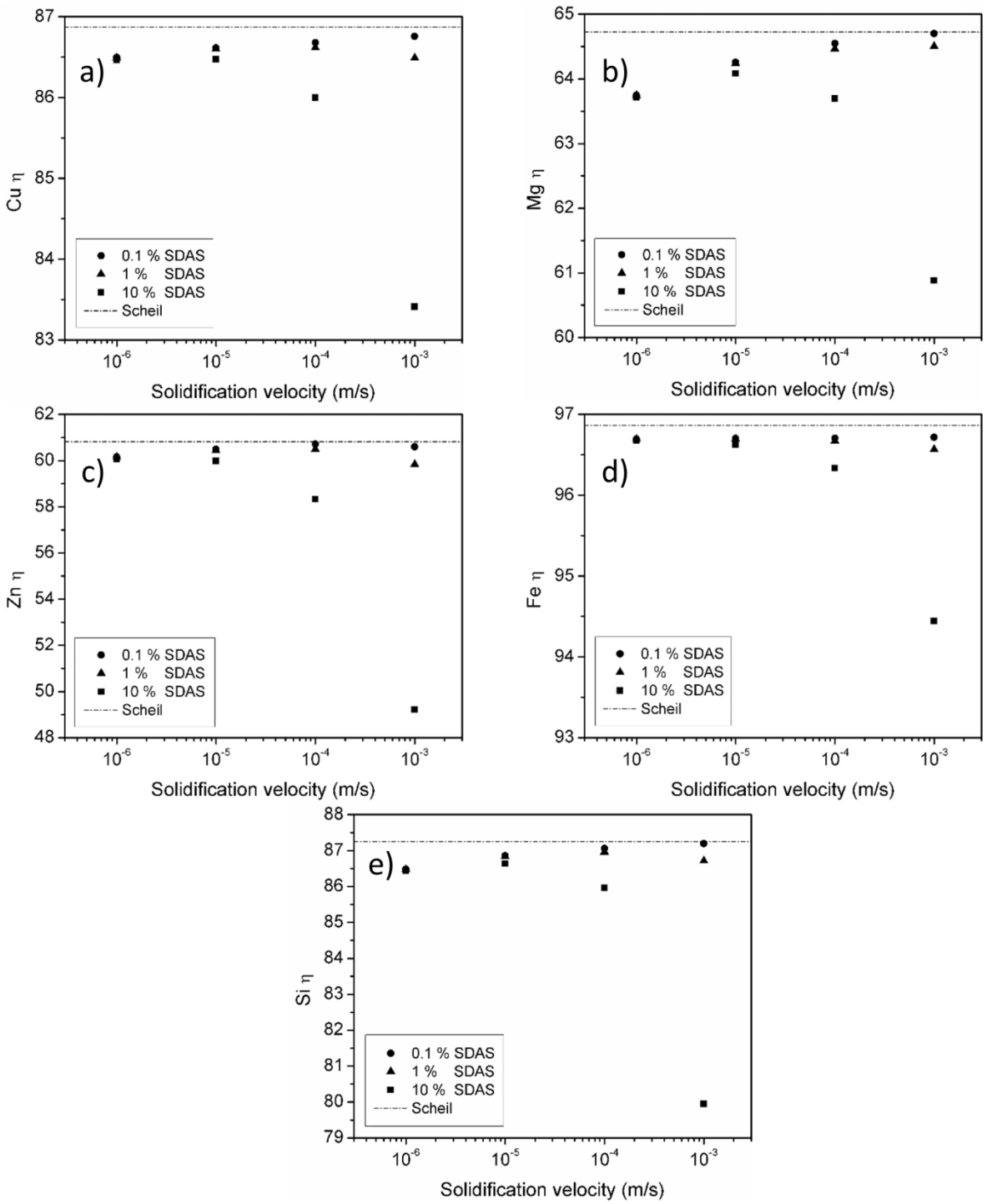

Figure 6-6. Refining efficiencies for (a) Cu, (b) Mg, (c) Zn, (d) Fe, and (e) Si, in the test as a function of solidification velocity and stirring conditions

6.5.2: Real Case Scenario: Aluminum Aircraft Scrap Refining

The Al scrap alloy selected for this study is based on a blend of Al components from a Bombardier CRJ-100ER aircraft. The resulting chemical composition of such blend corresponds to Al-2.43Cu-2.13Mg-4.67Zn (wt. %). The predicted liquidus projection of such alloy with additions of Fe and Si is presented in Figure 6-7. The projection does not show a wide range of crystallization region of primary Al FCC phase. In fact, the crystallization region is limited by the concentration of Fe. If the amount of Fe in the alloy exceeds approximately 1.3 wt. %, no primary Al FCC phase is formed and thus, refining by fractional crystallization cannot thermodynamically occur.

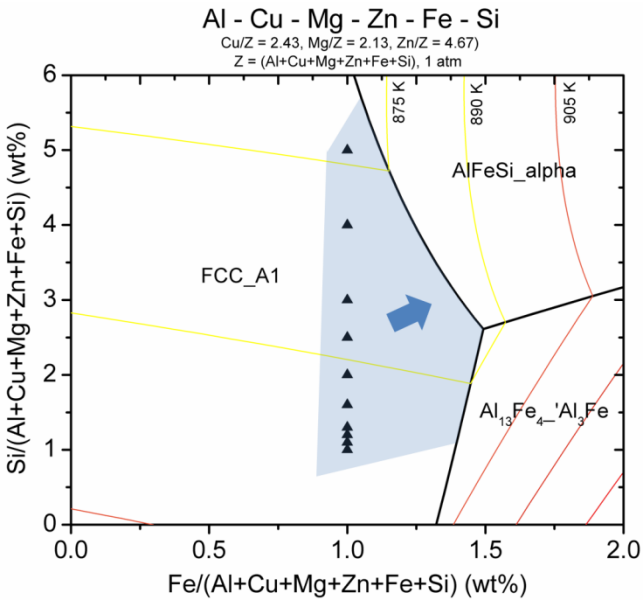

Figure 6-7. Liquidus projection of the Al rich corner in the multicomponent blended alloy with composition of Al-2.43Cu-2.13Mg-4.67Zn (wt. %) coming from a Bombardier CRJ-100ER aircraft.

The phase formation preference varies with the concentration of Si in the alloy as shown in Figure 6-7. It can be seen that at low Si concentration, the primary phase to be formed is Al FCC followed by the secondary $Al_{13}Fe\_Al_3Fe$ phase. In contrast, if the concentration of Si increases, the AlFeSi_alpha phase is formed instead of the $Al_{13}Fe\_Al_3Fe$ phase. The solidification range for the

alloys containing a concentration of Fe between 1 and 1.3 wt. % and Si between 1 and 5 wt% is depicted in Figure 6-8. It can be observed that the solidification range for the scrap alloy with additions of Fe and Si is not significantly large. In fact, the maximum solidification range is observed in the alloy containing 1 wt. % of Fe and Si. If the concentration of Fe is slightly increased up to 1.3 wt. %, the range is substantially decreased. Thus, in order to efficiently refine aircraft Al alloys, the temperature during solidification have to be strictly controlled to avoid the precipitation of phases rich in solutes such as the $Al_{13}Fe$_Al_3Fe and the AlFeSi_alpha phases. The formation of these phases during the fractional crystallization process will reduce substantially the overall refining process.

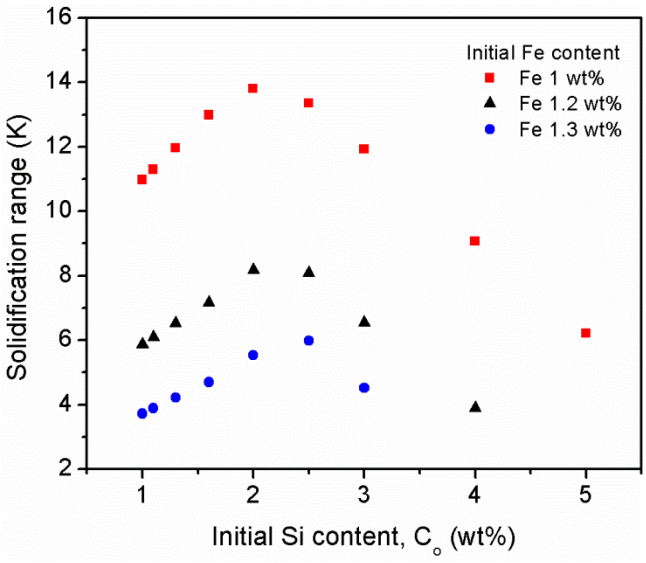

Figure 6-8. Solidification range for the blended aircraft scrap composition of Al-2.43Cu-2.13Mg-4.67Zn (wt. %) with different additions of Fe and Si.

In order to present the functionality of the present solidification model, the refining efficiency at a microstructure level was estimated for the aircraft Al scrap composition of Al-2.43Cu-2.13Mg-4.67Zn-1Fe-1Si (wt. %). The combined effect of the solidification velocity and stirring condition, i.e., δ, on the refining efficiency of the aircraft scrap alloy is depicted in Figure 6-9 for each solute in the selected alloy. Independently of the solidification velocity, Fe and Si present refining

efficiencies close to Scheil conditions followed by Cu, Zn, and Mg when high stirring levels are applied. It is likely to think that at solidification velocities higher than 1.0 x 10^{-5} m/s. the best refining efficiencies can be achieved. Nonetheless, these efficiencies can only be obtained at the expense of intense stirring in order to remove the piling-up of impurities in front of the solid-liquid. If the stirring is not strong enough, the effective partition coefficient increases decreasing the refining efficiency. Thus, solidification velocities lower than 1.0 x 10^{-5} m/s are desired since the effect of stirring is not significant.

Experimentally, Mehmetaj et al. [6.10] and Sillekens et al. [6.11] carried out fractional crystallization experiments on Al alloys. Specifically, Mehmetaj et al. [6.10] studied the refining the Al-7.2Si (wt.%) alloy by means of a static layer crystallizer reporting a Si removal efficiency of ~50 % at a growing rate of 1 x 10^{-6} m/s, while Sillekens et al. [6.11] studied the Al-6Si (wt.%) alloy using the zone melting process reporting a Si removal efficiency of ~70 % at a growth velocity of 1.67 x 10^{-6} m/s. The efficiencies obtained by Mehmetaj and Sillekens are much lower than the predicted by the present model. Nevertheless, it is important to mention that the overall concentration of Si reported by the previous authors was obtained by spectroscopy techniques from the bulk solidified samples. If the cooling conditions are not properly controlled during fractional crystallization, the formation of second phases rich in solute will affect the overall refining efficiency.

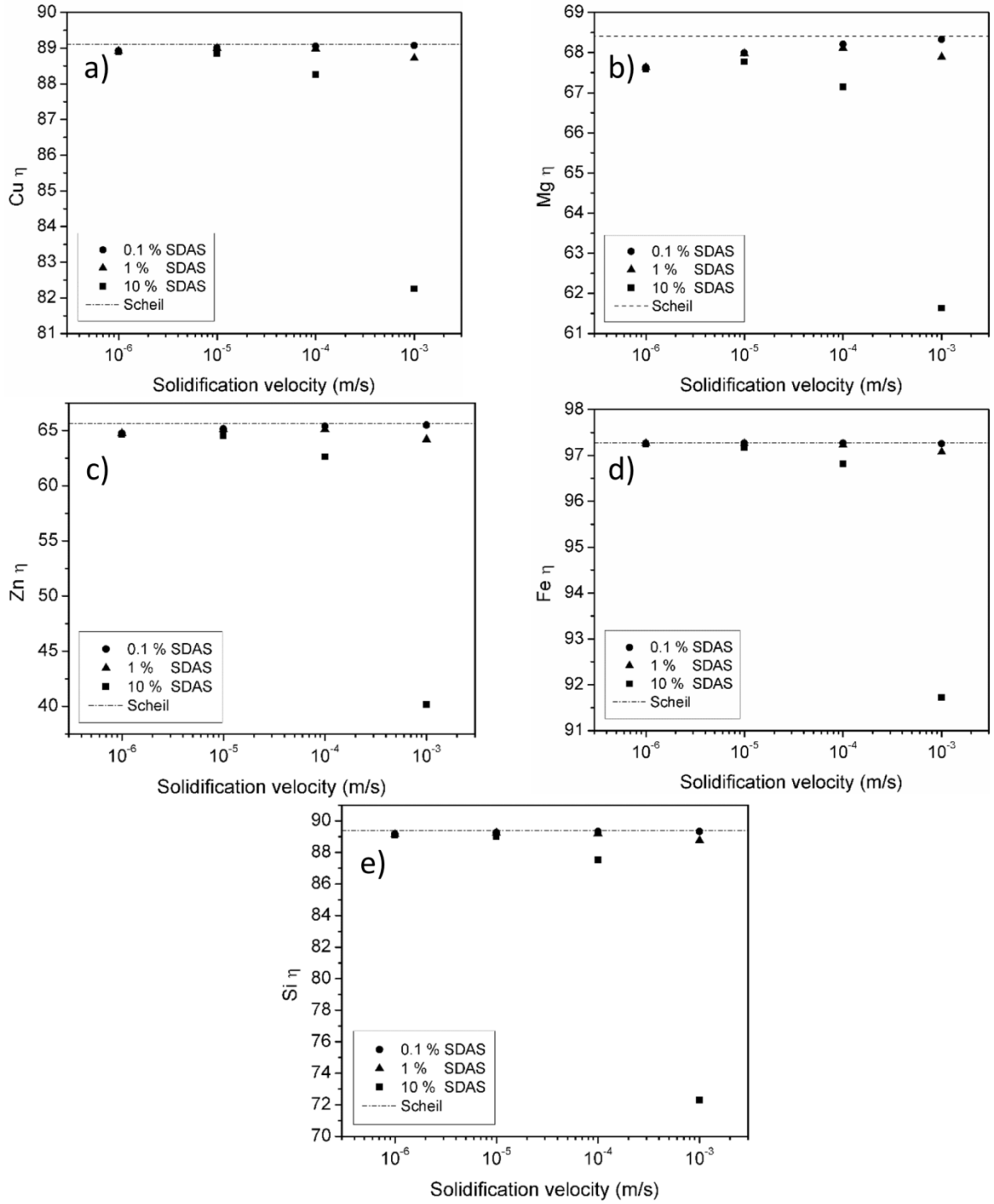

Figure 6-9. Refining efficiencies for (a) Cu, (b) Mg, (c) Zn, (d) Fe, and (e) Si, in the Al-2.43Cu-2.13Mg-4.67Zn-1Fe-1Si (wt. %) aircraft scrap alloy as a function of solidification velocity and stirring conditions

In order to study the recovery of refined Al, a solidification velocity of 1 x 10^{-6} m/s and a high stirring (δ = 0.1 % of SDAS) have been selected. The weight percent of Al that can be recovered as a function of the Si and Fe concentration, is presented in Figure 6-10. It can be observed that the general trend of Al recovery is similar than the solidification range shown in Figure 6-8. As the content of Fe increases from 1 w% to 1.3 wt.%, the recovery of Al decreases. When the Fe concentration is 1 wt.%, the maximum recovery of 31 wt.% is obtained at 2.5 wt.% of Si. Additionally, when the Fe concentration are 1.2 and 1.3 wt.%, the maximum yield of 19 and 15 wt.% will also take place at approximately at 2.5 wt.% of Si respectively. A similar range of recovery values have been reported by Boender et al. [6.19]. According to their analysis of the binary and ternary systems, Si, Fe, and Cu could be removed from Al if 20 to 40 % of the original liquid is fractionally solidified. The reason of similarity between the recovery values reported by Boender and the ones predicted by the present model is merely due to the low effect of the effective partition coefficient at low solidification velocities, where the effective partition coefficient is closed to the equilibrium and the dominant factor controlling the refining process is back diffusion.

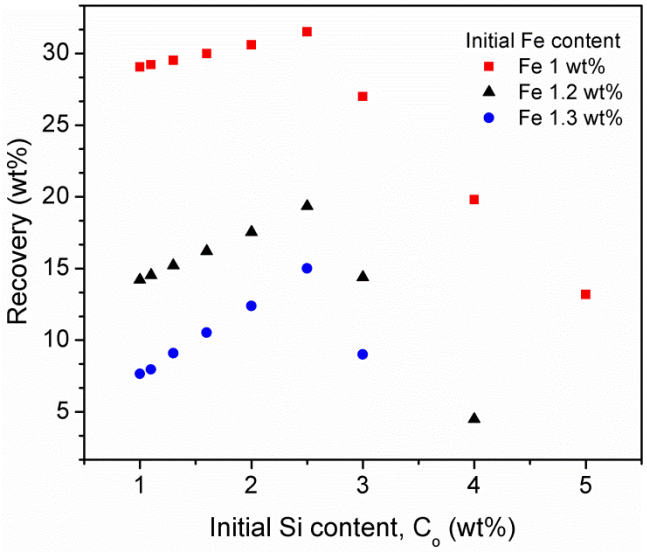

Figure 6-10. Predicted Al recovery at a solidification velocity of 1 x 10-6 m/s and a high stirring level (δ = 0.1% of SDAS).

6.6: Conclusions

A one-dimension multicomponent solidification model that considers back diffusion in the solid and an effective partition coefficient controlled by the solidification velocity and degree of melt stirring, has been used to predict the refining and recovery efficiencies of fractional crystallization applied to a blend of aircraft Al components. The effect of stirring at solidification velocities in the range of 1.0×10^{-6} and 1.0×10^{-5} is not the dominant factor affecting the refining efficiency being back diffusion the governing effect. In contrast, at solidification velocities higher than 1.0×10^{-5} m/s the effective partition coefficient determines the refining efficiency at the micro scale.

A refining scenario of aircraft Al alloys has been also studied. The feasibility of the process strictly depends on the concentration of Fe in the scrap alloy. If the concentration of this impurity is higher than 1.3 wt. %, the solidification range, and thus the fraction of primary Al FCC phase is decreased. The solidification model has been applied to a selected alloy containing 1 wt% of Fe and Si. The optimum solidification velocity where minimum stirring is required has been found to be at solidification velocities of 1.0×10^{-5} m/s giving rise to a calculated refining efficiency of ~97 % if the formation of second phases rich in solutes is avoided. However, if such phases form, the refining efficiency might decrease. Thus, the cooling of the process has to be strictly controlled.

According to the present study, recycling aircraft Al alloys by means of fractional crystallization is a viable option to obtain high-grade Al alloys that potentially could be re-used in the aerospace industry. However, the successful implementation of this technique will strongly depend on the added value of the obtained products versus the processing costs which is not studied in the present work.

AUTHOR INFORMATION

Corresponding author

*Mathieu Brochu. E-mail: Mathieu.brochu@mcgill.ca. Tel.:+514-398-2354

6.7: Acknowledgments

The authors would like to thank the Consortium de Recherche et d'Innovation en Aérospatiale au Québec (CRIAQ), Bombardier, Bell Helicopter, Sotrem-Maltech, BFI, Nano Quebec, and Aluminerie Alouette for funding this project.

6.8: References

[6.1] Aviation, U., End of life solutions: Retirement is not what it used to be., in Aircraft Technology-Engineering & Maintenance. 2011. p. 60-65.

[6.2] AFRA. Aircraft Fleet Recycling Association. 2014; Available from: http://www.afraassociation.org/.

[6.3] AFRA. Aircraft Fleet Recycling Association.: Aircraft Retirement Tsunami. A 1000 Aircraft a Year to leave Service by 2023. 2014; Available from: http://www.afraassociation.org/news.cfm?newsid=162.

[6.4] Airbus, S.A.S. Eco-efficiency and Sustainability -G9- Issue 1. Process for Advanced Management of End of Life of Aircraft Available from: http://ec.europa.eu/environment/life/project/Projects/index.cfm?fuseaction=home.showFile&rep=file&fil=ACADEMY_PAMELA.pdf.

[6.5] CRIAQ-ENV412. Process for advanced management and technologies of aircraftend-of-life. 2015; Available from: http://www.polymtl.ca/env412/index.php.

[6.6] Das, S.K., J. G., Light metals., 2007: p. 1161-1166.

[6.7] Green, J.A.S., Aluminum Recycling and Processing for Energy Conservation and Sustainability. 1-271, ASM International, 2007.

[6.8] Staley, J.T., Microstructure and Toughness of High-Strength Aluminum Alloys, ASTM STP 605, in Properties Related to Fracture Toughness. 1976, American Society for Testing and Materials: Montreal, CA. p. 71-103.

[6.9] Zhang, L., Gao, J., Damoah, L.N.W. Robertson, D.G., Miner. Process. Extr. Metall. Rev., 2012. Vol. 33(2): p. 99-157.

[6.10] Mehmetaj, B., Bruinsmab, O.S., Koola, W.H., Jansensb, P.J., Katgermana, L. Aluminium scrap recycling with solid layer fractional crystallization. in 15th International Symposium on Industrial Crystallization (ISIC-15), Sorrento, Italy. 2002.

[6.11] Sillekens, W.H., Westrum, V., Schade, J.A. Bruinsma, O.S., Mehmetaj, B., Nienoord, M., Recycling of Metals and Engineered Materials, 2000: p. 963-977.

[6.12] Kahveci, A.I., Unal, A., Recycling of Metals and Engineered Materials, 2000: p. 979-991.

[6.13] De Vries, P.A., and Wouters, H. A., Method for fractional crystallisation of a molten metal. U.S. Patent 7,419,530 B2. 2008, Aleris Switzerland GmbH c/o K+P Treuhangesellschaft, Schaffhausen, CH.

[6.14] Wouters, H.A., Beunder, E.M., Boender, W., Hogenboom, M.A., Kieft, R., Storm, J.C., Crystallisation method for the purification of a molten metal, in particular recycled aluminium. U.S. Patent 7,892,318 B2. 2011, Aleris Switzerland GmbH c/o K+P Treuhandgesellchaft, CH.

[6.15] Verdier, J.F., Butruille, J.R., Leroy, M., Valax, D., Process for recycling aluminum alloy scrap coming from the aeronautical industry. U.S. Patent 8,202,347 B2,. 2012, Constellium France.

[6.16] Regner, A., Method of separating constituents of alloys by fractional crystallization. U.S. Patent 2,471,899. 1949, United Chemical and Metallurgical Works National Corporation, Prague, Czechoslovakia.

[6.17] Qiu, K., Duan, W., Chen Q. Basic principles of control of continuous crystallizer in metal refining. Mineral Processing and Extractive Metallurgy, 2001. 110, 161-164 DOI: doi:10.1179/mpm.2001.110.3.161.

[6.18] Sillekens, W.H., Verdoes, D., Van, W., Schade, J.F.M. Refining aluminium scrap by means of fractional crystallisation: technical feasibility. in Proceeding of the Fourth ASM International Conference and Exhibition on the Recycling of Metals, ASM Europe. 1999.

[6.19] Boender, W., Waringa, C.J., Krielaart, G.P., Folkertsma, A., Verdoes, D. Refining aluminium scrap with fractional crystallisation: Assessing its feasibility with

thermodynamics. in Light Metals: Proceedings of Sessions, TMS Annual Meeting. 2002. Warrendale, Pennsylvania.

[6.20] Bale, C.W., et al., Calphad, 2009. Vol. 33(2): p. 295-311.

[6.21] Paliwal, M., Kang, D., Essadiqi, E., Jung, In-Ho, Metall and Mat Trans A, 2014. Vol. 45(8): p. 3308-3320.

[6.22] Paliwal, M. and I.-H. Jung, J. Cryst. Growth, 2014. Vol. 394: p. 28-38.

[6.23] Paliwal, M., Kang, D., Essadiqi, E., Jung, In-Ho, Metall and Mat Trans A, 2014. Vol. 45(8): p. 3596-3608.

[6.24] Burton, J.A., R.C. Prim, and W.P. Slichter, The Journal of Chemical Physics, 1953. Vol. 21(11): p. 1987-1991.

[6.25] Kattamis, T. and M. Flemings, Transactions of the Metallurgical Society of AIME, 1965. Vol. 233(5): p. 992-&.

[6.26] Rappaz, M. and W.J. Boettinger, Acta Mater., 1999. Vol. 47(11): p. 3205-3219.

[6.27] Pfann, W.G., Normal Freezing and the Distribution Coefficient, in Zone Melting. 1958, John Wiley & Sons New York. p. 8-27.

[6.28] Krumnacker, M. and W. Lange, Kristall und Technik, 1969. Vol. 4(2): p. 207-220.

[6.29] Martin, E.P., A.F. Witt, and J.R. Carruthers, J. Electrochem. Soc., 1979. Vol. 126(2): p. 284-287.

[6.30] Bridgers, H.E., J. Appl. Phys., 1956. Vol. 27(7): p. 746-751.

[6.31] Yang, G., et al., Cryst. Res. Technol., 2014. Vol. 49(4): p. 269-275.

[6.32] Ghosh, K., V. Mani, and S. Dhar, J. Cryst. Growth, 2009. Vol. 311(6): p. 1521-1528.

[6.33] Kim, K.-H., S.-H. Lee, and D. Lee, J. Mater. Eng. Perform., 1996. Vol. 5(5): p. 651-656.

[6.34] Voller, V.R., Int. J. Heat Mass Transfer, 2000. Vol. 43(11): p. 2047-2052.

[6.35] Du, Y., et al., Materials Science and Engineering: A, 2003. Vol. 363(1–2): p. 140-151.

7: Summary and Future Work

Rising environmental consciousness and the increasing number of end-of-life aircraft have persuaded the aerospace sector on the importance of aircraft recycling. As a result, different research initiatives, such as PAMELA, AFRA, and AIMERE, were undertaken during the last 10 years. These projects were primarily designed to improve aircraft dismantling techniques in order to facilitate the recuperation of high-value components while the rest of the materials, such as polymers, composites, titanium, Al, etc., were sent to their respective recycling routes. Al, which is the most abundant metallic material present in the aircraft airframes, represents approximately 80% of the total aircraft weight. It is well known that recycling Al can save about 95% of the energy required for the primary production of Al from bauxite; however, the major recycling advantage, from the economic point of view, is obtained when downgrading of the alloy is avoided. There are three main problems associated with the recycling of Al from end-of-life aircraft fuselage, the first being the safe removal of the hexavalent Cr-containing primers, coatings and paints from the fuselage. The second complication is associated with the complex Al alloys present in the airframe, specifically compositions with high concentrations of alloying elements such as Cu and Zn which are very difficult to remove. Finally, if the concentration of Fe and Si in the alloys increases during the dismantling and handling of the airframe, downgrading of the alloy is unavoidable when traditional recycling processes are employed. In this regard, under the scope of the CRIAQ-ENV412 research project, the primary objective of this work was to study the recycling process of Al components from a Bombardier CRJ-100ER aircraft using a liquid state route in order to avoid downgrading the alloy quality. Particular attention was devoted to the removal of impurities associated with the aircraft corrosion protection coating, the content of alloying elements, and the potential pick-up of Fe and Si during handling of the scrap metal.

Prior to this project, no investigations associated with the decoating of aerospace components at the end of life condition were found in the open literature. Thus, a fundamental study on the thermal decoating of aerospace Al alloys coming from the CRJ-100ER aircraft was carried out. In this study, it was highlighted that the aircraft coating is an important source of impurities representing approximately 5 % of the Al substrate weight of the aircraft under study. The processing parameters such as temperature and time, the energy barrier for thermal decoating, and

the nature of the residues after decoating were determined. In this sense, the minimum temperature and residence time required to thermally remove the aircraft coating from Al substrates correspond to 480°C and ~4 minutes, respectively, involving a maximum activation energy of 170 kJ/mol. Additionally, the main inorganic components identified after decoating correspond to strontium chromate ($SrCrO_4$), titanium dioxide (Rutile-TiO_2), calcium silicate, ($CaSiO_3$), and barium sulfate ($BaSO_4$) from the pigments and fillers used in the coatings. The $SrCrO_4$ is considered to be a carcinogenic compound due to the presence of hexavalent chromium Cr(VI). Hence, the concentration of Cr(VI) in the $SrCrO_4$ prior to decoating was determined. It was found that 2.6 ± 0.1 µg of Cr(VI)/mm^2 was contained in the Al substrate with an overall particle size distribution of D_{50}= 1.96 µm. These findings led to the conclusion that adequate particulate matter control must be taken into consideration during thermal decoating of aircraft Al substrates to avoid Cr(VI)-residues becoming airborne contaminants. It is worth to mention that alternative surface treatments and primers free of chromate compounds are becoming the standard products in new commercial aircraft. Nevertheless, in old aircraft such as those waiting for final disposal, the typical conversion coatings and primers containing chromates are still found. In general terms, thermal decoating is possible and effective to remove the surface layer. However, an environmental study must be performed to evaluate if industrial scale filters and scrubbers would be effective enough to catch any pollutants evolving from thermal processes.

In addition to the pyrolytic paint removal process, the chemical route has been also explored for coated components coming from the CRJ-100ER aircraft. Chemical stripping has the advantage of keeping hazardous materials such as Cr(VI) in a damp state, decreasing its probability of becoming an airborne contaminant. In this part of the project, four hot stripping solutions provided by Greensolv® were tested on the external section of the aircraft fuselage under study which contained an epoxy-polyamide primer and a polyurethane topcoat. The same stripping solutions were also evaluated on the internal section of the airframe which contained only an aged epoxy-polyamide primer applied to the aircraft at the time of construction. The coating system in the external section of the fuselage was effectively removed by the four stripping solutions in times ranging from 2.10 to 3.75 h at 80 °C. However, the coating on the internal section of the fuselage was eliminated by only one stripping solution in approximately 2.10 h. The chemical stripping solution able to clean the aircraft substrates from all organic coatings was the G-293WL, which

was composed of a mixture of dimethyl sulfoxide, sodium hydroxide, and activators property of Greensolv®. The effective performance of this solution was attributed to the molar volume of the active solvent and to the alkalinity of the solution. Nevertheless, the excellent stripping efficiency of this solution was not constant and decreased as the solution life decreased probably due to the water lost during the hot chemical stripping process. Thus, in order to industrially use this technique, the chemical composition of the stripping solution baths should be constantly monitored to ensure a constant high stripping efficiency.

Overall, chemical stripping is an alternative method to remove the surface primers and paints. The project showed that all coating layers aside from the internal one can be removed without difficulty. Hence, it is important to select a stripping agent able to remove the coatings on both sides of the substrates. A key factor for the adoption of the chemical stripping route is how the scrap must be processed before decoating. One option would be to analyze if the use of paint stripping racks, as holders for multiple dismantled aircraft components, would be an efficient aid during the removal of coatings from the joints. This would not be problematic if a part-by-part dismantling process would be considered. Nevertheless, this approach might not be viable due to the complexity of the dismantling process. Another option would be to safely shred the aircraft components to a determined scrap size and carry out the stripping process in baths containing vibratory racks to allow the processing of high scrap volumes; by this option, most of the joints would be exposed to the solution allowing the removal of paint from these sections.

In summary from the scrap pre-treatment section, thermal and chemical coating removal routes are viable to be used in the recycling of aircraft aluminum components. The main advantage of the chemical route over thermal decoating is the control of particles containing Cr(IV). Nevertheless strict control of the stripping baths in terms of the chemistry of the solutions is required. In order to adopt any of the previous decoating techniques, a cost-comparison and an environmental assessment of the thermal vs chemical decoating routes should be carried out to select the most cost-effective and environmentally friendly process.

To improve the aircraft scrap quality, the dismantling process for aircraft components must not only consider technical feasibility, but also the systematic selection of areas to be dismantled based on the desired final chemical composition of the recycled alloys. Hence, identifying the

representative chemical compositions that can be obtained from the aircraft components is imperative during the recycling process. The goal of this section of the project was to identify the chemical compositions that could be obtained when the main components of the aircraft such as the fuselage, wings, vertical, and horizontal stabilizer are blended. Based on the mass balance analysis carried out in this project, alloys such as AA7036, AA7050, AA7055, AA7150, AA7155, AA7064, and AA7068 can be theoretically obtained by combining different aircraft sections. However, the presence of coated substrates, components containing Fe as a main alloying element, composites, Ti alloys, and any other Al alloy not belonging to the AA2000 and AA7000 series must be avoided in the scrap stream.

This section of the project has demonstrated that aircraft structures developed 25-30 years ago were not designed for recycling. The primary design consideration was functionality, hence the justification for mixing 2000 and 7000 series alloys. A key suggestion would be to design for recycling at end of life, thus taking into consideration possibilities for alloy mixing during the materials selection. During the course of the project, the sponsors have confirmed that aircraft design guidelines have shifted in this direction. Another key recommendation would be careful dismantling of the aircraft in order to avoid contamination with Si (i.e.: sand from the ground) and Fe (i.e.: residues from the saw blades and hydraulics pliers).

After the aircraft is dismantled, sorted, and decoated, the next step in the recycling process is refining. Refining consists of the elimination of impurities contained in the alloys such as inclusions, hydrogen, and undesirable elements such as Fe and Si. It is well known that Fe and Si are difficult to remove from Al and react with alloying elements to form detrimental precipitates. In order to remove the impurities Fe and Si, in addition to the intrinsic alloying elements of the aircraft alloys, the technical viability of fractional crystallization was analyzed in the last part of this work. For this purpose, a thermodynamic analysis of a blend of different aluminum components of the aircraft with overall composition of Al-2.43Cu-2.13Mg-4.67Zn (wt. %) has been carried out to determine the concentration limit of Fe and Si that can be treated by fractional crystallization. Then, a one-dimensional multicomponent solidification model that considered back diffusion in the solid and an effective partition coefficient was applied to a specific scrap composition to predict the refining efficiency at the microstructure scale. From this model, the critical parameters such as solidification velocity and stirring level that yield the maximum

efficiency have been determined. From the thermodynamic analysis it has been found that the feasibility of the process strictly depends on the concentration of Fe in the scrap alloy. If the concentration of this impurity is higher than 1.3 wt. % in the blended scrap alloy, the solidification range and thus, the fraction of primary Al FCC phase is decreased. The direct consequence of high content of Fe in the scrap alloy on the fractional crystallization process is the decrement of the Al yield. The one-dimensional multicomponent solidification model has determined that the optimum solidification velocity to recycle aircraft aluminum alloys is 1×10^{-6} m/s or lower. At this solidification velocities, the back diffusion of solutes is the dominant factor on determining the refining efficiency compared with the effect of stirring. Under this condition, refining efficiencies up to 97 % can be obtained. Nevertheless, it is important to mention that if the temperature is not properly controlled during cooling, the formation of second phases rich in solutes can occur which decreases the overall efficiency. The Al recovery has also been determined in terms of the total fraction of solid formed during the solidification process. For the blend of aircraft alloys studied in this work, a maximum Al yield of 31 wt% was obtained at a solidification velocity of 1×10^{-6} m/s when the concentration of Fe and Si in the alloys were 1 wt% and 2.5 wt% respectively.

In order to increase the Al yield, alternative processes could be adopted in addition to fractional crystallization. The first process could be to adopt a simple dilution in order to increase the amount of FCC_Al area in the phase diagram. As a result, a high amount of refined aluminum could be obtain. Another possibility is to promote the formation of intermetallic compounds containing Fe and Si in the remaining liquid rich in solutes. Then, processes such as sedimentation, electromagnetic separation, or filtration could be applied to remove the intermetallic compounds which gives rise to an increase in the Al yield.

In general terms, refining aircraft Al scrap by means of fractional crystallization is a technically viable option to obtain high-grade Al alloys. Nonetheless, the simulation study performed in this project showed that at most 31 wt% of a furnace load could be sufficiently refined. The remaining 69% would have to be further processed either by cascade recycling (lower Al grades) or be highly diluted with pure Al to reduce the impurity content down to acceptable levels. The successful implementation of this technique will strongly depend on the added value of the obtained products versus the processing costs which is not studied in the present work. Additionally, further studies

are needed to experimentally quantify the refining ratios. These experiments are recommended to be carried out if the business analysis satisfies the recycler's interests.

8: Conclusions

This section contains a summary of the conclusions presented in previous chapters.

1. Thermal decoating process was investigated as a scrap pre-treatment for aircraft Al scrap. This process is possible and effective to remove the organic coatings which represent approximately 5 wt% of the Al aircraft skin weight under study. The estimated time to remove the coatings was approximately 4 minutes when the substrates are isothermally decoated at 480 °C involving an activation energy of 170 kJ/mol associated with the oxidation of char. The residues of the process contain particles of strontium chromate ($SrCrO_4$). The concentration of such particles in the Al substrates was found to be 2.6 ± 0.1 μg of Cr(VI)/mm^2 with an overall particle size distribution of D_{50}= 1.96 μm. Thus, appropriate particle matter control must be considered during thermal decoating of aircraft Al components.

2. Chemical stripping using non-dimethyl chloride solvents has been also explored as an alternative process to remove the organic coatings from aircraft Al components. Four commercial solutions were tested where the main difference between the products was their active ingredient and the presence or absence of an alkaline activator. The organic coatings present in the external section of the fuselage were removed without difficulty in times ranging from 2.10 to 3.75 h in a bath held at 80 °C. The organic coating present in the internal section of the fuselage was not easily removed. This coating was only removed by a solution containing DMSO and NaOH. The low molecular volume associated with the solvent DMSO and the alkaline environment provided by the activator NaOH contributed to swell the organic film and to attack the Al substrate to promote stripping. However, in order to maintain a high stripping efficiency, the chemical composition of the stripping solution has to be constantly monitored.

3. The representative chemical compositions that can be obtained from different aircraft components was carried out by a mass balance approach. This analysis provides the methodology to improve the aircraft scrap quality in terms of chemical composition. Additionally, it provides the tools for a "smart" aircraft dismantling process if the production of high value alloys is targeted. From the analysis of the aircraft under study, a CRJ100 ER, it was concluded that alloys such as AA7036, AA7050, AA7055, AA7150, AA7155, AA7064, and AA7068 can be theoretically obtained by combining different aircraft sections. However, any material not belonging to the AA2XXX and AA7XXX series must be avoided in the scrap stream. Additionally, it is suggested that the aircraft must be carefully dismantled to avoid contamination with Si and Fe during the handling of the scrap.

4. The last step in the Al aircraft recycling process is refining. In this sense, the technical viability of fractional crystallization was studied by a one-dimensional multicomponent solidification model. The model considered back diffusion in the solid and an effective partition coefficient where the solidification velocity and stirring, two important parameters in fractional crystallization, were included. The model is able to predict the refining efficiency of any aircraft blend at the microstructure scale. According to the modeling results, fractional crystallization is a technically viable option to obtain high-grade AA from aircraft Al scrap. The feasibility of the process is determined by the concentration of Fe in the scrap. If the amount of Fe is higher than 1.3 wt%, the fraction of primary Al FCC phase decreases. Thus, a low Al yield is obtained. The optimum solidification velocity to recycle aircraft Al alloys is 1×10^{-6} m/s or lower. At this condition, refining efficiencies up to 97 % can be obtained. If the concentration of Fe and Si are 1 wt% respectively, the maximum Al recovering that can be obtain is 31 wt% from the original mass.

9: Contribution to Original Knowledge

The main contributions to original knowledge of the present thesis are stated as follows:

For the first time,

- This study presents the conditions to effectively remove the corrosion protection coating by a thermal process from aircraft at the end of service life. The processing parameters such as temperature and residence time, the energy barrier required to thermally decomposed the aged aircraft coatings, and the concentration of Cr(VI) remaining in the coating have been determined.

- The chemical stripping efficiency of the internal and external sections of an aircraft fuselage subjected to recycling using non-dimethyl chloride stripping agents is reported.

- The Flory-Rehner model has been correlated with the stripping efficiency of the solvents dimethyl sulfoxide and N-methyl-2-pyrrolidone applied to aged aircraft coatings.

- The combined effect of stirring energy and solidification velocity on solute distribution was explored in a one-dimension solidification model applied to fractional crystallization of aircraft Al scrap. The model predicts the processing conditions of fractional crystallization to obtain the highest Al recovery and refining efficiency of aircraft Al scrap.

10: Appendix A. Estimation of the Aircraft Aluminum Scrap Chemical Composition by a Mass Balance Approach

One of the issues concerning the recycling of aircraft Al components to produce high-value added alloys, is the presence of high levels of alloying elements such as Cu and Zn from the 2XXX and 7XXX series alloys. If these elements are present together at a high concentration in the scrap stream, the production of premium alloys becomes a difficult task and dilution with pure Al is unavoidable. To optimize the recycling of Al components, the aircraft scrap has to be pre-sorted in the dismantling and disassembly operations. In the ideal scenario of aircraft recycling, it is preferred to sort the Al alloys into their main families or alloy type [9.1, 9.2]. Nevertheless, this strategy usually involves high operational cost and it is labor intensive [9.3]. One of the options to optimize the recycling process is to disassemble the aircraft in a certain order "smart dismantling", that permits to obtain a high quality scrap instead of a scrap stream were all the aircraft alloys are mixed. Nevertheless, the dismantling decision is based on the scrap chemical composition that can be obtain from different sections of the aircraft air frame.

In this part of the study, the estimation of the scrap chemical composition resulting from the aircraft under study has been carried out using a mass balance approach. An experimental matrix comprising the blend of the main aircraft sections such as fuselage, wings, and the vertical and horizontal stabilizer, was used in this study. It has been found that the chemical composition of some alloys from the 7XXX series can be potentially matched by commingling different sections of the aircraft.

10.1.1: Experimental Procedure

The total weight of each section and the corresponding distribution and weigth fraction of each alloy, were provided by Bombardier. Nevertheless, this information is Bombardier proprietary and confidential information. Hence, the mass balance calculation methodology will be symbolically illustrated. The experimental matrix employed for the mass balance calculations is summarized in

Table 10-1, where the aircraft sections corresponding to the vertical stabilizer, horizontal stabilizer, fuselage, and wings, are represented by the letters A, B, C, and D, respectively. The calculations were carried out in the individual components considering their own alloy composition, as well as in commingled components such as A+B, A+C, A+B+C, etc..

Table 10-1. Experimental matrix containing the aircraft blends employed in the mass balance calculations

Aircraft sections	**A**	**B**	**C**	**D**
A	A	A+B	A+C	A+D
B		B	B+C	B+D
C			C	C+D
D				D
A+B			A+B+C	A+B+D
A+C				A+C+D
B+C				B+C+D
A+B+C				A+B+C+D

A= Vertical stabilizer, B= Horizontal stabilizer, C= Fuselage, D= Wings

Table 10-2, represents the calculation steps to obtain the weight fraction ω, of each alloy in commingled aircraft sections. Each aircraft part to be blended is represented by the letter P, where the subscrips 1, 2, · · ·j, correspond to different aircraft sections. For instance, if the vertical stabilizer is blended with the horizontal stabalizer (A + B), P_1 will represent the vertical stabilizer while the symbol P_2 will represent the horizontal stabilizer. If more than two sections have to be blended, a third or fourth section will be represented by j.

The alloys distributed in the aircraft sections are represented by the letter A, where the subscrips 1, 2, · · ·n, correspond to a specific alloy. After determining the weight fraction ω, of each alloy in a blend of aircraft components, the total concentration of Cu. Mg, and Zn in the blend are estimated.

Table 10-2. Determination of the weigth fraction corresponding to each alloy present in commingled aircraft sections.

Alloy	Alloy mass per aircraft part			Total mass	Weight fraction
	Part 1, P_1	**Part 2, P_2**	**Part j, P_j**		
A_1	m_{P_1,A_1}	m_{P_2,A_1}	m_{P_j,A_1}	$m_{A_1} = \sum_{i=1}^{j} (m_{P_i,A_1})$	$\omega_{A_1} = \frac{m_{A_1}}{m_{TOT}}$
A_2	m_{P_1,A_2}	m_{P_2,A_2}	m_{P_j,A_2}	$m_{A_2} = \sum_{i=1}^{j} (m_{P_i,A_2})$	$\omega_{A_2} = \frac{m_{A_2}}{m_{TOT}}$
·	·	·	·	·	·
·	·	·	·	·	·
A_n	m_{P_1,A_n}	m_{P_2,A_n}	m_{P_j,A_n}	$m_{A_n} = \sum_{i=1}^{j} (m_{P_i,A_n})$	$\omega_{A_n} = \frac{m_{A_n}}{m_{TOT}}$
				$m_{TOT} = \sum_{i=1}^{n} (m_{A_n})$	$\omega_{TOT} = \sum_{i=1}^{n} (m_{A_n})$

Table 10-3, shows the procedure to calculate the total concentration of the main alloying elements Cu, Mg, and Zn in a blend of aircraft components. The letters X, Y, and Z, represent the average concentration of Cu, Mg, and Zn of each commercial Al alloy A_n, as in

Table 10-4. The resulting chemical composition of commingled aircraft components was used to identify if any wrought commercial Al alloy could be produced from aircraft scrap.

Table 10-3. Determination of the concentration of Cu, Mg, and Zn in commingled aircraft sections.

Alloy	**A_1**	**A_2**	**. . .**	**A_n**	**Total weight (%)**
Cu	$X_1 * \omega_{A_1}$	$X_2 * \omega_{A_2}$	· ·	$X_n * \omega_{A_n}$	$Cu_{TOT} = \sum_{i=1}^{n} (X_n * \omega_{A_n})$
Mg	$Y_1 * \omega_{A_1}$	$Y_2 * \omega_{A_2}$	· ·	$Y_n * \omega_{A_n}$	$Mg_{TOT} = \sum_{i=1}^{n} (Y_n * \omega_{A_n})$
Zn	$Z_1 * \omega_{A_1}$	$Z_2 * \omega_{A_2}$	· ·	$Z_n * \omega_{A_n}$	$Zn_{TOT} = \sum_{i=1}^{n} (Z_n * \omega_{A_n})$

Table 10-4. Representation of the standard average chemical composition.

Element	**Alloy composition (wt%)**			
	A_1	**A_2**	**. . .**	**A_n**
Cu	X_1	X_2	· ·	X_n
Mg	Y_1	Y_2	· · ·	Y_n
Zn	Z_1	Z_2	· · ·	Z_n

10.1.2: Results and Discussions

Table 10-5, summarize the chemical composition of the main alloying elements of 2XXX and 7XXX series, Cu, Mg and Zn, in blended and non-blended aircraft components. Assuming that these estimated compositions are close to the reality, it would seem that the resulting scrap compositions could not produce high-value Al alloys from the 2XXX series due to high concentrations of Zn in the scrap stream. According to the international alloy designation and chemical composition limits for Al alloys [9.4], the maximum permissible concentration of Zn in alloys from the 2XXX series must not exceed 0.9 wt%. Hence, if the recycling process of high-

value alloys has to be optimized and dilution with primary Al is to be avoided, the production of alloys from the 7XXX series seems to be the ideal solution.

Based on the present analysis, different Al alloys from the 7XXX series can be obtain from the aircraft under study. The primary selection criteria for these alloys was the concentration of Cu. If the concentration of this element is above 2.6 wt%, most of the alloys from the 7XXX series cannot be produced. As a result, all the blends where the chemical composition of Cu was higher than 2.6 wt% were discarded. Based on this criteria, the commingled aircraft components that match the Cu concentration limits of 7XXX series alloys, are presented in Table 10-6. From this table, it can be observed that if the wings are separated from the aircraft, the resulting chemical composition matches more alloys than the rest of the blends. Similarly, if the wings are mixed with the vertical stabilizer or the horizontal stabilizer, the obtained composition can be able to produce a mayor quantity of alloys compared with other blends. On the other hand, if all the components are mixed, i.e., vertical stabilizer + horizontal stabilizer + fuselage + wings, and Zn and Mg are properly adjusted, the resultant chemical composition matches the composition of the alloys 7036, 7050, 7055 7150, 7155, 7064, and 7068.

In order to effectively produce these 7XXX series alloys, attention must be paid on the maximum concentration of Fe and Si that the alloys can accept. If the aircraft scrap exceeds the concentration of these elements, the recycled alloys cannot be used for aerospace applications that are based on fatigue crack growth rates and fracture toughness parameters (critical applications) unless an effective refining treatment and further validation are carried out [9.2]. If no refining treatment is done to decrease the amount of Fe and Si, an evaluation of the mechanical performance of these high Fe and Si-containing alloys has to be conducted. The evaluation has to define if the recycled alloys could be used for non-critical applications in the aerospace industry or if the alloys could find a niche in others industries such as the automotive or construction.

Table 10-5. Potential chemical composition of blended and non-bended aircraft components.

Blends	Alloy composition (wt%)			
	Cu	Mg	Zn	Al+others
A	3.4	1.8	2.7	Balance
B	2.8	2.0	3.4	
C	2.9	2.0	3.6	
D	1.9	2.2	5.6	
A+B	3.2	1.9	3.0	
A+C	3.0	1.9	3.5	
A+D	2.0	2.2	5.4	
B+C	2.9	2.0	3.6	
B+D	1.9	2.2	5.5	
C+D	2.3	2.1	4.7	
A+B+C	2.9	2.0	3.5	
A+C+D	2.4	2.1	4.7	
A+B+D	2.0	2.2	5.3	
B+C+D	2.4	2.1	4.7	
A+B+C+D	2.4	2.1	4.6	

A= Vertical stabilizer, B= Horizontal stabilizer,
C= Fuselage, D= Wings

Table 9-6. Commercial aluminum alloys from the 7XXX that could be produced by blending aircraft sections if the concentration of Fe and Si are within the permissible limits.

Aircraft sections	7036	7136	7040	7140	7050	7050A	7075	7150	7055	7155	7064	7068	7075	7175	7178	7278A	7349
D																	
A+D																	
B+D																	
C+D																	
A+C+D																	
A+B+D																	
B+C+D																	
A+B+C+D																	

A= Vertical stabilizer, B= Horizontal stabilizer, C= Fuselage, D= Wings

10.1.3: Conclusions

A simple mass balance methodology to estimate the chemical composition resulting from blended and non-bended aircraft components from a Bombardier CRJ-100ER has been proposed. The mass balance results suggest that the wings can be directly recycled into different 7XXX series alloys. Furthermore, if the wings are combined either with the vertical or with the horizontal stabilizer, the result is similar. Another observation of the present study is that if no separation is carried out, as a case in point, the vertical stabilizer, horizontal stabilizer, fuselage, and wings are blended to form a single scrap stream, the scrap composition matches the alloys 7055 and 7068.

However, the presence of coated substrates, components containing Fe as main alloying element, composites, Ti alloys, and any other Al alloy not belonging to the AA2000 and AA7000 series have to be avoided in the scrap stream. Additionally, the pickup of impurities such as Si and Fe must be minimized during the handling and shredding of the scrap. A high concentration of these impurities, usually higher than 0.5 wt%, limits the recyclability of aircraft components into high quality alloys such as those from the 7000 series

In this part of the study, the estimation of the scrap chemical composition resulting from the aircraft under study has been carried out using a mass balance approach. An experimental matrix comprising the blend of the main aircraft sections such as fuselage, wings, and the vertical and horizontal stabilizer, was used in this study. It has been found that the chemical composition of alloys from 7XXX series can be match by commingling different sections of the aircraft.

10.1.4: References

[9.1] Mascle, C., et al., Procedia CIRP, 2015. Vol. 26: p. 299-304.

[9.2] Das, S.K., J. G., Light metals., 2007: p. 1161-1166.

[9.3] Sabaghi, M., et al., Resources, Conservation and Recycling, 2015. Vol. 102: p. 163-169.

[9.4] The Aluminum Association. International Alloy Designations and Chemical Compositions for Wrought Aluminum and Wrought Aluminum Alloys. 2009, The Aluminum Association: Arlington, VA.